2-1-2021

Design and Biomechanical Evaluation of a Clutch-Based Energy Storage and Release Assistive Knee Brace

Ericber Jimenez Francisco
University of Massachusetts Amherst

DESIGN AND BIOMECHANICAL EVALUATION OF A CLUTCH-BASED ENERGY STORAGE AND RELEASE ASSISTIVE KNEE BRACE

A Dissertation Presented

By

Ericber Jiménez Francisco

Submitted to the Graduate School of the

University of Massachusetts Amherst

in partial fulfillment of the requirements for the degree of

DOCTOR OF PHILOSOPHY IN MECHANICAL ENGINEERING

February 2021

DESIGN AND BIOMECHANICAL EVALUATION OF A CLUTCH-BASED ENERGY STORAGE AND RELEASE ASSISTIVE KNEE BRACE

A Dissertation Presented

By

Ericber Jiménez Francisco

Approved as to style and content by:

Frank C. Sup IV, Chair

Katherine Boyer, Member

Xian Du, Member

Sundar Krishnamurty
Department Head
Mechanical Engineering

ACKNOWLEDGMENTS

First and foremost, I would like to thank God for providing the health and time that allowed me to put my work and dedication into this project. I would like to thank my loving wife for her continuous support and patience during the most demanding times of this journey.

I am genuinely grateful to my advisor Dr. Frank Sup for giving me the opportunity of becoming part of his team and succeeding under his guidance. I am especially grateful to Dr. Katherine Boyer for all the knowledge, guidance, and trust put given to me; I will always treasure the welcome arms shown by the MOBL. I would also like to thank Dr. Xian Du for his timely guidance and advice. I am fortunate to have such a dissertation committee.

I would like to thank my fellow lab members at the Mechatronics and Robotics Research Laboratory for all the support and all the good memories that I will always treasure with me. Likewise, I would like to thank every colleague, friend, and family member that showed support at any point during my doctoral journey.

Last but not least, I would like to thank LASPAU and the Fulbright Scholarship Program for believing in me and giving me the opportunity and resources to come to this institution and pursue my dreams.

I will always be grateful.

ABSTRACT

DESIGN AND BIOMECHANICAL EVALUATION OF A CLUTCH-BASED ENERGY STORAGE AND RELEASE ASSISTIVE KNEE BRACE

FEBRUARY 2021

Ericber Jiménez Francisco

B.Eng. Mechatronics, Instituto Tecnológico de Santo Domingo

M.Sc. Mathematics, Instituto Tecnológico de Santo Domingo

Ph.D. Mecanical Engineering, University of Massachusetts Amherst

Directed by: Dr. Frank C. Sup IV

Knee osteoarthritis (OA) is a serious degenerative disease affecting over 240 million people around the world. The most disabling symptoms are joint pain, joint stiffness, and reduction in joint functionality. Medial compartment knee OA is the most common case of unicompartmental knee OA, and pain and progression have been associated with tibiofemoral alignment in early to moderate knee OA patients, mainly due to its association with knee loading as measured by knee adduction moment (KAM) and tibiofemoral contact forces (KCF). Valgization knee

braces have been developed to correct the malalignment at the tibiofemoral joint, but they have no direct effect on knee OA progression and joint contact forces. This has been explained by increased muscular activity, and neural adaptation to external knee brace loading, since muscle forces are the main contributors to knee contact forces. Muscular activity reduction has been achieved on healthy subjects through the implementation of exoskeletons and active orthoses. Integrating similar approaches into current knee bracing methods may reduce muscle activity around the knee joint, therefore achieving a reduction in KCF, and potentially reducing knee OA symptoms and slowing down disease progression.

After identifying the specific external knee assistance requirements for level walking, stair ascent, stair descent, stand-to-sit-to-stand, a clutch-based knee brace was built to meet the corresponding behavior for each of these daily life activities. The device was tested to quantify its biomechanical effects on one healthy subject during these activities, and changes in knee muscle co-contraction index, knee joint internal contact forces, and kinematics were reported. Stand-to-Sit-to-Stand (STS) showed the highest peak contact force reduction due to external assistance, moreover, the reduction in knee contact forces for the STS task was found to be directly proportional to the level of external assistance applied.

Our research reveals the capacity of semi-active knee bracing as a tool for tibiofemoral contact forces reduction, and its potential to be extrapolated as a non-invasive treatment to slow down the disease progression in knee osteoarthritis patients.

Contents

List of Figures

List of Tables

Chapter 1

INTRODUCTION

1.1 Introduction

Knee osteoarthritis (OA) is a serious degenerative disease affecting over 240 million people around the world, the most disabling symptoms are joint pain, joint stiffness, and reduction in joint functionality. Medial compartment knee OA is the most common case of unicomparmental knee OA, and pain and progression have been associated with tibiofemoral alignment in early to moderate knee OA patients; mainly due to its association with knee loading as measured by knee adduction moment (KAM) and tibiofemoral contact forces (KCF). Valgization knee braces have been developed to correct the malalignment at the tibiofemoral joint, and this approach has been found to be effective for reducing pain and improving joint functionality. Knee braces have effectively reduced medial KCF in patients with instrumented implants after undergoing total knee arthroplasty (TKA); however, pre-TKA patients have different kinematics and knee braces seem to have little to no direct

effect on knee OA progression and joint contact forces. This has been explained by increased muscle activity, and neural adaptation to external knee brace loading, since muscle forces are the main contributors to knee contact forces.

One way in which muscle activity reduction has been achieved on healthy subjects is through the implementation of exoskeletons and active orthoses. Integrating similar approaches into current knee bracing methods may reduce muscle activity around the knee joint, therefore achieving reduction in KCF, and potentially reducing knee OA symptoms and slowing down disease progression. The preliminary data shown in this proposal suggests different knee assistance requirements depending on the task being executed; current knee exoskeletons and active orthoses do not follow the required assistance patters, and therefore can not be directly applied to reduce joint loading in knee OA patients.

Knowing the effects of semi-active assistive knee bracing in healthy people, could help extrapolate this technique to be applied on knee OA patients. For that reason, this research aims to explore the effect of clutch-based knee bracing on knee muscles co-contraction index, knee joint internal contact forces, and kinematics during daily life activities.

1.2 Motivation

Knee Osteoarthritis (OA) is a progressive disease that compromises the structural and functional integrity of the knee joint cartilage. Clinical symptoms for OA include swelling, joint pain, and joint stiffness; this commonly leads to functional disability

and muscle weakness. The risk of developing knee OA depends on factors such as genetics (Huetink et al., 2016), Body Mass Index (BMI), changes in BMI throughout life, and history of knee injury (Claes et al., 2013; Murphy et al., 2008). Knee OA has a significant global prevalence, affecting 240 million people around the world (Vos et al., 2015).

Symptomatic OA has a significant impact on the quality of life of patients; a 2015 study involving 147 hip or knee OA patients aged 20 to 55 years reported a 35% reduction in Health-Related Quality of Life scores and the prevalence of psychological distress was over 4 times higher when compared with a population of similar age (Ackerman et al., 2015). The measures used to quantify these outcomes included independent living, relationships, mental health and senses, and levels of anxiety, depression, and worry.

The principal and most disabling symptom of knee OA is pain, this fact is magnified when we consider that OA is a degenerative disease and that OA pain increases as the disease progresses (Bihlet et al., 2019). This indicates that progression is a key component of the OA problem, as it will cause both pain and functional disability to increase.

Pain and disease progression are closely tied to knee loading. Varus alignment and peak knee adduction moment (KAM) have been particularly associated with pain in advanced stages of knee OA (Shimura, Kurosawa, Sugawara, et al., 2013; Henriksen et al., 2012). KAM also seems to be a significant contributor to OA progression, as it has been associated with medial condyle joint space narrowing (Miyazaki et al., 2002; Chehab et al., 2014). Muscle activation patterns also play an

important role in knee loading, as Hodges et al. (2016) found faster OA progression due to augmented medial knee muscles co-contraction duration in the gait cycle. Co-contraction and knee joint moments have one key feature in common; they are surrogates for knee joint contact forces (KCF) (Trepczynski et al., 2018; Kutzner et al., 2013). This indicates that KCF is the underlying target when referring to knee joint loading.

1.3 Problem Statement

The prevalence of knee OA has been difficult to mitigate due to the degenerative nature of the disease and the lack of effective treatment. The initial management of OA is advised to be non-operative and intended to reduce the symptoms and improve functionality to delay surgical procedures. Although TKA is the most common definitive procedure for knee OA, it is generally reserved for patients with severe OA due to its invasiveness, cost and risk of complications such as infection, loosening, wear, instability and stiffness (Koh et al., 2014; Roche et al., 2018).

Nonsteroidal anti-inflammatory drugs (NSAIDs) are commonly implemented, however, they have been associated with risk of myocardial infarction and cardiovascular death (Bhala et al., 2013; Trelle et al., 2011). Other techniques include activity modification, physical therapy, weight loss, intraarticular injections, and load modifying techniques such as the use of wedged insoles, and knee bracing. Salam et al. (2019) suggest that insoles can significantly reduce pain and improve quality of life; however, a systematic review has been suggested, as disagreement has

been reported among studies in the literature (Chen et al., 2019).

On the other hand, offloader knee braces have been proposed as a treatment for knee OA for a long time, mainly because tibiofemoral alignment has been associated with functional disability and disease progression. However, a recent systematic review found that the literature supports knee bracing for improving pain, while functionality and stiffness improvement remains unclear, and no conclusion is provided regarding KCF (Gohal et al., 2018). It is then clear that effective external assistive devices to mitigate knee loading and knee OA progression are yet to be developed.

Since joint loading has been associated with knee OA progression, load-modifying techniques such as assistive exoskeletons can potentially extend the life of the joint by modifying the internal knee loads caused by muscle activity and joint torque. Evaluating this approach could provide a new noninvasive method to improve the functionality of knee OA patients and delay knee replacement surgery. The problem described is summarized in Fig. 1.1.

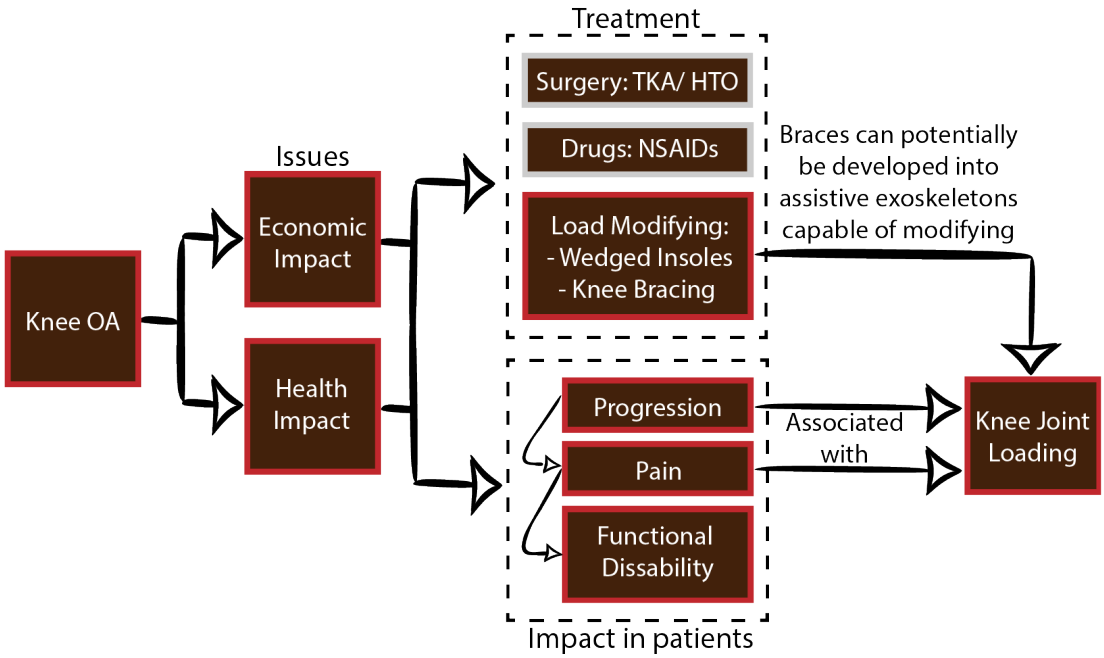

Figure 1.1: Problem description.

1.4 Research Objectives and Scope

This research aims to develop a clutch-based energy storage and release knee bracing approach and quantify its effect in knee muscles co-contraction index (CCI), knee joint internal contact forces (KCF), and lower limb kinematics during four daily life activities; walking, sit and stand, stair ascent, and stair descent. This work implements a case study to evaluate the prototyped device and answer the following questions.

- What is the relationship between external assistive moment magnitude and peak KCF and CCI for medial and lateral sides of the assisted knee during

walking, sit and stand, stair ascent, and stair descent tasks?

- How does external knee assistive moment alter the peak HFM and ADM of assisted and contralateral limb during walking, sit and stand, stair ascent, and stair descent tasks?
- How does external assistive moment timing relative to peak KCF affect the changes in KCF and CCI for medial and lateral sides during walking, sit and stand, stair ascent, and stair descent tasks?

The specific objectives to answer these questions are as listed below.

- To develop a clutch-based assistive knee brace capable of storing elastic energy and releasing it during eccentric knee extension torque with selected timing during walking, sit and stand, stair ascent, and stair descent tasks.
- Formulate and execute an experimental protocol to collect motion data, external loads, and muscle activity to obtain information for musculoskeletal modeling and data analysis.
- Implement musculoskeletal models to estimate the changes internal KCF through simulations to determine the knee joint loading variations caused by the knee brace external assistance.
- Measure muscle activity using electromyography (EMG) to quantify changes caused by the knee brace in motor control patterns and CCI.
- Quantify changes in the kinetics of knee, ankle, and hip joints by comparing joint moment and angle as a function of time to observe alterations in locomotion caused by the knee brace.

Chapter 2

Literature Review

2.1 Knee Osteoarthritis

2.1.1 Impact and Pathology of Knee OA

Knee Osteoarthritis (OA) is a disease that degrades the knee joint cartilage as it progresses. OA onset risk depends on multiple factors; previous knee injury and obesity seem to be two of the most important according to Silverwood et al. (2015) and Muthuri et al. (2011). Meniscal injury and a combined meniscus and ACL injury can increase the risk of developing knee OA by 6 times (Poulsen et al., 2019). Genetics and changes in BMI also play an important role (Huetink et al., 2016; Murphy et al., 2008). The global prevalence of OA is therefore, not surprising; in 2013, knee or hip OA affected 242 million people across the world, adding up to 13 million YLDs (Vos et al., 2015). This seems to become an underestimation for some populations, as nearly 1 in 2 people in the US will develop symptomatic knee

OA in at least one knee by age 85 years; more than 1 in 2 among those with knee injury history and nearly 2 in 3 among obese people (Murphy et al., 2008).

Symptomatic knee OA has a significant impact on the daily life of patients; a 2015 study involving 147 hip or knee OA patients aged 20 to 55 reported a 35 % reduction in Health-Related Quality of Life scores, and the prevalence of psychological distress was over 4 times higher when compared to a population of similar age (Ackerman et al., 2015). This age range serves as an indicator of the incidence of OA, as younger populations will likely live with the disease for longer than previous generations did, representing a new public health challenge (Ackerman et al., 2017).

Healthcare costs and joint replacement rates often serve as indicators of the burden of OA. In the US and Canada, the rate of primary total knee arthroplasty (TKA) procedure increased by 66 % and 83 % respectively from 2001 to 2007 (Ravi et al., 2012); moreover, Sloan et al. (2018) estimated that the number of primary TKA procedures in the US will increase by 85 % from 2004 to 2030, totaling 1.26 million procedures in 2030.

According to Kotlarz et al. (2009), the annual medical care expenditure in the US due to OA was $ 185.5 billion between 1996 and 2005. It is also estimated that 10 % of the lifetime direct medical cost for symptomatic OA patients can be attributed to this disease, and they spend 50 % of their postdiagnosis life expectancy between treatments while waiting for Total Knee Arthoplasty (TKA) (Losina et al., 2015). Knee arthoplasty, however, fails to mitigate the economic impact of OA for the individual affected; patients that undergo this procedure spend over twice

in medical costs during the first two years following surgery when compared to patients that remain under conservative treatment, as it was found by Ong et al. (2019). This impact is scaled up when observed from a broader perspective; in 2009, a US study estimated hospital expenditures due to knee replacements to be $ 28.5 billion (Murphy & Helmick, 2012).

Indirect individual costs should not be ignored to avoid significantly underestimating the burden of OA (Gupta et al., 2005). OA job-related indirect costs due to loss of productivity have been estimated at $ 3.4 to $ 13.2 billion per year (Leigh et al., 2001). This type of costs are mainly due to work loss, premature retirement, reduction in productivity and compensation for household work performed by others (Hunter et al., 2014); this is caused by the disabling nature of symptomatic OA.

Joint pain is the principal and most disabling symptom of knee OA. OA pain is a type of nociceptive pain and it has been associated with inflammation, mainly synovitis, detrimental mechanical stress and peripheral sensitization (Shimura, Kurosawa, Ishijima, et al., 2013; Dieppe & Lohmander, 2005). This type of pain can manifest in two distinct ways; an intermittent and intense pain, and a persistent 'background' aching pain (G. Hawker et al., 2008). Pain impacts negatively the quality of life of OA patients; G. Hawker et al. (2008) reported negative effects in mood, ability to participate in recreational activities, sleep onset, and sleep maintenance. In fact, 70 % of older adults with OA reported poor sleep in a study by G. A. Hawker et al. (2010); this deficiency in sleep quality was found to be related to fatigue and OA severity. This fact is magnified when we consider that OA is a degenerative disease and that OA pain increases as the disease progresses, as

it was evidenced in a recent study that associated radiographic knee OA severity and knee pain with bone and cartilage biomarkers (Bihlet et al., 2019).

Knee OA progression has also been found to increase the dynamic joint stiffness. Zeni Jr & Higginson (2009) reported an increase in dynamic joint stiffness in severe OA populations as compared to moderate OA patients and suggested that this was an adaptation strategy to overcome the decrease joint stability, decreased proprioception, and reduced afferent response to changes in external forces (Shakoor et al., 2008; Hortobágyi et al., 2004; Sharma & Pai, 1997; Fitzgerald et al., 2004) .

2.1.2 Knee OA Progression

In the healthy knee, kinematics and contact surface shape affect the functional adaptation of knee articular cartilage morphology (Koo et al., 2011), as pressure applied during everyday activities stimulate a positive adaptation (Koo & Andriacchi, 2007). Regional cartilage thickness variations are influenced by loading and number of loading cycles; Koo et al. (2011) associated the location of the thickest cartilage in the medial condyle with the knee flexion angle at heel strike during level walking. However, this relationship has been found to be altered by factors such as aging, obesity and whether the loading is generated by body size or subject-specific mechanics (Blazek et al., 2014).

While knee loading is usually beneficial for the healthy knee, it can lead to onset and progression of knee OA. Andriacchi et al. (2004) set a framework for knee OA

onset pointing out the contribution of knee loading location change within the cartilage due to changes in kinematics, generally caused by knee injury or aging. Several studies have related knee loading with medial compartment OA progression. A $6yr$ longitudinal study involving 106 OA patients found significant relationship between KAM and medial compartment joint space narrowing (Miyazaki et al., 2002); showing that that the risk of progression of knee OA increased 6.46 times with a 1% increase in KAM. Likewise, Chehab et al. (2014) associated tibial and femoral medial to lateral thickness ratio with KFM and KAM, suggesting the relevance of this surrogates of knee joint loading for intervention and treatment design. This study found a -0.064 unit change in the tibial medial to lateral thickness ratio per each 1% body weight times height change in the peak KFM. Another study, involving 54 OA patients over a $5-8yr$ period, showed that a 1 unit increase in knee loading increased the progression towards TKA by 5.7 times Hatfield et al. (2015).

Overweight and tibiofemoral alignment has also been correlated to knee OA progression (Yusuf et al., 2011). A $1yr$ study found faster OA progression due to augmented medial knee muscles co-contraction and that increased duration of lateral muscles co-contraction protected against medial cartilage loss; revealing an estimated 0.14% increase in cartilage loss per each 1% increase in medial muscles co-contraction duration in the gait cycle (Hodges et al., 2016). This indicates that biomechanical techniques to modify muscle activation patterns are potential candidates to slow disease progression.

2.1.3 Knee OA Treatment

The initial management of OA is advised to be non operative. Although TKA is the most common definitive procedure for knee OA, it is generally reserved for patients with severe OA, due to its invasiveness, cost and risk of complications such as infection, loosening, wear, instability and stiffness (Koh et al., 2014; Roche et al., 2018). While showing high survival rates (Liu et al., 2016; Julin et al., 2010), TKA is not advisable in the young patient due to a two to three-fold increase in risk of revision surgery (Chawla et al., 2017). Even though TKA patient satisfaction can change over time (Shannak et al., 2017), a study involving 1703 primary TKA patients revealed that approximately 1 in 5 were not satisfied with the outcome (Bourne et al., 2010).

Other surgical procedures to treat OA include high tibial osteotomy (HTO) and unicompartmental knee replacement (UKR). HTO cannot be considered a definitive treatment and can make future TKR more difficult (Sutton & Holloway, 2013). On the other hand, failed UKR may be associated with significant bone loss making revision surgery more difficult (Sutton & Holloway, 2013). Hang et al. (2010) suggest that revision of a failed UKR to a second UKR is associated with a threefold risk of further revision compared to patients revised to a TKR.

These findings show that nonoperative methods are recommended to reduce OA symptoms and improve functionality to delay surgical procedures. Commonly implemented treatments include non steroidal anti inflammatory drugs (NSAIDs), activity modification, physical therapy, weight loss, intraarticular injections (IA), use

of wedges and insoles and knee bracing. (Gohal et al., 2018; Sutton & Holloway, 2013; Boyer, 2018). NSAIDs are commonly implemented, however, they have been associated with risk of myocardial infarction and cardiovascular death (Bhala et al., 2013; Trelle et al., 2011). Some studies suggest that insoles can significantly reduce pain and improve quality of life (Salam et al., 2019); however, a systematic review has been suggested, as disagreement has been reported among studies in the literature (Chen et al., 2019).

Combining load-modifying treatments with pharmaceutical pain treatment has been recommended, as the load-modifying devices may support the beneficial gait adaptation that can protect the diseased joint, whereas the pharmaceutical interventions would address the inflammation and resulting noxious stimuli that can limit ambulatory function (Boyer, 2018). Offloader knee braces have been used as a knee OA treatment for a long time, mainly because tibiofemoral alignment has been associated with functional disability and disease progression (Shimura, Kurosawa, Sugawara, et al., 2013; Henriksen et al., 2012). However, a recent systematic review found that the literature supports knee bracing for improving pain, while functionality and stiffness improvement remains unclear, and no conclusion is provided regarding KCF (Gohal et al., 2018).

2.2 Locomotion and Knee OA

It has been widely observed that gait mechanics in OA patients differ from those in healthy subjects regardless of the severity of the disease; smaller knee flexion

angles (KFA) and smaller peak knee flexion moment (KFM) have been found during level walking in unilateral knee OA patients as compared to healthy subjects (Huang et al., 2008; Mündermann et al., 2005; Kaufman et al., 2001).

Frontal plane mechanics alterations are commonly reported during walking and seem to be more beneficial for mild knee OA patients rather than advanced knee OA patients. Mündermann et al. (2005) reported greater first peak knee adduction moment (KAM) and smaller hip adduction moment (HAM) in severe knee OA patients (K/L $\geq$ 3) as compared to less severe OA patients (K/L $\leq$ 2) and healthy subjects. Additionally, he found an increased axial loading rate in all joints of the lower extremity in severe OA subjects, and suggested that this could lead to faster OA progression. Huang et al. (2008) found a reduced knee extension moment in mild knee OA patients, while maintaining the same knee abduction moment at the affected knee; this was achieved mainly through listing and anterior tilting of the pelvis. Severe OA patients were able to reduce the knee extension moment by increasing the hip abduction, knee extension, and ankle plantarflexion angles; however, this resulted in an increased hip abduction moment. But gait adaptations are not always beneficial for non-severe OA patients, Metcalfe et al. (2013) found an increased adduction moment impulse at the knees and the contralateral hip in unilateral knee OA patients as compared to control subjects, and pointed out that this increased load could represent a risk for these healthy joints. Moreover, detrimental loading due to kinematics adaptations; in a study involving 117 knee OA subjects, Thorp et al. (2006) found a positive relationship between peak KAM and radiographic knee OA severity.

Sit to stand activity has been explored by Turcot et al. (2012), who reported an asymmetrical adaptation. Knee OA patients reduced the peak KFM by nearly 30 % by leaning the torso towards the contralateral side, resulting in a 10 % increase in contralateral limb loading.

Similarly, Hicks-Little et al. (2011) explored the kinematics of stair ascending in OA patients, and reported greater hip abduction angle at foot strike and smaller peak knee flexion during support as compared to control subjects. Knee loading under the same task was explored by Asay et al. (2009), who showed that severe knee OA patients lean the trunk forward as a compensatory strategy to reduce the demand of knee extension torque. Meireles et al. (2019) reported the same torso leaning strategy, combined with slow ascending speeds, to be effective for total knee contact forces (KCF) reduction in knee OA patients.

Body mechanics adaptation seems to be a more complex problem than simply reducing knee contact forces. Meireles et al. (2014) found an increased peak KCF magnitude in severe knee OA patients during walking, however, the medio-lateral component of the KCF was reduced, suggesting a possible trade-off to minimize shear forces within the joint. Brandon et al. (2014) studied the effects of muscle activation alterations in OA patients during gait, explaining the increased KCF as the result of a strategy to increase joint stiffness without considerably increasing the KCF.

2.3 Muscle Activity and Knee OA

Muscle activity plays an important role in knee joint loading, accounting for roughly 60 % of medial condyle loading during normal gait (Winby et al., 2009). Muscle activity can be quantified through the electrical activity manifested on the motor units recruited during muscle contraction, or myoelectric (ME) signals (De Luca, 1979). The sign, shape and magnitude of the electric signals obtained through electromyography (EMG) are dependent on factors such as the orientation of the electrodes with respect to the active muscle fibers, the direction from which the muscle membrane depolarization reaches the recording site, the diameter of the muscle fiber, the distance between the active fiber and the reading site, the filtering properties of the electrode, and the tissue between the active fibers and the electrode (De Luca, 1979; Lindström, 1973; Rosenfalck, 1969).

To study muscle activity during a time interval or a specific task, EMG envelope is commonly used. The inherent variability in EMG signals is commonly addressed with normalization techniques. EMG normalization is required for clinical interpretation as well as for comparison between different muscles within a subject, and for comparison between subjects (Lehman & McGill, 1999). Normalization factors have been obtained by maximal voluntary isometric contraction (MVIC), the mean of a task being studied, peak EMG reading of a task, and maximal or submaximal dynamic task (Sinclair et al., 2012; Burden, 2009; Benoit et al., 2003; Merletti & Di Torino, 1999). Burden et al. (2003), however, suggested implementing MVIC over dynamic tasks to obtain normalization factors, explaining that using isokinetic

MVC methods did not reduce variability as compared to other methods and that it was not more representative of muscle activity than MVIC for gait. Burden (2009) also signaled MVIC as the preferred method, while pointing out that it did no guarantee to reveal the activity of a muscle relative to its maximum activation capacity.

Electromyography is particularly useful to study neuromuscular strategies for given musculoskeletal tasks. During locomotion, agonist and antagonist muscles act on joints, this is known as co-contraction, and has been regarded as a mechanism to improve movement efficiency and joint stabilization (van Ingen Schenau et al., 1992; Falconer & Winter, 1985). Excessive co-contraction, however can increase metabolic cost (Peterson & Martin, 2010) and has been associated with internal knee loading and disease progression in knee OA patients(Dixon et al., 2018; Hodges et al., 2016).

Rudolph et al. (2000) quantified muscular co-contraction by defining the co-contraction index (CCI) as in Eq. 2.1 where $EMGS$ and $EMGL$ are the level of activity of the less active and the more active muscle respectively.

$$CCI = \frac{EMGS}{EMGL} * (EMGS + EMGL) \tag{2.1}$$

Knarr et al. (2012) Compared this method with the MCCI derived from the joint moment caused by individual muscles, as in Eq. 2.2, where LM is the magnitude of the smaller muscle moment, and HM is the magnitude of the larger muscle moment at a given time. Knarr et al. (2012) suggested the application of both CCI

methods to obtain a more complete description of co-contraction.

$$MCCI = \frac{|LM|}{|HM|} * (|LM| + |HM|) \tag{2.2}$$

Since MCCI can account for passive muscle forces not accounted for in EMG analysis, and includes muscle mechanical properties, it may provide a more confident description of muscle action (Knarr et al., 2012; Souissi et al., 2017), however, this method is directly dependent on the accuracy of the computer simulations used.

Muscle activity has been well studied in healthy and OA subjects during daily life tasks. A systematic review by Mills et al. (2013) found consistency in the literature, concluding that knee OA patients exhibited increased co-contraction amplitude and duration of lateral knee muscles, regardless of disease severity, along with up-regulation of medial knee muscles.

Liikavainio et al. (2010) characterized the Vastus Medialis (VM) and Biceps Femoris (BF) activation in healthy and knee OA subjects during level walking and stairs walking. Knee OA patients exhibited higher activity for the affected limb during the stance phase, while the contralateral side resembled the activity in healthy subjects; this reflected a difference in the strategy implemented by the OA patients to accomplish the same task. Patients were also found to increase the knee muscle loading with increasing walking speed.

The EMG activity for VM and BF during level walking found by Liikavainio et al.

(2010), shown in Fig. 2.1, resembles the preliminary results shown in Chapter 3 with both muscles being active primarily during early stance.

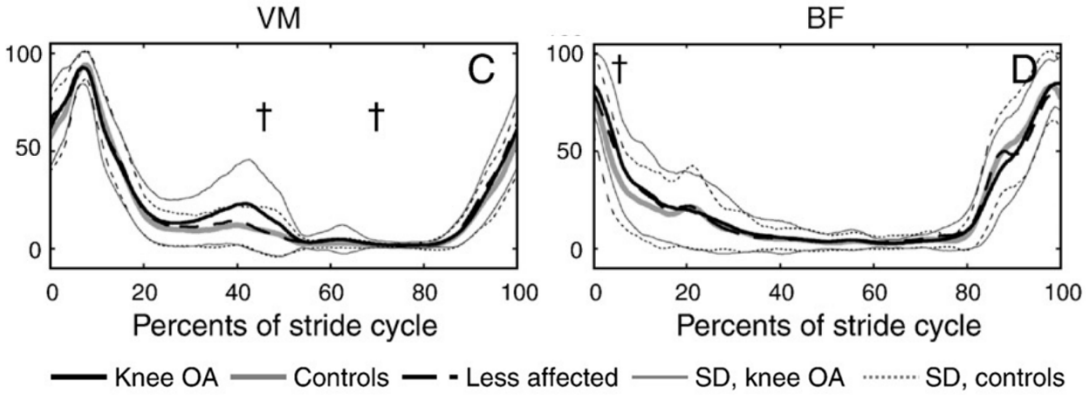

Figure 2.1: VM and BF activation during level walking at 1.5 m/s, normalized to dynamic maximum EMG. Toe off occurs at approximately 60 %. Adapted from Liikavainio et al. (2010)

For the stair ascending task (Fig. 2.2), Liikavainio et al. (2010) showed that besides having an increased muscle activity compared to healthy subjects, knee OA subjects had a more active BF as compared to the level walking task, similar to what is shown in Chapter 3.

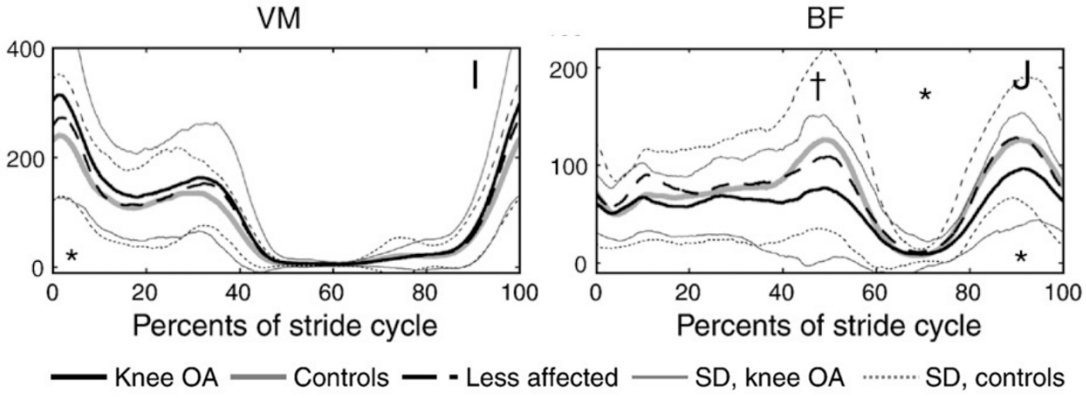

Figure 2.2: VM and BF activation during stair ascending at 0.8 m/s, normalized to dynamic maximum EMG. Toe off occurs at approximately 60 %. Adapted from Liikavainio et al. (2010)

Patsika et al. (2011) studied sit-to-stand task in female knee OA patients, finding a reduced force to EMG magnitude relation (efficiency) and an increased antagonist BF activation (RMS EMG). These neuromuscular changes in task strategy led to a slower task speed for OA subjects. Similarly, Bouchouras et al. (2015) found earlier and greater activation of hamstrings and increased muscle co-contraction in female knee OA subjects, and suggested this was a strategy to overcome pain and potential muscle trophy without compromising task duration. However, increased muscle activity in OA patients has been explained as part of the strategy to increase joint stiffness withouth considerably increasing the KCF (Brandon et al., 2014).

According to Al Amer et al. (2018) muscle activity can significantly vary depending on the initial position of the feet for the sit-to-stand task in unilateral knee OA subjects, hence, control of the initial position of the lower limb joints is recommended.

2.4 Simulation Approaches for KCF Determination

Muscle forces are the main contributors to joint loading (Herzog et al., 2003), albeit articular contact, ligament forces and other passive tissue strain, and external loading also contribute to joint loading (Fregly et al., 2012). Internal loading variables can not be directly measured in a clinical environment, and the redundant nature of the musculoskeletal system does not allow for a unique solution by means of rigid body mechanics (Erdemir et al., 2007).

Several studies have measured in vivo KCF by using instrumented implants following TKA intervention (Kinney, Besier, Silder, et al., 2013; Zhao, Banks, D'Lima, et al., 2007; Varadarajan et al., 2008; Mündermann et al., 2008), and have explored changes in contact forces under different gait patterns and external loading conditions. These measurements have allowed for comparison between experimentally measured and model estimated KCF (H. J. Kim et al., 2009; Lin et al., 2010; Purevsuren et al., 2016). However, joint kinematics have reportedly changed after TKA, indicating that some error may be introduced if this is ignored while estimating KCF on pre-TKA patients, by implementing modeling approaches validated with in vivo force readings from instrumented implants. Hatfield et al. (2011) studied 42 OA patients undergoing TKA, and found an increased knee flexion angle during the stance phase, while observing a reduction in midstance KAM and increased KFM during early stance.

2.4.1 Evolution of Musculoskeletal Simulation Techniques

The initial attempts to predict knee loading date back to the 1970s and calculations were considerably simplified (Morrison, 1970). Seireg & Arvikar (1973) formulated the redundancy problem through linear programming and solved it by means of a simplex algorithm; using EMG data as a validation tool. Algorithms to solve the musculoskeletal redundancy problem have evolved since then, and have been categorized into three groups: reduction method, forward dynamics method, and inverse dynamics method (Erdemir et al., 2007).

Reduction methods simplify the redundancy problem in such a way that the number of unknown matches the number of equations available to solve the musculoskeletal problem (Erdemir et al., 2007). The simplification typically eliminates unknown muscles or combines muscles with similar functions; this method, however, does not account for measured muscle activation patterns and muscle co-contraction (Fregly et al., 2012).

The inverse dynamics approach to solve the redundancy problem rely on static optimization methods, where the force distribution is solved at each instant in time by minimizing an objective function subject to constraints that satisfy the results determined by inverse dynamics such as joint torque and motion. Anatomical parameters are also used as constraints to ensure physiological feasibility.

Forward dynamics approaches integrate the equations of motion to determine muscle forces and body kinematics simultaneously. Forward dynamics can be EMG driven or can rely on optimization methods to generate muscle excitation patterns in order to generate body locomotion (Fregly et al., 2012).

Fig. 2.3 illustrates the inverse and forward dynamics approaches for muscle force determination. Inverse dynamics-based static optimization minimizes the objective function J and constraints are satisfied. Forward dynamics-based methods can include dynamics data tracking to update muscle excitations or can include optimal control strategies to update muscle excitations based on the minimization of a phisiologically based cost function (Erdemir et al., 2007).

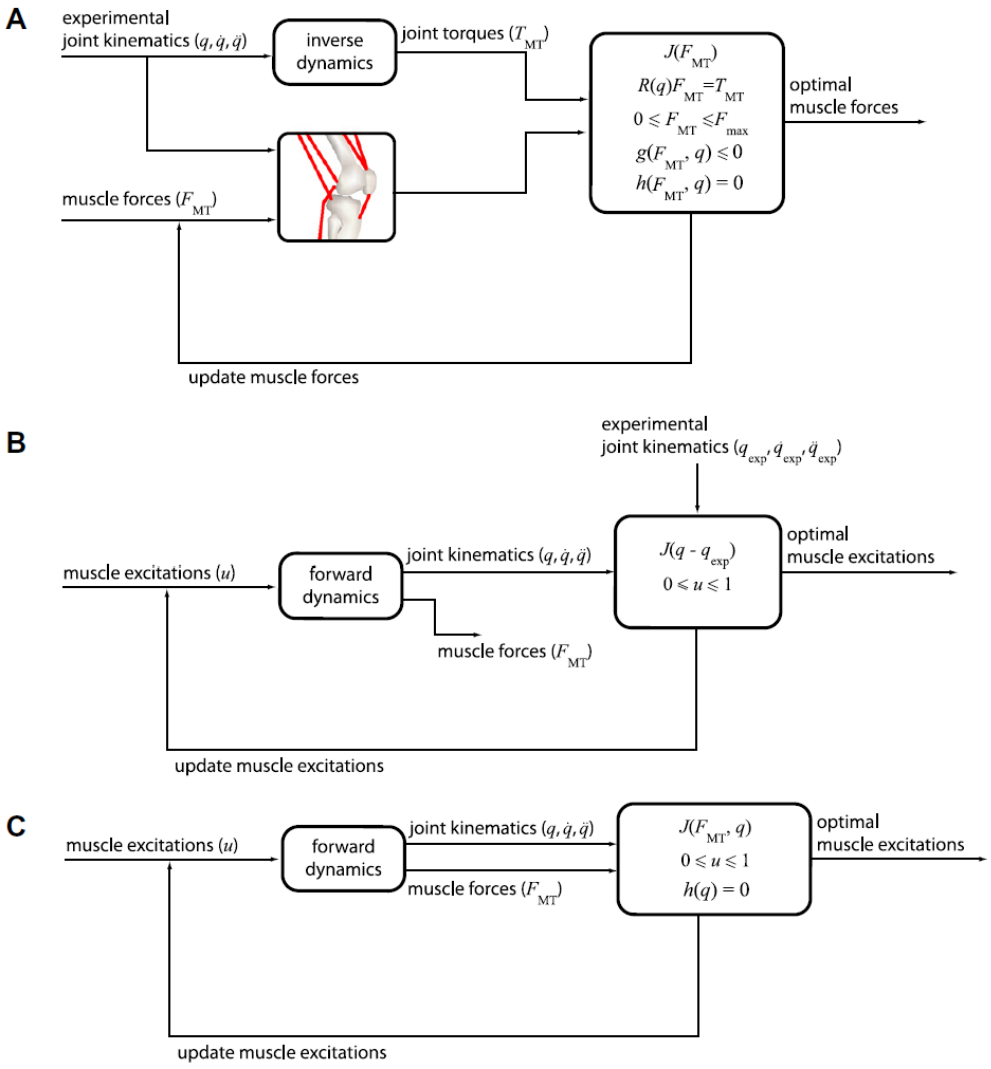

Figure 2.3: (A) Inverse dynamics-based static optimization. (B) Forward dynamics-assisted data tracking. (C) Forward dynamics based on optimal control strategies. Adapted from Erdemir et al. (2007)

When forward dynamics-based optimization is formulated independently from experimental data, it is called predictive simulation (Anderson & Pandy, 2001). This approach has been gaining popularity in musculoskeletal simulation research, as it has been recently implemented to predict locomotion in healthy subjects in different walking scenarios (Lin et al., 2018; Dorn et al., 2015), as well as in subjects wear-

ing orthotics and prosthetics (Handford & Srinivasan, 2016; Nguyen et al., 2019). However, validation of results remains a challenge for all optimization-based methods, and experimental results are commonly implemented as a validation tool for predictive simulation approaches (Lin et al., 2018; Dorn et al., 2015).

The selection and validation of a simulation approach to study human locomotion will generally depend on the questions to be answered and the available experimental data. One of the main limitations of optimization approaches is that the cost function and constraints are not necessarily known, and optimization strategies may be different among individuals, especially those with musculoskeletal or neuromuscular impairment. EMG-driven simulation methods try to overcome this issue by using EMG signals to drive muscle activity, however, it is not possible to include muscles for which EMG can not be measured (Fregly et al., 2012), and it is dependent on EMG normalization techniques, which may not be representative of the mucle activity relative to its maximum activation capacity (Burden, 2009).

2.4.2 Validation of Simulations for KCF Estimation

Solving the muscle redundancy problem does not solve the indetermination of the tibiofemoral contact forces problem, where forces at two contact locations must be determined in order to separate medial and lateral KCF. This again leads to a simulation-based approach, however, in vivo KCF measurements are generally used to validate simulation approaches to predict KCF (Fregly et al., 2012).

The Grand Knee Challege organized by Fregly et al. (2012) provided a frame-

work to evaluate different musculoskeletal simulation approaches for KCF through comparison with in vivo KCF values. From the four winner from 2010 to 2012, two of them implemented deformable contact models, however, the last two winners (2012) obtained some of the lowest RMS errors and highest accuracy without using contact models (Kinney, Besier, D'Lima, & Fregly, 2013).

Knowlton et al. (2012) reported the lowest RMS error (RMSE) for average total KCF, along with the best curve fitting ($R^2 = 0.82$); they implemented a parametric numerical model to determine a space of possible KCF solutions. On the other hand, Manal & Buchanan (2012) used an EMG-driven simulation approach, and reported the lowest RMSE for average lateral KCF. The lowest average medial KCF RMSE was reported during the 2010 competition by Y.-H. Kim et al. (2010), who implemented a deformable contact model. However, upon adjustments after unblinding the results, the EMG-driven model by Manal & Buchanan (2012) reported the lowest RMSE for average medial KCF.

While the $RMSE$ and R^2 values characterize the similarities between predicted and measured KCF during a time interval, it is often specific events, such as the peak values, that are of interest. Lerner et al. (2015) showed that correct anatomical information was determinant for accurate prediction of KCF, finding 12.4 % error for medial KCF using a fully informed model, as opposed to 63.1 % error when using a generic model. Lerner et al. (2015) Used the same data from the Grand Knee Challenge (Fregly et al., 2012) and developed a musculoskeletal model based on (DeMers et al., 2014); the fully informed model included subject-specific tibiofemoral alignment and contact locations determined through radio-

graphic analysis. To include these subject-specific values, Lerner et al. (2015) modified the knee joint as shown in Fig. 2.4; two revolute joints are attached to the medial and lateral compartments fixed on the tibial plateau, the two joints are also attached to the sagittal articulation frame, this allows for the simulation to resolve the joint reactions as medial and lateral KCF. The intercondylar distance can be adjusted by modifying $d1$ and $d2$; the tibiofemoral alignment can be modified through the femoral and tibial weld joints by setting θ_1 and θ_2 respectively.

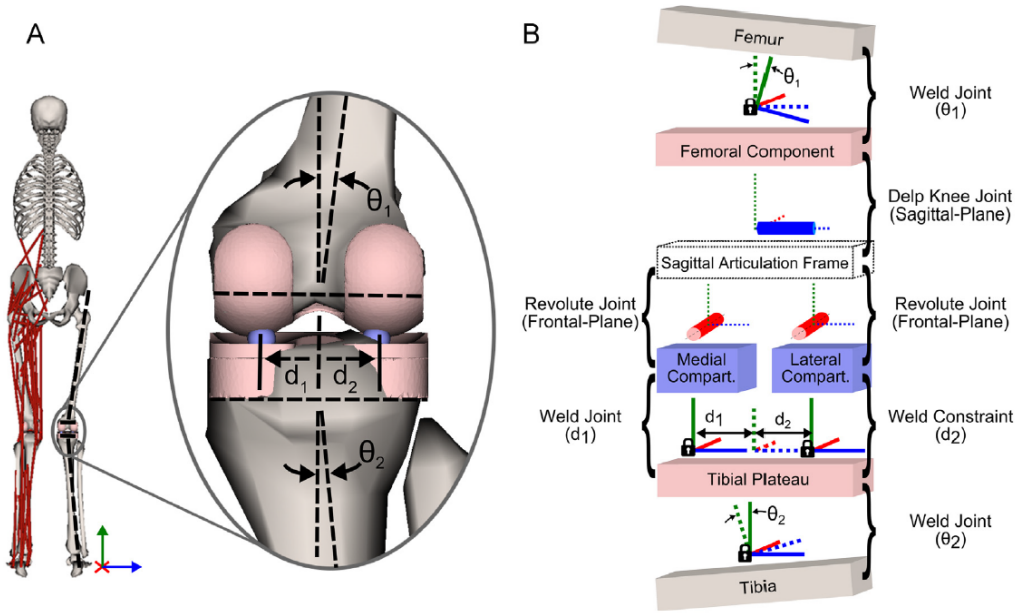

Figure 2.4: (A) Model illustration and schematic. (B) Diagram of knee joint model structure. Adapted from Lerner et al. (2015)

In order to estimate the muscle forces, Lerner et al. (2015) implemented static optimization simulation with custom muscle actuator weights. The joint reactions were determined using OpenSim Joint Reaction Analysis tool (Seth et al., 2011).

Winby et al. (2009) presented a different approach, predicting muscle forces by means of an EMG-driven musculoskeletal model, but relying on static equilibrium

equations to solve for medial and lateral KCF as depicted in Fig. 2.5. The external moment acting about the medial condyle (M^{MC}) was assumed to be balanced exclusively by the lateral joint reaction force (F_{LC}) and the muscle forces (F_{musc}); ditto for the medial joint reaction force (F_{MC}). In order to set the intercondylar distance (d_{IC}), Winby et al. (2009) made estimations from epicondylar width based on regression equations derived from MRI images.

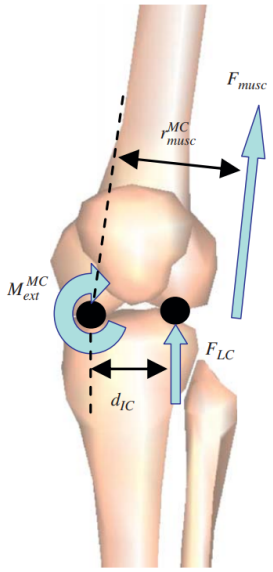

Figure 2.5: Schematic of the loads acting about the knee joint. Adapted from Winby et al. (2009)

Although able to predict the correct behavior, this model was not validated against experimental data, unlike Lerner et al. (2015). Additionally, the results from those simulations may be underestimates, because passive structures of the knee were not included in the model. Another limitation in this study was the fact that the calculations were made exclusively in the frontal plane, assuming that the only force components contributing to KCF were those generating frontal plane moment (Winby et al., 2009); this also prevents the simulation to properly account

for muscle co-contraction.

Although less explored, KCF have been estimated for other activities such as stair ascending, and sit to stand (Konrath et al., 2019; Van Rossom et al., 2018). Konrath et al. (2019) reported a peak KCF for stepping up (approximately 3.5 BW) in agreement with experimental values found by Taylor et al. (2004); while the KCF values for sit to stand (approximately 2 BW) are comparable to those reported by Zhao, Banks, D'Lima, et al. (2007).

Van Rossom et al. (2018) implemented a well defined knee joint finite elements model and the results are comparable to Zhao, Banks, D'Lima, et al. (2007), however, no validation procedure is implemented; rather, the results are used to compare between various rehabilitation tasks.

Tables 2.1 and 2.2 summarize notable experiments involving knee contact forces estimation through simulation. Among the walking studies, Lerner et al. (2015) showed the lowest error; this method represents a suitable candidate for KCF determination in this proposed research project. Among the higher knee flexion tasks, sit to stand and stair ascending, the approach taken by Van Rossom et al. (2018) seems to be the most detailed in terms of model definition and the results presented were in agreement with experimental data from the literature; however, no direct validation is provided.

The regression method used by Winby et al. (2009) to determine the intercondylar distance is practical and can be used to inform the subject-specific musculoskeletal modeling approach taken from Lerner et al. (2015). However, tibiofemoral alignment will need to be determined for each subject.

Table 2.1: Summary of experiments predicting KCF during walking. LW = Level Walking. P_1 and P_2 are 1^{st} and 2^{nd} peak KCF respectively. BW = Body Weight.

Ref./ Activity	**Model**	**Muscle force estimation**	**KCF estimation**	**Limitations**	**Peak KCF**	**Accuracy/ Validation**
(Y.-H. Kim et al., 2010) LW	Lower extremity 7 segments, 24DoF. Changing contact points location in FE model.	Static Optimization. Obj: Sum of squared muscle activations.	Quasi static FE analysis. Rigid to elastic contact. Ligaments modeled as non-linear springs.	Frictionless 3D rotation with predefined center of rotation (CoR) Single subject.	P_1 Medial: Approx 1400N P_1 Lateral: Approx 700N P_2 Medial: Approx 1800N P_2 Lateral: Approx 500N	RMSE = 229N R^2 = 0.82 Winner of 2010 Grang Knee Challenge.
(Hast & Piazza, 2013) LW	Opensim 23DoF Full body. Ligaments modeled as tensile spring with quadratic relationship.	Opensim CMC Forward Simulation.	Rigid body spring model.	2D Kinematics Generic model, aside from maximum isometric force scaling. Single subject.	P_1 Medial: approx 2BW P_1 Lateral: Approx 0.6BW	RMSE = 312N (approx 25% of max values). R^2 = 0.5 Winner of 2011 Grang Knee Challenge.
(Lerner et al., 2015) LW	Full body, 18 segments, 98 muscle-tendon actuators. Subject specific alignments and intercondylar distance from radiographs.	Static Optimization. Obj: Sum of squared muscle activations. Custom muscle weights.	OpenSim Joint Analysis	Single subject No knee rotation or adduction	P_1 Medial: 827N - 1002N P_1 Lateral: 635N - 825N P_2 Medial: 559N - 987N P_2 Lateral: 399N - 714N	12.4% error peak medial KCF. 11.9% error peak lateral KCF. Data from Grand Knee Challenge.
(Winby et al., 2009) LW	Full body 13 musculotendon units. Simplified intercondylar distance determination.	EMG-driven forward simulation.	Static equilibrium equations.	Passive structures ignored. Co-contraction not accounted for. Only frontal plane static equilibrium.	P_1 Medial: 2.1 - 3.3 BW P_1 Lateral: 0.92 - 3.06 BW	No direct validation.

Table 2.2: Summary of experiments predicting KCF during stairs ascent and sit to stand. SA = Stairs Ascent, ST = Sit to Stand. BW = Body Weight.

Ref./ Activity	**Model**	**Muscle force estimation**	**KCF estimation**	**Limitations**	**Peak KCF**	**Accuracy/ Validation**
(Konrath et al., 2019) SA	Full body 39 DoF (Anybody)	Inverse dynamics. No muscle forces directly determined.	KAM, ground reaction forces and moments, and body kinematics used as input.	Passive structures ignored. Muscle forces not directly considered (no co-contraction) Intercondylar distance not reported.	P_1 Total: approx 3.5BW P_2 Total: approx 3BW	RMSE = 0.89 $\pm$ 0.32 compared to inertial method. No direct validation.
(Konrath et al., 2019) ST	Full body 39 DoF (Anybody)	Inverse dynamics. No muscle forces directly determined.	KAM, ground reaction forces and moments, and body kinematics used as input.	Passive structures ignored. Muscle forces not directly considered (no co-contraction) Intercondylar distance not reported.	Approx 2BW	RMSE = 0.40 $\pm$ 0.14 compared to inertial method. No direct validation.
(Van Rossom et al., 2018) ST	Full body 44 musculotendon actuators. Knee Joint: 6 DoF for patellofemoral and tibiofemoral joint.	SIMM optimization of muscle activation and kinematics. Minimization of squared muscle activation and contact energy.	Nonlinear elastic foundation formulation based on the penetration depth of the surfaces. Force obtained from pressure and contact area.	Friction and tissue deformation was neglected. Neutral joint alignment assumed.	Medial: Approx 1BW Lateral: Approx 2BW	No direct validation.

2.5 Knee Exoskeletons and Knee Bracing

2.5.1 Knee Bracing as a Treatment for OA

During the stance phase of gait, where peak joint loading occurs, most of the joint load is supported by the medial tibial plateau in patients with neutral tibiofemoral alignment, being estimated to represent around 75% of the total load (Johnson et al., 1980; Zhao, Banks, Mitchell, et al., 2007; Hsu et al., 1990). This load increases in patients with varus alignment (Meireles et al., 2017), which is the most common case of unicompartmental knee OA. This results in a higher varus alignment as OA progresses, further increasing the loading in the already damaged compartment. Functional disability and pain in OA patients have been associated with tibiofemoral alignment (Srivastava et al., 2011; Shimura, Kurosawa, Sugawara, et al., 2013).

The malalignment of the lower limb has also been identified as a risk factor for the progression of knee OA, due to its association with joint load. Moyer et al. (2010) reported a 3.2 Nm increase in KAM for each 1° increase in knee varus alignment; while Zhao, Banks, Mitchell, et al. (2007) had directly correlated increased KAM with increased medial KCF. Felson et al. (2004) had already reported a 1.08 odds ration of progression for each 2 unit increase in BMI in malaligned OA affected knees, particularly pointing out that neutrally aligned and severely malaligned knees were not significantly affected in terms of disease progression. Therefore, correcting the joint alignment seems to be a reasonable approach to counteract OA symptoms and progression; this is the reasoning behind offloader

or valgization knee braces, aiming to correct the alignment at the tibiofemoral joint by applying an external valgus moment.

Effectiveness of knee bracing, however, is not universally accepted. A recent systematic review including 31 studies on the effectiveness of offloader braces found that the majority of literature supports its use for improving pain in medial compartment OA. However, it remained unclear whether this method improves function and stiffness or not, and disease progression was not assessed (Gohal et al., 2018). Meanwhile, Steadman et al. (2016) had explored the literature, showing agreement on the effectiveness of knee bracing on pain and functionality improvement, but concluding that unloading the medial compartment through this method did not significantly mitigate disease progression.

The lack of effectiveness of knee bracing to counteract OA progression may be directly related to its effectiveness to truly unload the medial knee compartment. Pollo et al. (2002) found an average medial KCF reduction of $114N$ (11%) and 179 (17%) for 4° and 8° of valgization angle respectively. However, these estimations were made based on a musculoskeletal model that did not include muscle forces, which have been regarded as the primary contributor to KCF (Winby et al., 2009).

Kutzner et al. (2011) studied the effect of knee bracing on knee loading by measuring in vivo KCF on three post TKA subjects with an instrumented implant, achieving 23 % and 30 % reduction in medial load for first and second peak of stance phase of gait respectively. The medial load reduction was found to be caused by both a shift from medial to lateral compartment and an overall reduction of the total force at the joint. However, high variability was reported between

subjects and the valgization configuration used ($8°$) was reportedly not tolerable to be continuously used. Additionally, Kutzner et al. (2011) did not analyze joint kinematics; which tend to change after TKA (Hatfield et al., 2011), and therefore experimental results from post-TKA patients may not always be applicable to pre-TKA patients.

Recent literature seems to support the idea that knee bracing does not effectively unload the medial knee compartment. Hall et al. (2019) studied the effects of knee bracing on KCF and muscle forces implementing an EMG-driven musculoskeletal model, finding no significant changes in KCF at a group level (Fig. 2.6). Additionally, the contribution of muscle forces to KCF relative to external loading were not significantly different between brace and no-brace conditions. Moreover, when using the brace, subjects showed significantly higher peak extensor-flexor muscle co-activation. These findings were interpreted as a possible muscle activity modulation to counteract the brace-generated valgus moment, thereby not affecting the KCF.

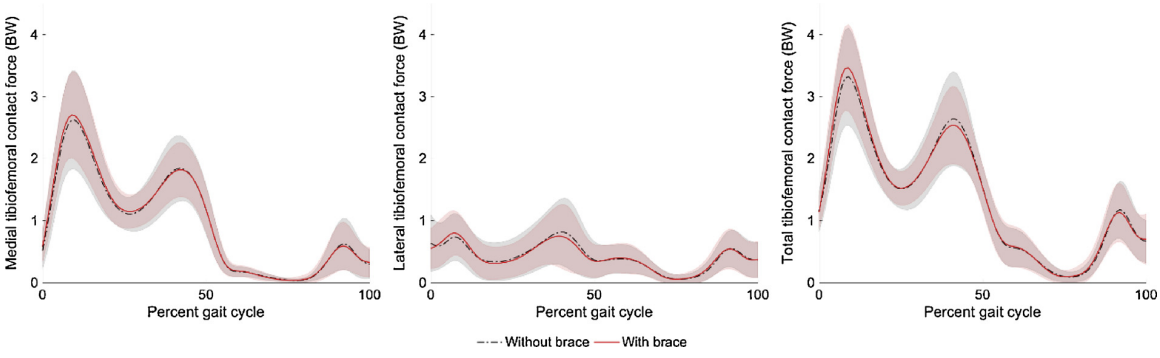

Figure 2.6: Tibiofemoral contact forces normalized to body weight (BW). Adapted from Hall et al. (2019)

Knee bracing alone may, therefore, not be an effective method to reduce KCF,

and alternative ways to reduce internal or external load contributions to tibiofemoral loading may be needed. One way in which lower limb muscle activity has been achieved is the use of assistive exoskeletons. Reduced ankle plantarflexor activity has been achieved by increasing torque and net work in ankle exoskeletons (Steele et al., 2017). Chaichaowarat et al. (2018) developed a knee exoskeleton to enhance cycling and found a significant reduction in EMG activity of the quadriceps even at higher cycling power output. Similarly, Ramanujam et al. (2018) tested an $Ekso^{TM}$ powered exoskeleton on healthy subjects and reported reduced lower limb muscular activity.

2.5.2 Knee Exoskeletons and Active Orthoses

An exoskeleton is defined as an active mechanical device that is essentially anthropomorphic in nature, is "worn" by an operator and fits closely to his or her body, and works in concert with the operator's movements (Dollar & Herr, 2008b; Herr, 2009). In general, the term "exoskeleton" is used to describe a device that augments the performance of an able-bodied wearer. An active orthosis is described as a device used to increase the ambulatory ability of a person suffering from a leg pathology. Exoskeletons are integrated with either: actuators, visco-elastic components, sensors, or control elements (Jun et al., 2015).

Exoskeletons have been functionally classified into serial-limb and parallel-limb. Serial-limb exoskeletons have reportedly increased jump height but have not been able to improve running speed or metabolic cost (Herr, 2009). Parallel-limb ex-

oskeletons, on the other hand, focus on the transfer of large loads to the ground in parallel with the body, lowering the load to be transfer by the body and therefore the metabolic cost (Herr, 2009). Other parallel mechanisms focus on improving strength by augmenting joint torque (Jun et al., 2015).

2.5.3 Knee Exoskeletons Design Approaches

Knee exoskeletons can be considered rigid or flexible based on the level of compliance shown during load transmission. Extremely compliant methods, such as knee sleeves have proven to have immediate effect on joint mechanics, reportedly mainly because of increased proprioception Schween et al. (2015). However, for load transmission purposes, stiff components must be added.

The knee joint in particular, is a complex joint with large range of motion in the sagital plane and small range of motion in the frontal and transverse plane. During walking, kinematics and kinetics have been characterized for OA patients; this information is of extreme importance when designing and evaluating knee exoskeletons. Considering a common 80 kg individual, peak KFM and KAM would be close to 24 Nm and 40 Nm respectively for OA patients (Deluzio & Astephen, 2007). In a healthy knee, peak KFM and KAM are around 32 Nm (Landry et al., 2007).

In terms of actuation, knee exoskeletons can be active or passive. Shepherd & Rouse (2017) developed an active exoskeleton designed to assist at full torque during sit to stand motion, and was able to deliver 80 Nm at $3\ rad/s$ (see Fig. 2.7).

These performance values surpass the common values for knee mechanics during sit to stand task; peak KFM ranges between $0.5 - 0.8\ Nm/kg$ and knee velocities do not exceed $3.0\ rad/s$ (Wretenberg & Arborelius, 1994; Roebroeck et al., 1994; Spyropoulos et al., 2013). Flexion torque was measured through a fiberglass beam incorporated in the transmission mechanism and torque control was implemented. This system however, had no compliance as the transmission mechanism included no elastic elements; another disadvantage is that this device had one degree of freedom, contrary to the complexity of the knee joint.

Figure 2.7: Orthosis structure. (Left, Center) CAD renderings excluding electronics box and with transmission revealed; (Right) photograph of complete system, including electronics box. Adapted from Shepherd & Rouse (2017)

An active design that takes into consideration the rolling nature of the knee joint was implemented by Liao et al. (2015) for level walking, stairs ascent, and stairs descent (see Fig. 2.8). The maximum torque capacity was 18 Nm, considerably inferior to expected knee joint moments during the performed activities. This design

did not allow frontal plane motion and power consumption and weight remained as limitations.

Figure 2.8: The bionic knee exoskeleton prototype. It's worn in front of human leg through the thigh belt and shank belt. Adapted from Liao et al. (2015)

More compliant mechanisms are also found in the literature, based on semi-active designs. An exoskeleton developed to assist during running activities implemented a quasi-passive mechanism with a spring that was engaged during the stance phase (Dollar & Herr, 2008a) (see Fig. 2.9). The spring would store energy at heel strike to then release it when the heel separated from the ground, reducing the work to be done by the quadriceps and the metabolic cost of running.

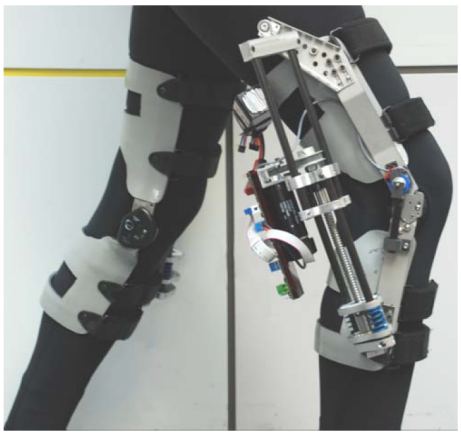

Figure 2.9: Exoskeleton prototypes being worn by a user. Adapted from Dollar & Herr (2008a)

Witte et al. (2017) developed a lightweight design ($0.76kg$) by implementing a tethered approach; the device was driven with Bowden cables and reached a capacity of $62.2Nm$ flexion torque. The big disadvantage of this design is that it can only be implemented in an experimental environment, since it needs to be remotely actuated.

Horst (2009) developed a commercially available knee orthosis for neurorehabilitarion (Fig. 2.10), capable of providing assistance during sit to stand, level walking and stairs walking. This design implements a continuous variable torque actuator (Flex CVA by Horst & Marcus (2006)), providing customized trade-off between force and speed and delivering up to 34 Nm of knee torque.

Figure 2.10: Tibion PK100 bionic leg orthosis. Adapted from Horst (2009)

While active exoskeletons have high torque capability, weight is usually a limitation. Conversely, passively actuated exoskeletons have lower weight, but at the expense of a considerably reduced torque capacity. Jun et al. (2015) developed a semi active parallel approach with compliance mechanism (Fig. 2.11), that deliv-

ered 0.6 Nm. The parallel plate mechanism however, causes the torque to develop as the knee flexes, making is dependent on the knee flexion angle. Torque output was modulated in the semi-active mode, but dependency on knee angle remained.

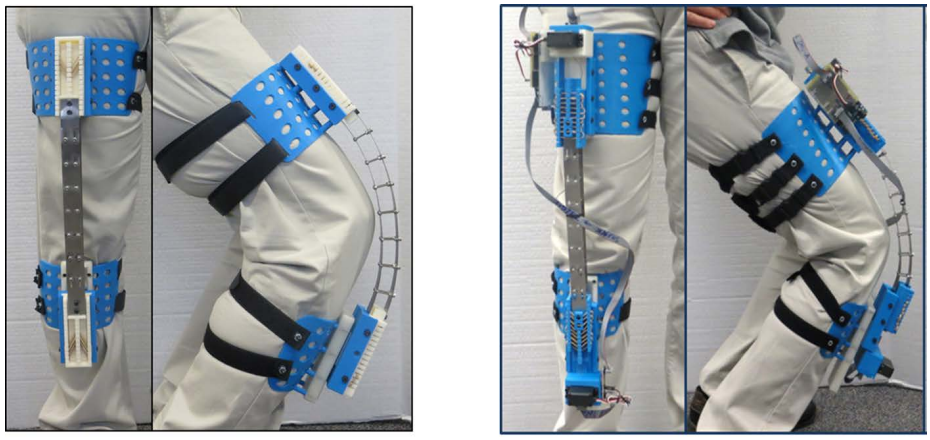

(a) (b)

Figure 2.11: Wearable prototype of (a) passive, and (b) semi-active knee brace. Adapted from Jun et al. (2015)

Table 2.3 summarizes notable knee exoskeletons found in the literature. Unlike what is available in the literature, the preliminary work shown in Chapter 3 suggests the application proposed in this work, would require a low weight knee bracing approach capable of applying high torque at small KFA during gait, and high torque at large KFA during sit-to-stand and stepping up. Therefore, a new actuation and control approach must be developed in the current work.

Table 2.3: Summary of experimental and commercially available exoskeleton and active orthoses. LW = Level walking, STS = Sit-to-stand, SA = Stairs ascend, SD = Stairs descend, R = Running, N/R = Not reported

Reference	**Task**	**Type**	**Max Torque**	**Max Speed**	**Control**	**Mechanism**	**Weight**	**Power**
(Shepherd & Rouse, 2017)	STS	Active	80Nm	>3.5 rad/s	Impedance	Rotational	1.8kg	200W motor
(Liao et al., 2015)	LW, SA, SD	Active	18Nm	N/R	Impedance	Rolling	N/R	N/R
(Dollar & Herr, 2008a)	R	Semi-Act	47.5Nm	N/R	Position	Rot. + Linear	2.5 kg	2W controller 200W motor Approx 115W peak demand
(Witte et al., 2017)	LW	Active	62.2Nm	N/R	Torque	Rotational	0.76kg	N/R
(Horst, 2009)	LW, SA , SD , STS	Active	34 Nm	>1.75rad/s	N/R	Rot. + Flex CVA	2.2 kg	70W
(Jun et al., 2015)	Bench testing	Semi-Act	0.6 Nm	User	N/R	Beam bending	0.6kg/ 1.5kg	N/R

Chapter 3

Redefining the Functional Requirements of Assistive Knee Braces

3.1 Introduction

As an initial evaluation of our approach, we developed a passive assistive knee brace based on an off the shelf Breg DUO knee brace for Osteoarthritis. We developed and executed a pilot testing protocol on one subject. The objective of this experiment was to quantify the effect of passive elastic knee external assistive moment in knee kinetics, knee contact forces KCF, and knee muscle activity. The results and observations obtained from this preliminary experiment served as the basis to develop the next version of the assistive device and its corresponding

testing protocol.

3.2 Methods

3.2.1 Dynamic Tasks

Three dynamic tasks were explored; walking at preferred speed, standing up from a sitting position and stepping up to a 215 mm step. Two conditions were tested for each task; Brace condition, and No Brace condition. The trials were not randomized, because a fixed body marker set was required to ensure consistency across all trials. Switching between conditions would potentially have altered marker positions and EMG data collection.

Walking Task

A total of 10 trials were collected for the Walking task; 5 for the No Brace condition and 5 for the Brace condition. However, one of the trials (NO_BRACE_WALKING0005) was regarded as an outlier due to a unusually high 2^{nd} peak KCF and KFA values; leaving the results data set with 4 No Brace condition trials.

Standing up Task

A total of 10 trials were collected for the Standing up task; 5 for the No Brace condition and 5 for the Brace condition. However, one of the trials (BRACE_STAND0004) was discarded, because the external knee brace moment (KBM) could not be de-

termined before 40% of the standing up phase; leaving the results data set with 4 Brace condition trials.

Stepping up Task

A total of 10 trials were collected for the Stepping up task; 5 for the No Brace condition and 5 for the Brace condition. However, one of the trials (BRACE_STEP0001) was discarded as an outlier, because it showed joint torque values significantly higher than the rest of the trials; leaving the results data set with 4 Brace condition trials.

3.2.2 Knee Brace KB2.0

This version of the assistive device (KB 2.0) was based on a Breg DUO knee brace; which is an adjustable valgization brace for OA. The brace was equipped with two assistive elastic bands to provide passive external knee extension torque. To obtain tensile load readings, two 20 kg flexion Micro Load Cell RB-Phi-119 were purchased from RobotShop and modified as indicated in Appendix A. All parts referenced in the drawing were obtained from McMASTER-CARR. The modified cells are shown in Fig. 3.1.

The load cells allow for direct measurement of the force produced by the elastic bands; this facilitates accurate estimation of KB 2.0 torque by cross multiplying the force vector with the moment arm vector created from the marker data obtained through motion capture. The location of the load cells on the brace is shown in

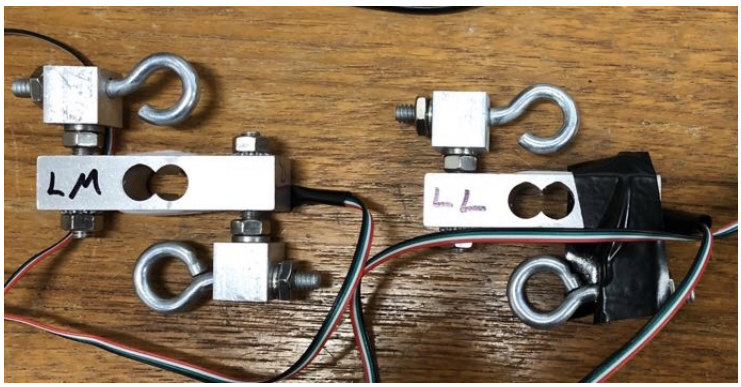

Figure 3.1: Modified load cells used in KB 2.0.

Fig 3.2.

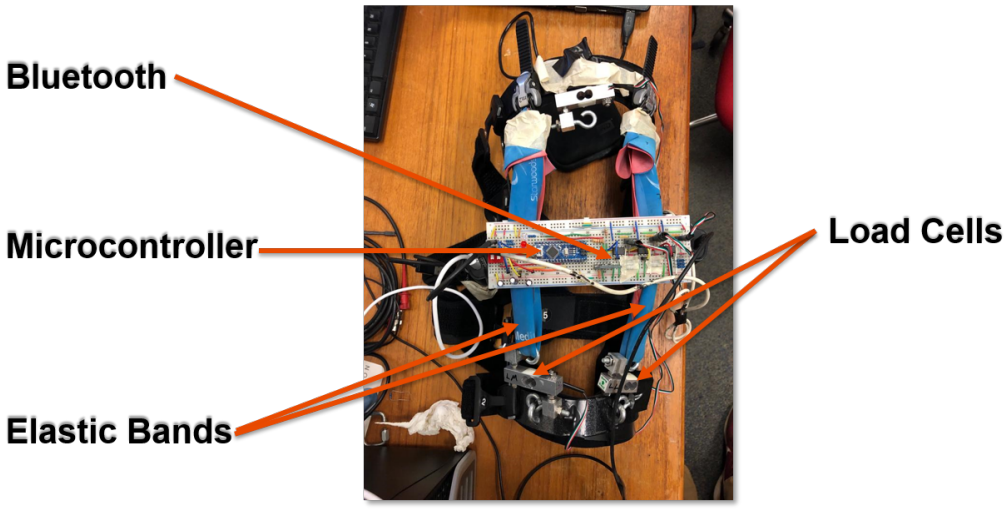

Figure 3.2: KB 2.0 components; elastic bands, load cells, and microcontroller/ bluetooth circuitry. The third load cell showed in the picture (but not signaled), was not used in the experiment.

Signal Conditioning

The signal from the load cells was amplified using AD620 instrumentation amplifiers and RC low pass filtered at 23.8 Hz; this cutoff frequency was found to eliminate most of the noise produced by the HC-05 Bluetooth module while allowing to

accurately capture the dynamic behavior of the elastic bands. The sampling frequency in the readings was set to 250 Hz using an Aruino NANO circuit board. The circuit prototype is also shown in Fig. 3.2.

The signal reading from the sync out connector in the Qualisys camera system was done with an Arduino DUE circuit board connected through a BNC cable. In order for the trigger feature to work, the Mode must be configured to 'Measurement time' and the TTL signal polarity must be configured to 'Negative' in the Sync Out property in the project settings in Qualisys QTM.

Communication

The system has three communication processes:

1. UART communication between the Arduino NANO and the Bluetooth module (HC-05), set to $115,200$ Bd.
2. Bluetooth communication between the bluetooth module and the computer, standard settings.
3. USB communication between the Arduino DUE and the computer, set to $115,200$ Bd.

User Interface

The user interface was developed using Visual Studio 2018 C# Windows Form. The UI, shown in Fig. 3.3, has the following functionalities:

- **Settings:** This tab has the options to connect a bluetooth module to the

software, enable a trigger COM port, and select the units or scale to plot the force data.

- **Start/Stop button:** This starts/ stops data collection; a bluetooth device must be connected to the software beforehand.
- **Save button:** This will save the last collected dataset to the path specified in "Save Path" under the name specified in "Name".
- **Stand by:** When selected, the system will wait for the trigger signal to start collecting data, after pressing "Start".
- **Time (s):** Sets the time to collect data for the current trial. When set to 0, data collection will not stop until "Stop" button is pressed.
- **Plotting area:** Plots the force readings in real time.

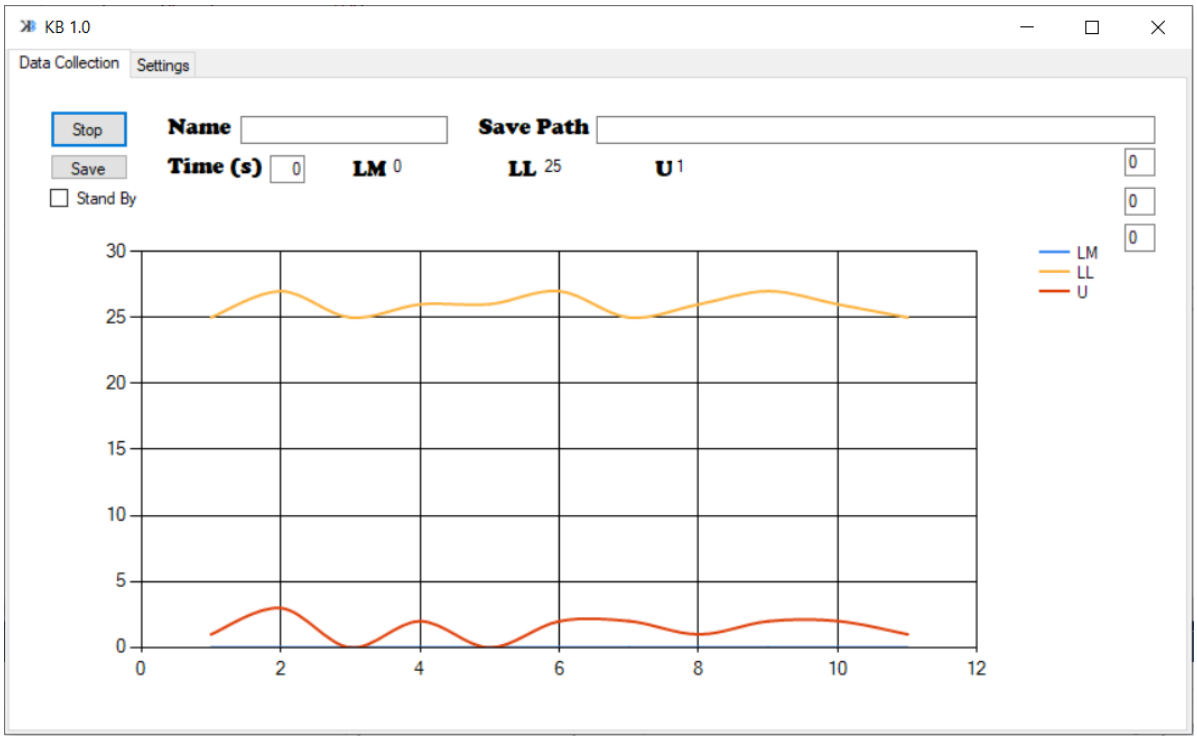

Figure 3.3: KB 2.0 User interface.

Calibration

The load cells were calibrated under tension, using an INSTRON 4411 universal testing machine. Static nominal loads were applied for a period of 10 s; data was read from the load cell and averaged to obtain a calibration measurement. The nominal calibration points were selected based on the expected tension load range, according to the expected knee angle range; 10 N, 20 N, 30 N, 40 N, 50 N, 60 N, 70 N, 80 N, 90 N, 100 N, 110 N, 120 N, and 130 N. The calibration data is shown in Appendix A, the maximum $\%$ error found was 0.72 %. The results from this calibration were used to adjust the relations between the arduino digital scale, and Newtons (N) unit of force, to correct the load cell readings.

In order to preserve the integrity of the load cells and use the same conditions as in the implementation, the calibration was made placing the load cells in line with the elastic bands as shown in Fig. 3.4. The calibration tables and curves are shown in Appendix A.

(a) Fixture set up. (b) Lower fixture setup.

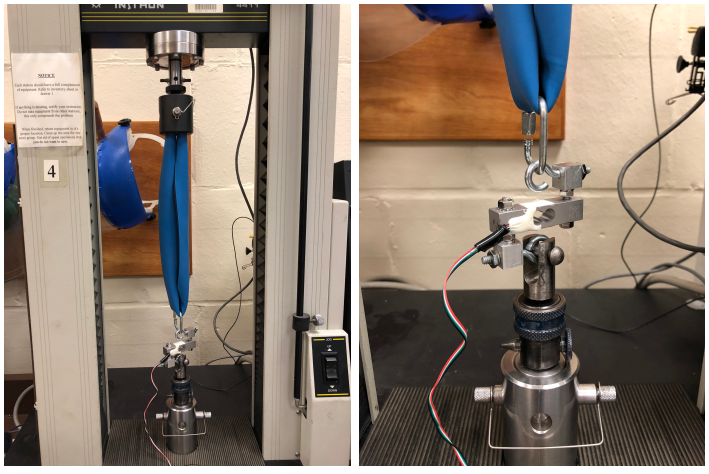

Figure 3.4: Testing fixture setup for load cell calibration under tension.

3.2.3 Data Collection

Motion data was collected for each trial using an 11-camera Qualisys motion capture system at 240 fps. Force data for ground reaction forces (GRF) was collected using AMTI force plates at $1,200$ Hz. EMG data was captured using a triggered Delsys Trigno EMG data system at $2,000$ Hz.

Force data collection from the knee brace was also triggered by the Qualisys motion capture system, the data collection system for the knee brace is summarized in Fig. 3.5.

Once the Qualisys system starts data collection, a trigger signal is sent to an Arduino microcontroller, which sends a command to the Visual Studio program indicating that data collection has started. The program then sends a command through bluetooth to the microcontroller in the knee brace, which then starts collecting data from the load cell and sending it back to the interface. Data collection continues until the collection time has elapsed. The comunication process before the brace starts collecting data, is delayed with respect to the initial Qualisys trigger command. To obtain the delay time, multiple trials were executed with the camera system in passive mode and the KB2.0 circuit board equipped with an infrared LED to indicate data collection start at the knee brace. The time delay between the initial trigger and the detection of the infrared LED by the camera system was averaged at 158 ms; this was later compensated during data collection.

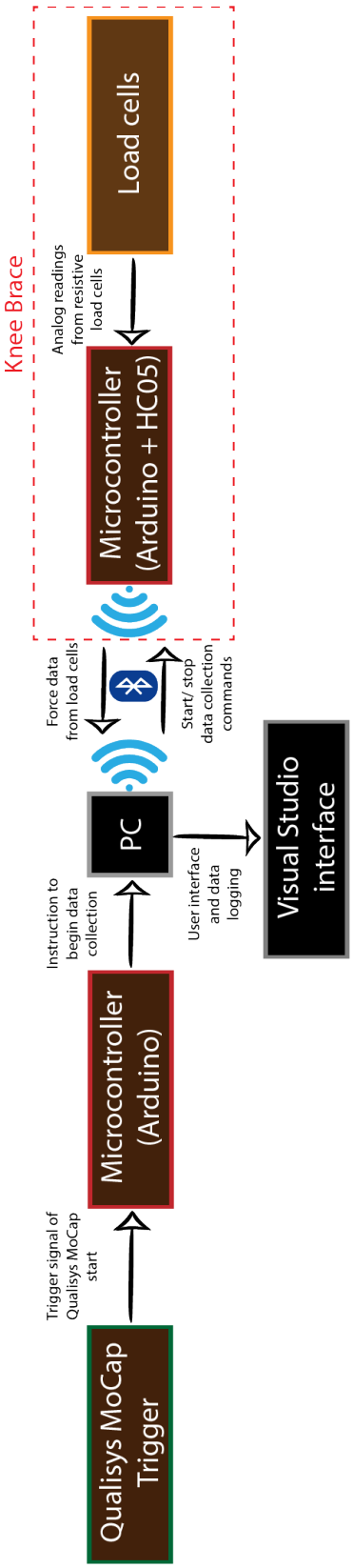

Figure 3.5: Data collection system diagram for KB2.0.

A lower limb and torso marker set was implemented, as shown in Fig. A.2. The marker set is detailed in Table 3.1.

Figure 3.6: Subject during walking trial with lower limb and torso marker set.

Table 3.1: Description of lower limbs and torso marker set implemented.

Markers	Description	Notes
TOR	Torso	-
RASI, LASI, RPSI, LPSI	L/R, A/P Asis	-
RGRT, LGRT	L/R Greater Trochanter	-
RTHUP, RTHUA, RTHLP, RTHLA	R Thigh cluster	-
LTHUP, LTHUA, LTHLP, LTHLA	L Thigh cluster	-
RLCO, RMCO	Right Knee condyles	No Brace trials
LLCO, LMCO	Left Knee condyles	-
RSHUP, RSHUA, RSHLP, RSHLA	R Shank cluster	-
LSHUP, LSHUA, LSHLP, LSHLA	L Shank cluster	-
RLMA, RMMA	Right Malleoli	-
LLMA, LMMA	Left Malleoli	-
RHLA, RHMD, RHPR	Right Heel	-
LHLA, LHMD, LHPR	Left Heel	-
R1MH, R5MH, RTOE	Right Metatarsal and Toe	-
L1MH, L5MH, LTOE	Left Metatarsal and Toe	-
B-UL, B-UM, B-LL, BLM, B-AL, B-AM, B-PL, B-PM	Knee Brace	Brace trials

EMG signals were collected for nine right lower limb muscles; Semitendinosis

(ST), Biceps Femoris (BF), Vastus Medialis (VM), Rectus Femoris (RF), Soleus (SOL), Medial Gastrocnemius (MG), Lateral Gastrocnemius (LG), and Tibialis Anterior (TA).

During the Brace trials, a mechanical interference between the knee brace and the VL transducer war reported. VL signals turned out to be considerably higher in magnitude as compared to the rest of the transducers and no consistent behavior was observed for the EMG envelope curve. For this reason, VL EMG data was was deemed not reliable and care should be taken to ensure signal reliability in future experiments.

3.2.4 Musculoskeletal Model

In order to estimate body kinetics and knee contact forces, musculoskeletal modeling was executed in OpenSim. Two models were created based on the Gait2392 model developed by Thelen et. al.

No Brace Model

This model was used in the simulations corresponding to No Brace trials data. The original Gait2392 model was added the marker set used during data collection and was scaled using the OpenSim **Scale** tool. The total squared error for model scaling was 0.0101 m, and the marker RMS error was 0.0153 m. To absorb noise and spikes during the Static Optimization simulations, a set of external actuators was added to each joint. This model is composed of 13 bodies, 12 joints, 92 musculo-

tendon actuators and has 23 degrees of freedom. The musculoskeletal model and the corresponding topology diagram are shown in Fig. 3.7.

(a) No Brace model.

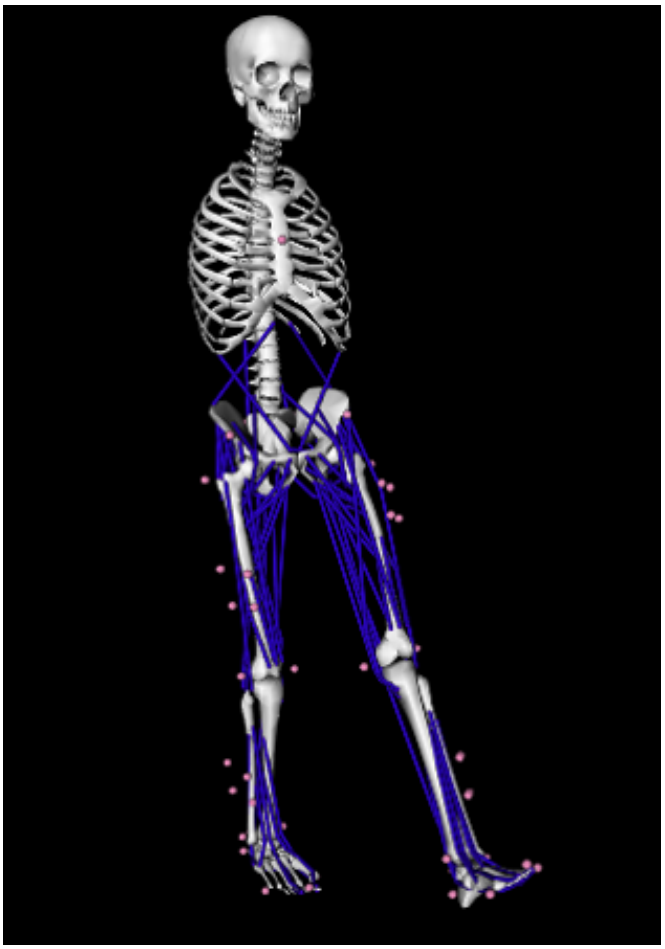

(b) No Brace model topology.

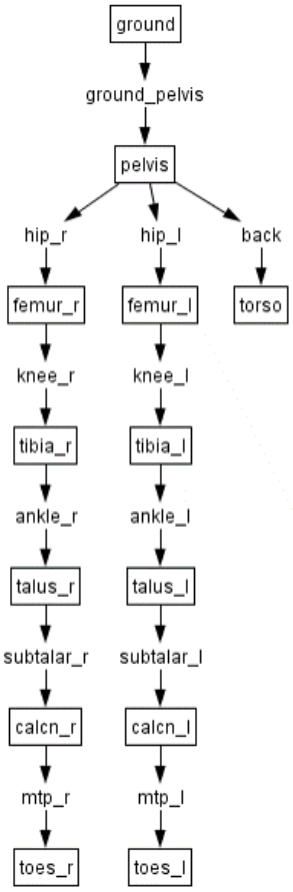

Figure 3.7: No Brace model and topology diagram. Model graphics and diagram is identical for the Brace model; the spring added is reflected at an actuation level.

Brace Model

The Brace model was constructed based on the No Brace model by adding a torsional spring to the right knee joint; this spring emulated the behavior of the knee brace by actively adjusting the elastic constant.

3.2.5 Data Processing

Data exported from Qualisys QTM included EMG data, marker data, and external forces data. EMG data was processed separately using the signal envelope method and marker and force data were converted into OpenSim format using a Matlab script. After conversion, this data was synchronized with the external force data from the knee brace and later processed using OpenSim and Matlab to execute inverse kinematics, inverse dynamics, static optimization, and joint reaction simulations. The data processing workflow is illustrated in Fig. 3.8.

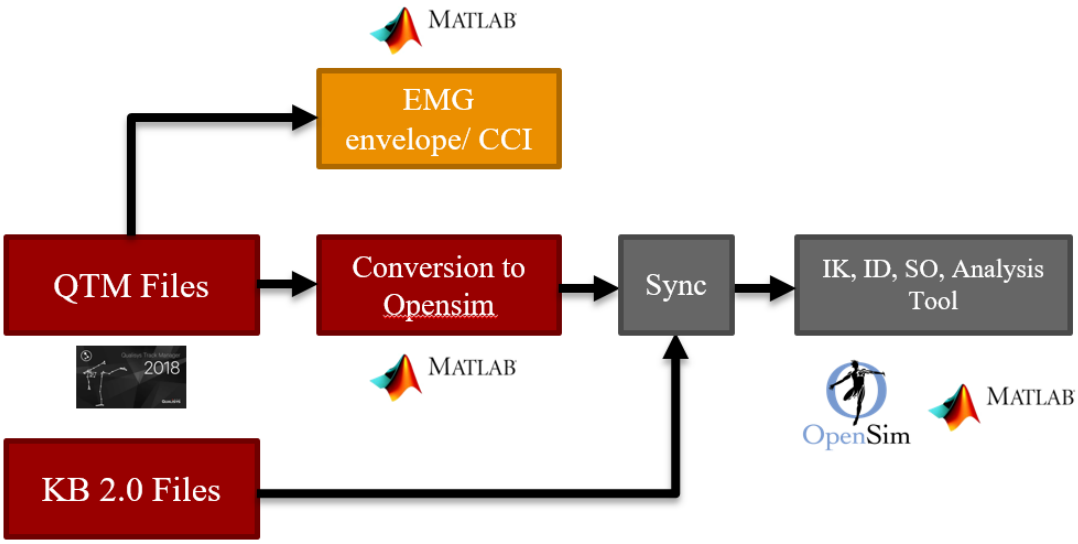

Figure 3.8: Data processing workflow for the testing trials.

KB 2.0 Force Data Processing

Force data from the knee brace was filtered with a moving average of 32 ms time window. Delay with respect to Qualisys motion capture system, produced during data collection, was compensated.

Brace torque was estimated as the cross product between the force vectors determined for the elastic bands and the moment arm vectors determined from the marker data obtained through motion capture. Force data obtained from the load cells is scalar, in order to convert it into a vector, unit vectors were created from marker data, using markers located in line with the elastic bands.

EMG Data Processing

EMG signals were band-pass filtered to remove noise (second order Butterworth filter at 20 - 500 Hz), rectified, and finally low-pass filtered at 10 Hz to obtain envelope curves.

Muscle activation co-contraction was determined, as defined by Rudolph et al. (2000), using Eq. 3.1, where $EMGS$ and $EMGL$ are the level of activity of the less active and the more active muscle respectively.

$$CCI = \frac{EMGS}{EMGL} * (EMGS + EMGL) \tag{3.1}$$

Musculoskeletal Simulations

Inverse kinematics and inverse dynamics were executed for all trials using the **OpenSim 3.3** IK and ID tools. After obtaining knee joint moment with ID, it was compensated with the estimated knee brace moment; it was assumed that the external moment from the brace was perfectly transferred to the knee joint.

Additionally, static optimization (SO) simulations were executed to estimate muscle forces. For SO in the Brace trials, the torsional spring at the right knee joint was manipulated at each time step in order to emulate the effect of the knee brace; Fig. 3.9 illustrates this process.

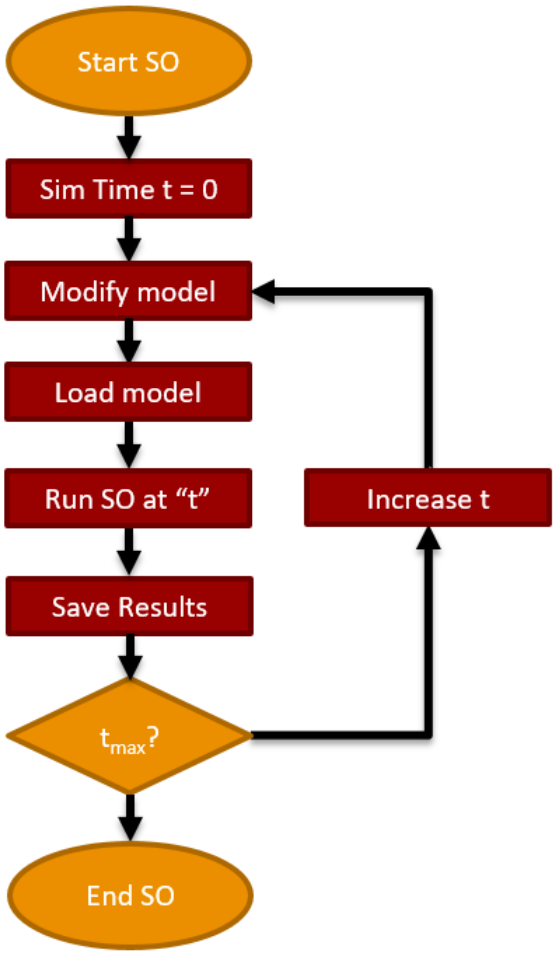

Figure 3.9: Static optimization (SO) simulation process for Brace trials.

When the simulation begins, the initial time is set to $t = 0$, the elastic constant of the torsional spring in the model model is subsequently modified, based on the knee angle at the given time point, to match the external torque prescribed as previously determined for that time point. The model is loaded and the simulation is

executed for one time point. After the results are saved, the time point is increased by the predetermined time step and the model is again modified to run a new simulation. This process continues until the maximum time point has been reached. All musculoskeletal simulations were executed on OpenSim through a Matlab script.

All musculoskeletal simulations were executed for the defined stance phase of the right leg (the braced leg), for each task. For Walking, the stance phase was defined based on ground reaction force magnitude, using a threshold of 10 N. For Standing Up, the stance phase was defined based on the variance of the knee angle, to detect when movement had started and when the final posture had been reached. For the Stepping Up task, stance phase was defined based on the variance of the ground reaction force of the stepping leg (braced leg).

3.3 Results

3.3.1 Walking

Kinematics

Relative knee flexion angle (KFA) during the stance phase of gait was not affected by wearing the brace, meaning that the shape in the knee flexion pattern was similar between conditions. However, the knee was found to be more flexed during the entire stance phase while wearing the brace compared to the no brace condition, as seen in Fig. 3.10. Additionally, the hip was significantly more flexed during the stance phase while wearing the brace as seen in Fig. 3.11. The ankle dorsiflexion

angle (Fig. 3.12) was not significantly affected by wearing the brace. This shows that the gait mechanics are affected by wearing the brace. This prototype provides external torque at all times and the resulting adaptation response was a crouch-like gait.

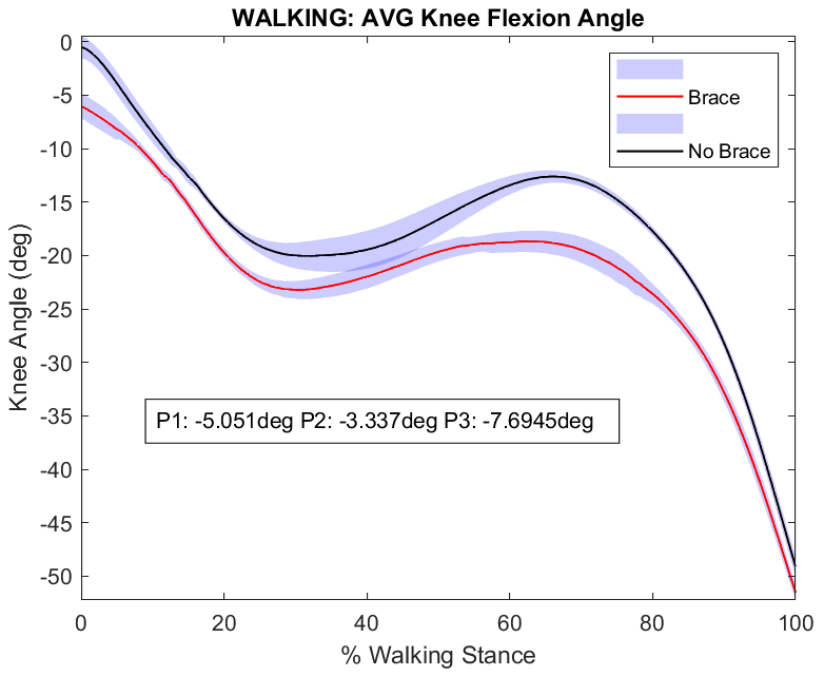

Figure 3.10: Average Knee Flexion Angle (KFA) during the walking trials (+ extension, - flexion). The KFA change effect caused by the knee brace at the three peak KCF is indicated in the plot.

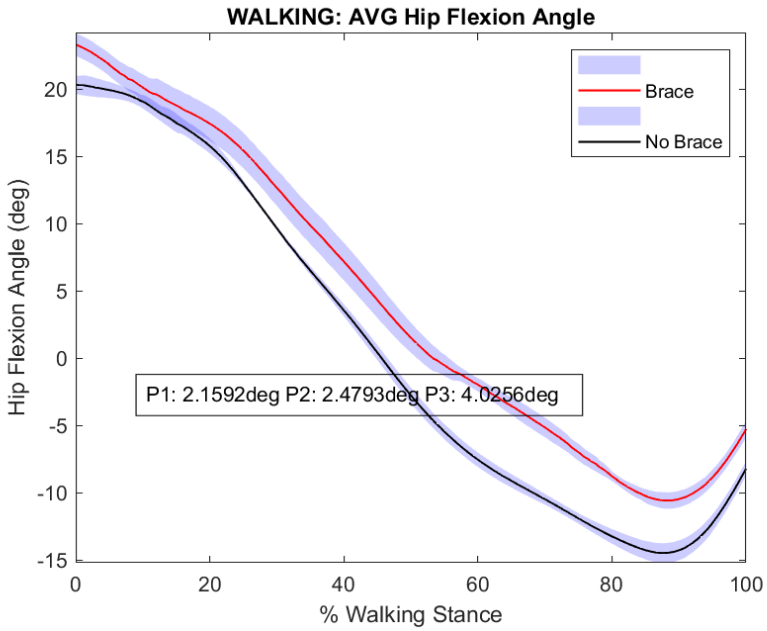

Figure 3.11: Average Hip Flexion Angle (HFA) during the walking trials. The HFA increase effect caused by the knee brace at the three peak KCF is indicated in the plot.

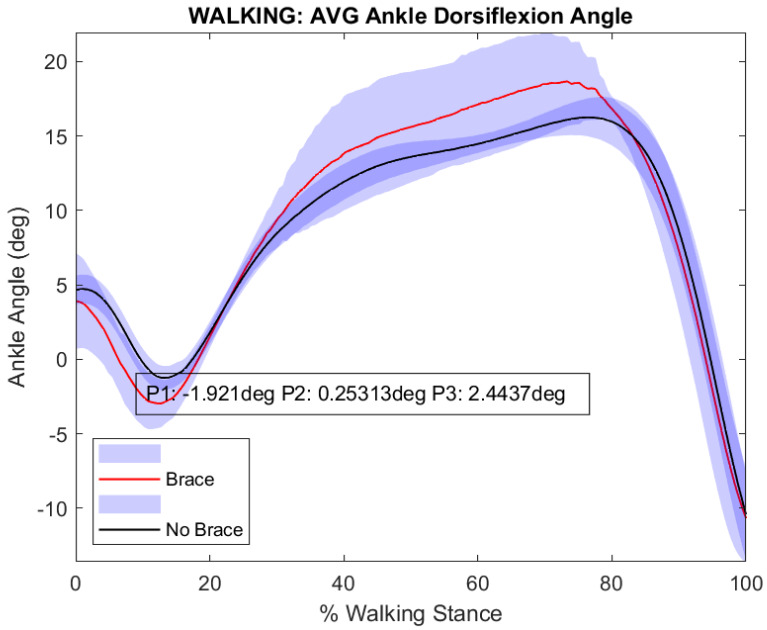

Figure 3.12: Average Ankle Dorsiflexion Angle during the walking trials. The ADA increase effect caused by the knee brace at the three peak KCF is indicated in the plot.

Joint Moments

The hip flexion moment (HFM) shows the same profile between Brace and No-Brace conditions, however, the hip extension moment peak at heel strike is smaller for the Brace condition. Similarly, the HFM is smaller from around 35 % stance until the end of the phase (Fig. 3.13).

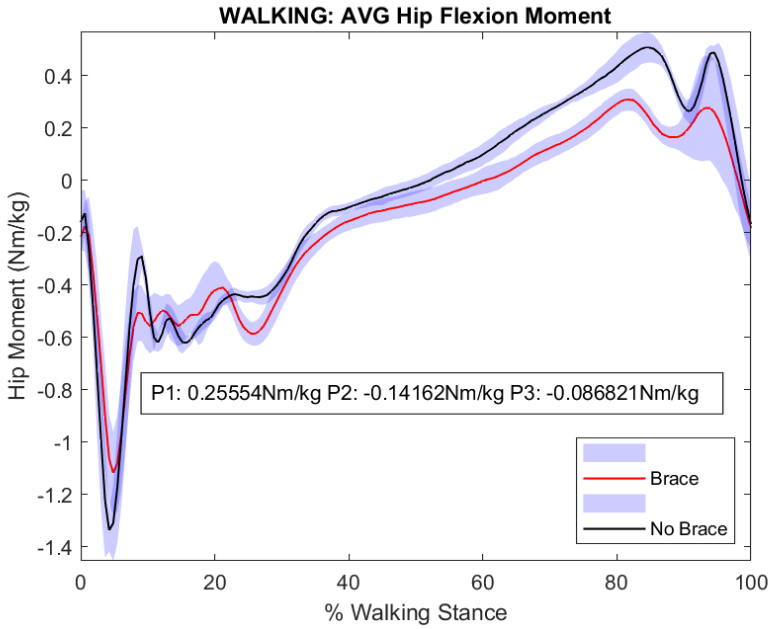

Figure 3.13: Hip Flexion Moment (HFM) during the walking trials. The change caused by the knee brace at the three peak KCF is indicated in the plot.

The initial Knee Flexion Moment (KFM) peak is reduced on the Brace trials. Moreover, KFM peak is reduced after midstance. At the end of the stance phase (80 % $+$), where higher KFA values happen, the effect of the elastic bands is evidenced in the KFM plot (Fig. 3.14), where a higher KFM is needed in order to overcome the external brace torque.

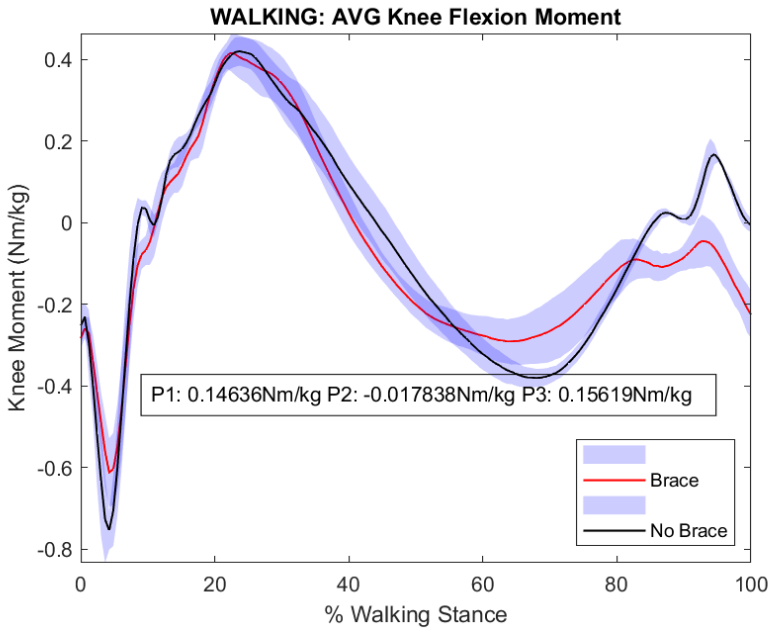

Figure 3.14: Knee Flexion Moment (KFM) during the walking trials.(- Flexion, + Extension) The change caused by the knee brace at the three peak KCF is indicated in the plot.

The Ankle Dorsiflexion Moment (ADM) remained closely similar between the Brace and No Brace conditions. However, the peak ADM is higher for the Brace condition (Fig. 3.15), this may be a consequence of muscle activity adaptation between conditions.

Due to the small magnitude of KFA during early to mid stance, the brace did not apply an external moment beyond the preload (6 Nm) until late stance (80 % $+$), as seen in Fig. 3.16.

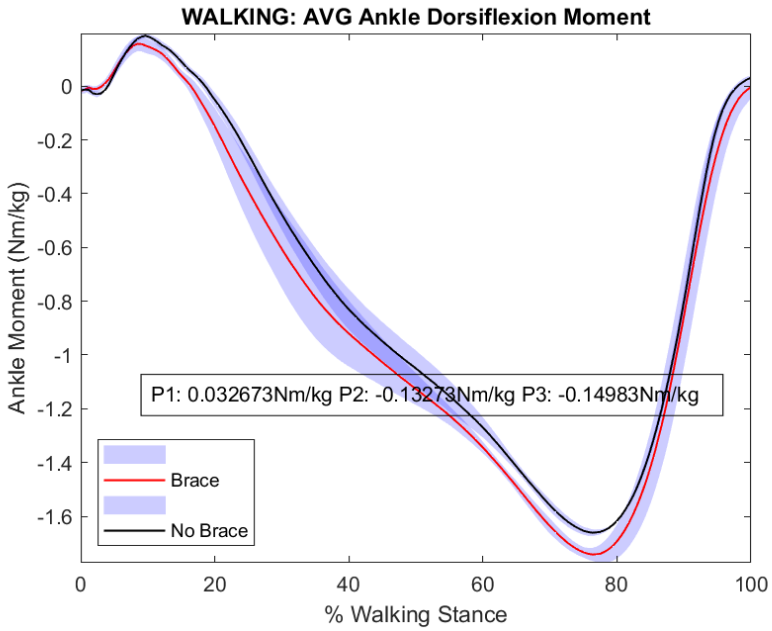

Figure 3.15: Ankle Dorsiflexion Moment (ADM) during the walking trials. The change caused by the knee brace at the three peak KCF is indicated in the plot.

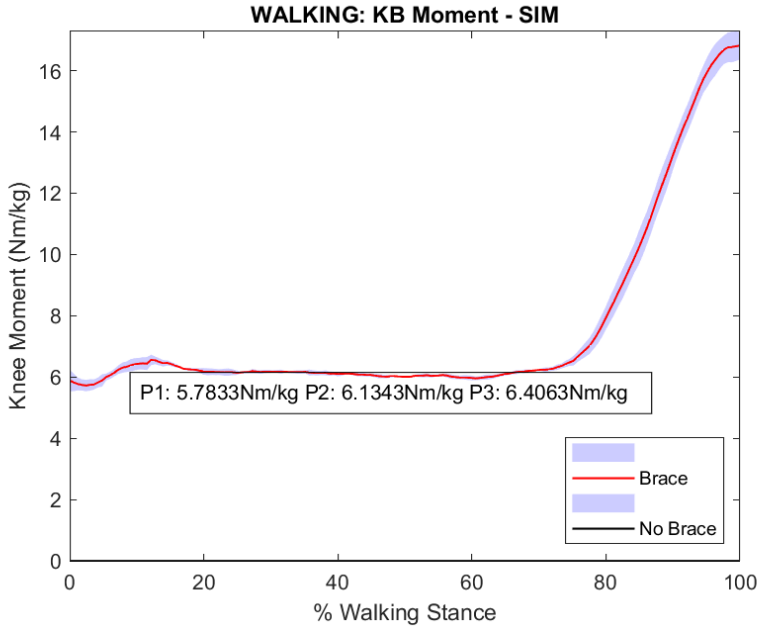

Figure 3.16: Average Knee Brace external moment during the stance phase of gait for the walking trials.

Knee Loading and Muscle Forces

The KCF plots are shown in Fig. 3.17. Table 3.2 indicates the muscle activity changes at the three peak KCF.

After heel strike the knee needs to flex, before contralateral toe off. Since the right knee is more flexed in the braced trials, less flexion moment is required during the first KFM peak (Fig. 3.14), this causes a reduced force demand from MG, LG, ST, and BF (Fig. 3.18), causing a reduction in the first peak KCF (Fig. 3.17).

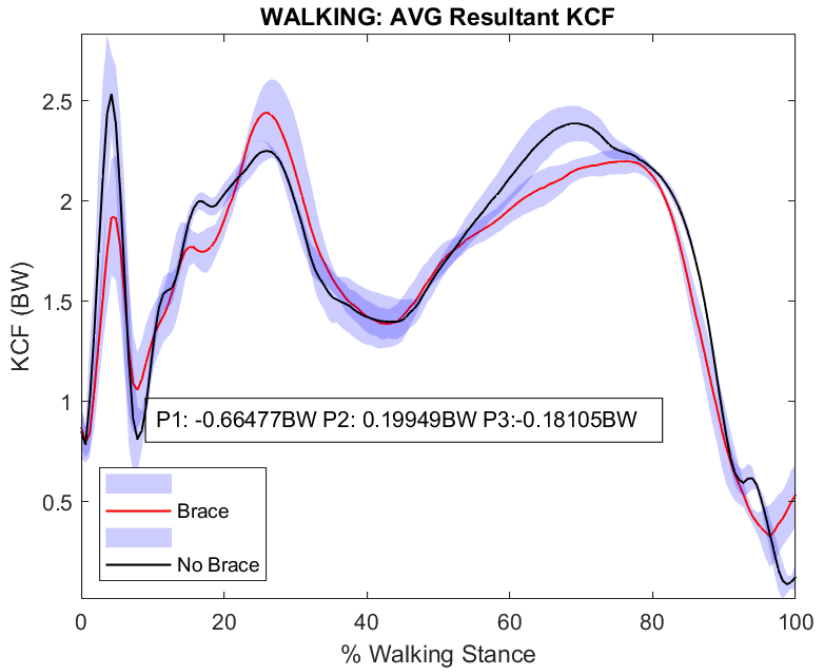

Figure 3.17: Average KCF during the stance phase of gait for the walking trials expressed in BW. The KCF change at the three peak locations is shown as P1, P2 and P3.

Table 3.2: Muscle activity changes at peak KCF.

Muscle	**P1 (↓)**	**P2 (↑)**	**P3 (↓)**	KCF Contributor?
BF	$\downarrow -1.19\ N/kg$	$\uparrow 0.53\ N/kg$	0	YES
LG	$\downarrow -0.22\ N/kg$	$\uparrow 0.02\ N/kg$	$\downarrow -0.38\ N/kg$	YES
MG	$\downarrow -1.22\ N/kg$	0	$\downarrow -2.30\ N/kg$	YES
RF	0	0	$\uparrow 1.01\ N/kg$	YES
ST	$\downarrow -0.36\ N/kg$	$\uparrow 0.13\ N/kg$	0	YES
SOL	0	$\uparrow$	$\uparrow$	NO
TA	$\downarrow$	$\downarrow$	0	NO
VL	0	$\uparrow 0.39\ N/kg$	0	YES
VM	0	$\uparrow 0.15\ N/kg$	0	YES

Immediately after foot down the quadriceps engage, as observed in the corresponding OSim Force plots (Fig. 3.18i, 3.18h, 3.18d) and the knee moment starts rising towards extension moment. At about 25% stance, close to where the second KCF peak is located (Fig. 3.17), the quadriceps are fully engaged, causing knee extension. The brace external moment is small here, due to the small knee flexion angle (Fig. 3.10), therefore no assistance to KFM is provided; the KFM (Fig. 3.14) remains unaltered and KCF (Fig. 3.17) shows a slight increase for the brace trials, however, statistical significance should be examined.

The third KCF peak occurs at about 75% of stance, when the knee extension peak is reached. The effect of the brace is minimal here and no reduction in quads activity due to it is observed. However, the knee is more flexed in the brace trials at this peak location and therefore less flexion moment is required in order to achieve the knee angle needed before toe off. Because of this higher knee flexion angle, the Soleus compensates (replacing MG and LG) for plantarflexion and an increased force production is observed for SOL (Fig. 3.18f), while reduced for MG

and LG (Fig. 3.18c and 3.18b). This change in muscle activity can also be confirmed by the corresponding EMG envelope plots in Fig. 3.19f, 3.19c and 3.19b. Unlike MG and LG, SOL does not actuate on the knee joint, therefore this shift in muscle activity causes a reduction in KFM (Fig. 3.14) and KCF (Fig. 3.17).

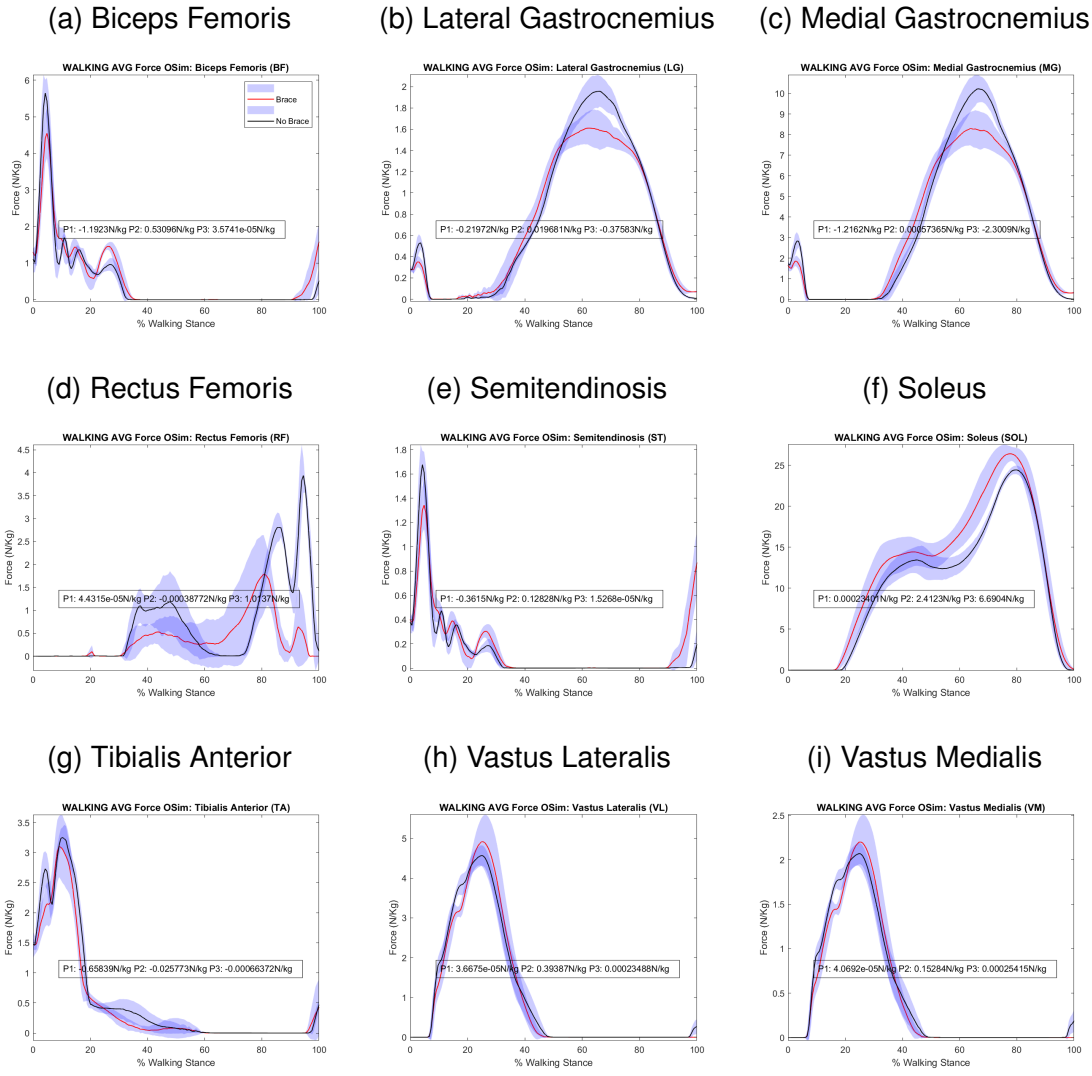

Figure 3.18: Static Optimization results for walking trials. Right leg muscle forces plots normalized to body weight in N/Kg.

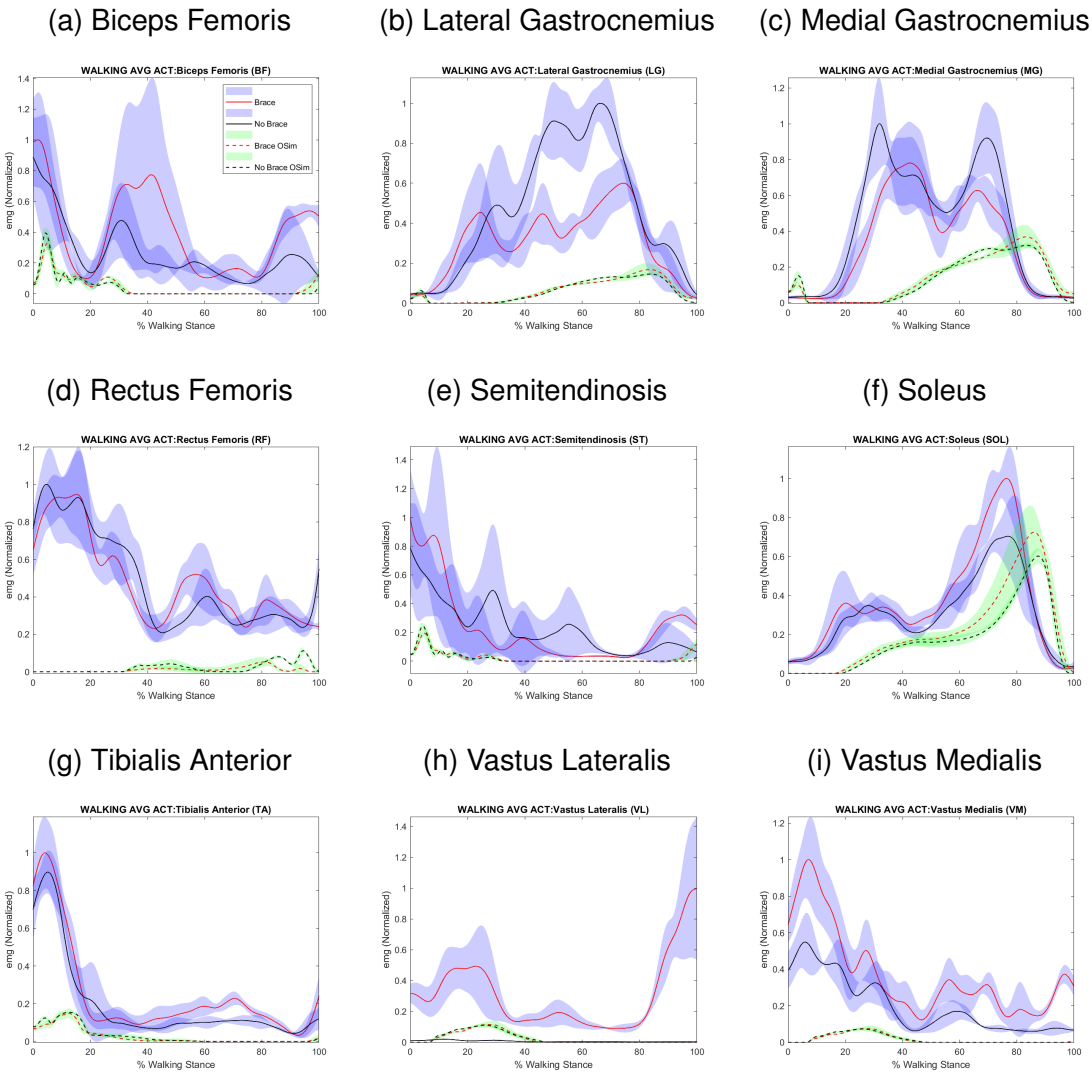

Figure 3.19: EMG envelope curves for right leg muscles during walking trials.

The highest external torque applied by the brace occurs during late stance, approaching toe off (Fig 3.16); at this point KFA is not significantly different between conditions and we can observe an increased KFM for similar KFA in the braced condition relative to the no braced. Consequently, an increased activity of the BF, ST, MG and LG is observed in the OSim muscle forces simulation results, causing an increase in the KCF; however, there is no peak muscle activity in this zone and

therefore no peak KCF. Although the brace did not apply significant external torque until late stance, the capacity of the brace to alter muscle activity is evidenced in these muscle activity changes between conditions.

3.3.2 Standing Up

Kinematics

Results from IK are shown in Fig. 3.20, 3.21, and 3.22. The ankle starts in a more dorsiflexed position for the no brace trials. Dorsiflexion occurs at the beginning of the cycle and plantarflexion starts after roughly 40%, as seen in Fig. 3.20.

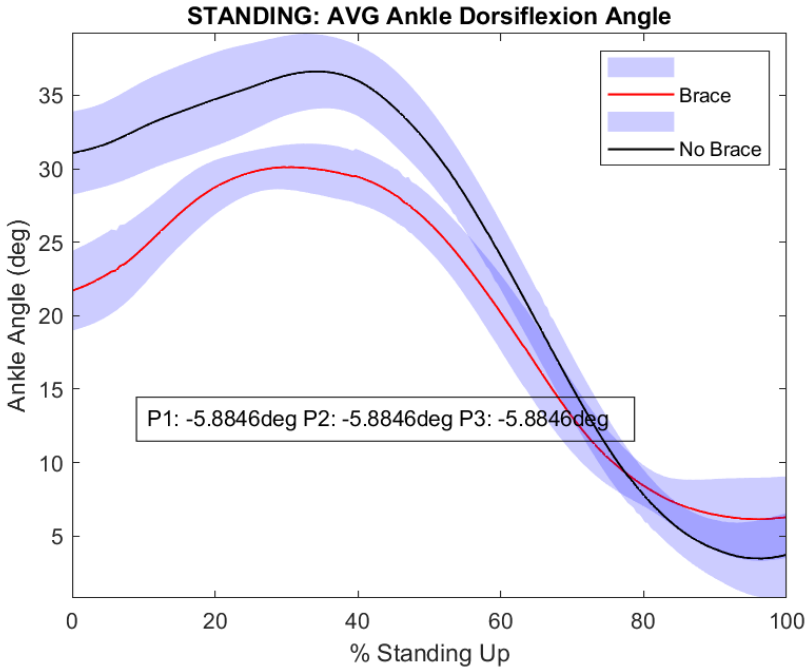

Figure 3.20: Average Ankle Dorsiflexion Angle during the standing up trials. The ADA change effect caused by the knee brace at the peak KCF is indicated in the plot.

The knee starts extending right at the end of the initial peak ankle dorsiflexion angle, at about 35% of the phase (Fig. 3.21). The knee brace limits the range of motion and this, combined with the persistent extension moment caused by the elastic bands, causes a smaller flexion angle at the beginning of the cycle in the brace condition as compared to the no brace. Similarly, at the end of the cycle, the knee is less extended in the brace trials as compared to the no brace.

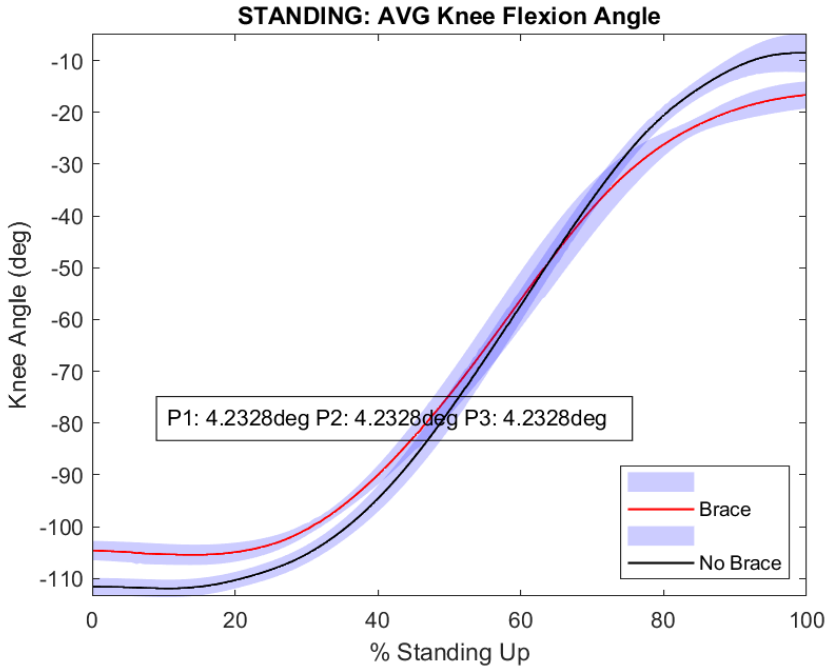

Figure 3.21: Average Knee Flexion Angle (KFA) during the standing up trials (+ extension, - flexion). The KFA change effect caused by the knee brace at the peak KCF is indicated in the plot.

The hip remains more flexed for the Brace trials during the entire standing up phase, as seen in Fig. 3.22. The final posture had a more flexed hip, knee and ankle for the Brace trials, showing a crouched posture, similar to what was observed for the walking trials.

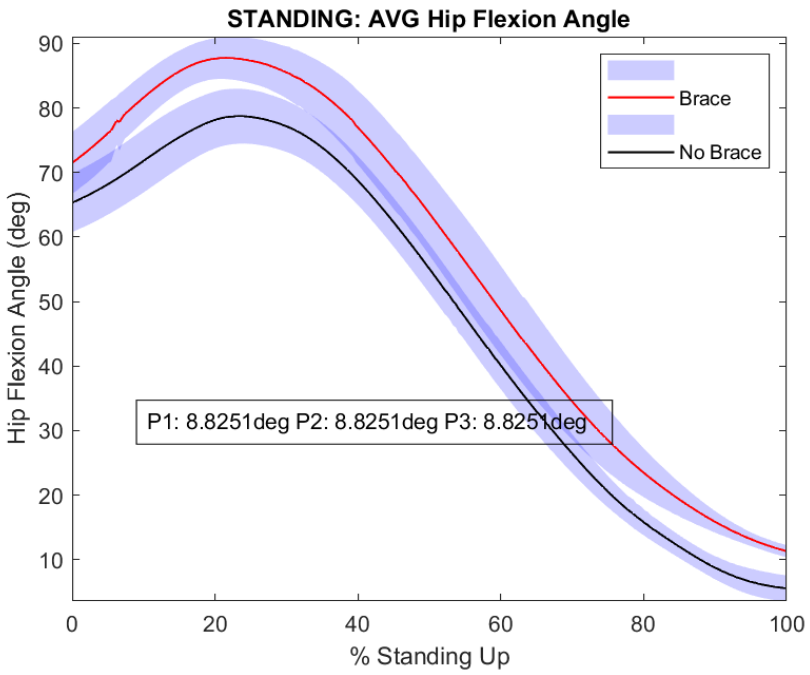

Figure 3.22: Average Hip Flexion Angle (HFA) during the standing up trials. The HFA change effect caused by the knee brace at the peak KCF is indicated in the plot.

Joint Moments and Muscle Forces

The smaller ankle dorsiflexion angle (ADA) at the beginning of the cycle caused an increased ankle dorsiflexion moment (ADM) for the brace trials (Fig. 3.23); as the subject leans forward, matching the knee angle between conditions (Fig. 3.21) before lifting the glutes from the seat. This increase is also evidenced in the OSim force and envelope EMG plots for the Tibialis Anterior (TA), acting in ankle dorsiflexion (Fig. 3.27g and Fig. 3.28g). The same can be observed for the no brace condition, although in smaller magnitude.

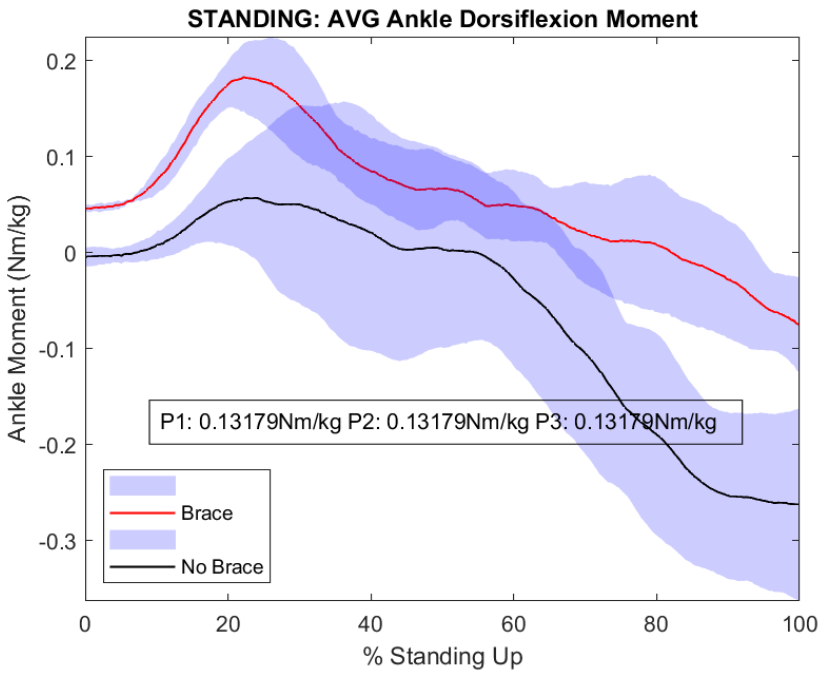

Figure 3.23: Ankle Dorsiflexion Moment (ADM) during the standing up trials. The change caused by the knee brace at the peak KCF is indicated in the plot.

At around 60% of the phase, an inflection point is observed for the ankle dorsiflexion angle in both conditions (Fig. 3.20); however, since the dorsiflexion angle was greater for the no brace condition, the corresponding rotational speed is higher, and a higher plantarflexion moment is required to bring the ankle joint to a stop as observed in Fig. 3.23. This is also reflected in the OSim force and EMG envelope plots for the SOL, MG and LG (Fig. 3.28 and Fig. 3.27).

The higher HFA for the Brace trials also causes higher hip flexion moment (HFM) throughout the standing up phase as seen in Fig. 3.24, finishing with the same value in the final posture.

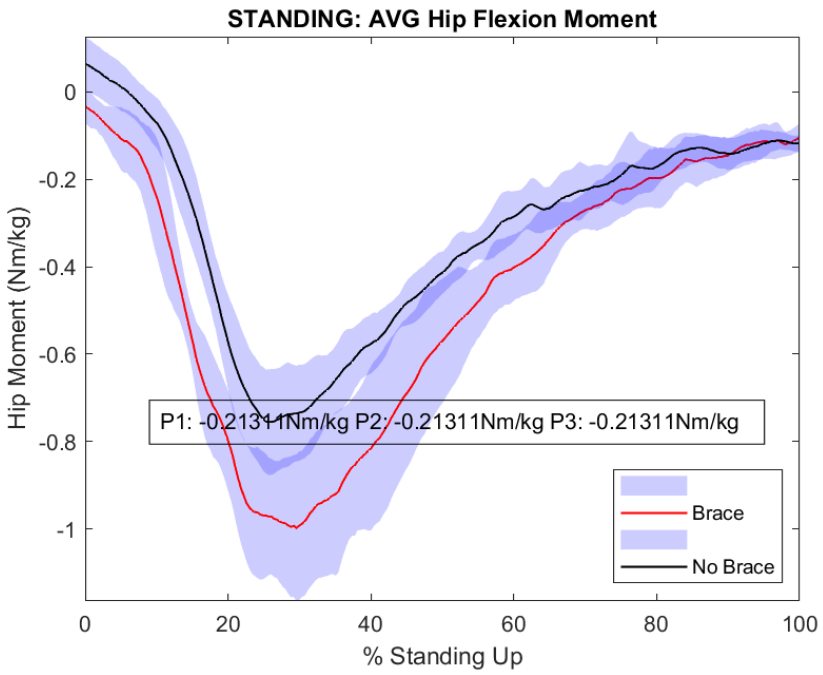

Figure 3.24: Hip Flexion Moment (HFM) during the standing up trials. The change caused by the knee brace at the peak KCF is indicated in the plot.

The peak knee extension moment (KEM) occurs at about 35%, right after knee extension starts happening (Fig. 3.25); the KEM starts dropping as the knee extends, because no further knee joint acceleration is required to take the knee to the final flexion angle.

High KFA is experienced during the Standing Up task and the knee brace provided the highest torque output possible for the configuration used (Fig. 3.26). During the peak KFM, the external knee brace moment is nearly at its maximum value.

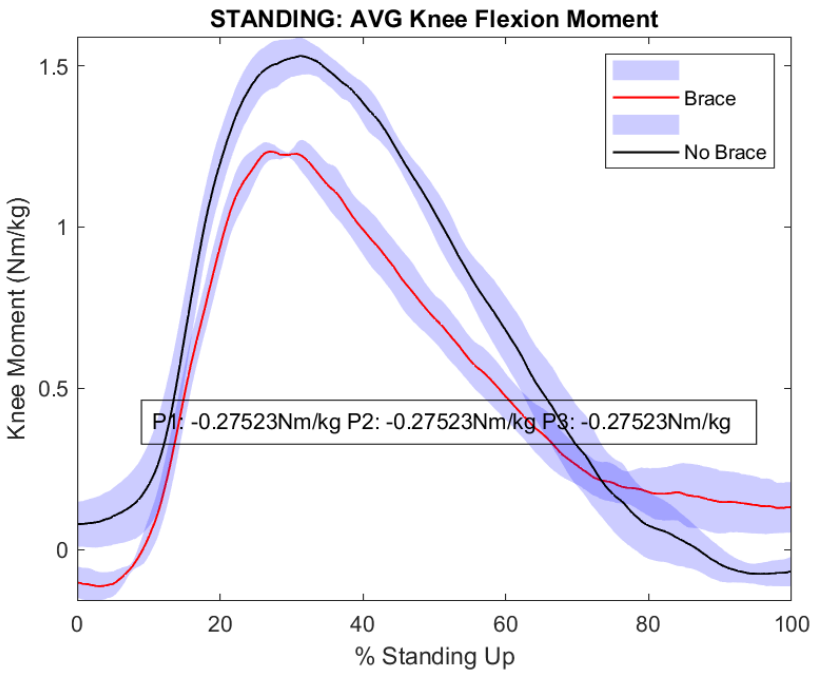

Figure 3.25: Knee Flexion Moment (KFM) during the standing up trials. The change caused by the knee brace at the peak KCF is indicated in the plot.

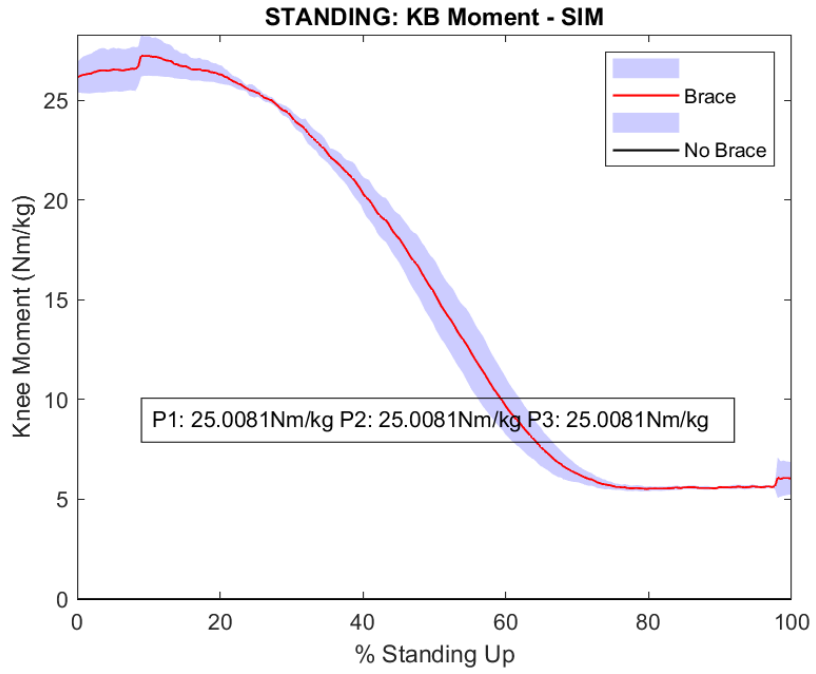

Figure 3.26: Average Knee Brace external moment for the standing up task, as simulated.

EMG envelope and OpenSim activation plots for the standing up trials are shown in Fig. 3.27. Although saturation is reached for TA, this is not a concern for the present work, because the total moment at the joint remains unaltered and the behavior of TA as a muscle-tendon unit does not affect the KCF. Muscle forces plots estimated with OpenSim are shown in Fig. 3.28.

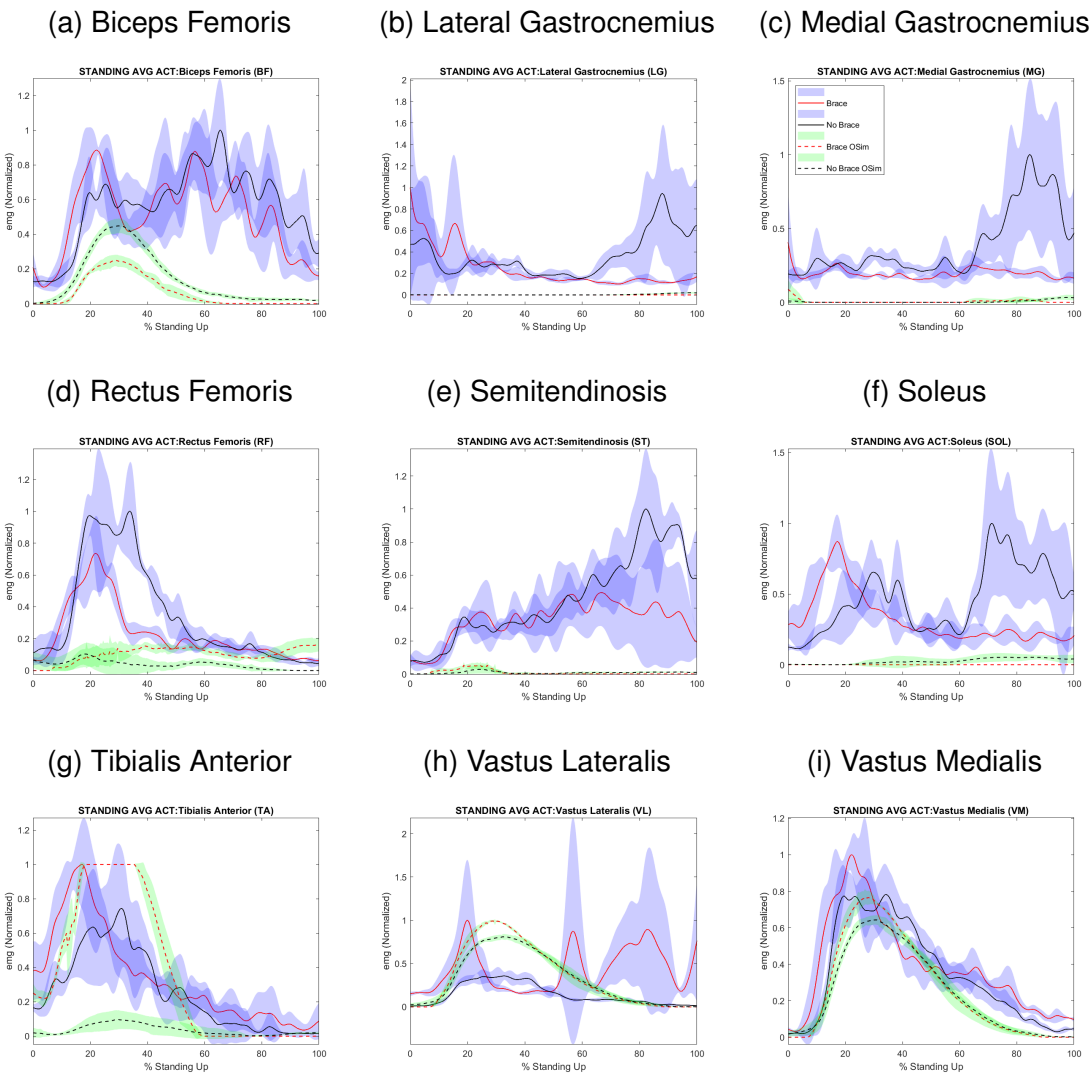

Figure 3.27: EMG envelope and OSim activation for right leg muscles during the standing up trials.

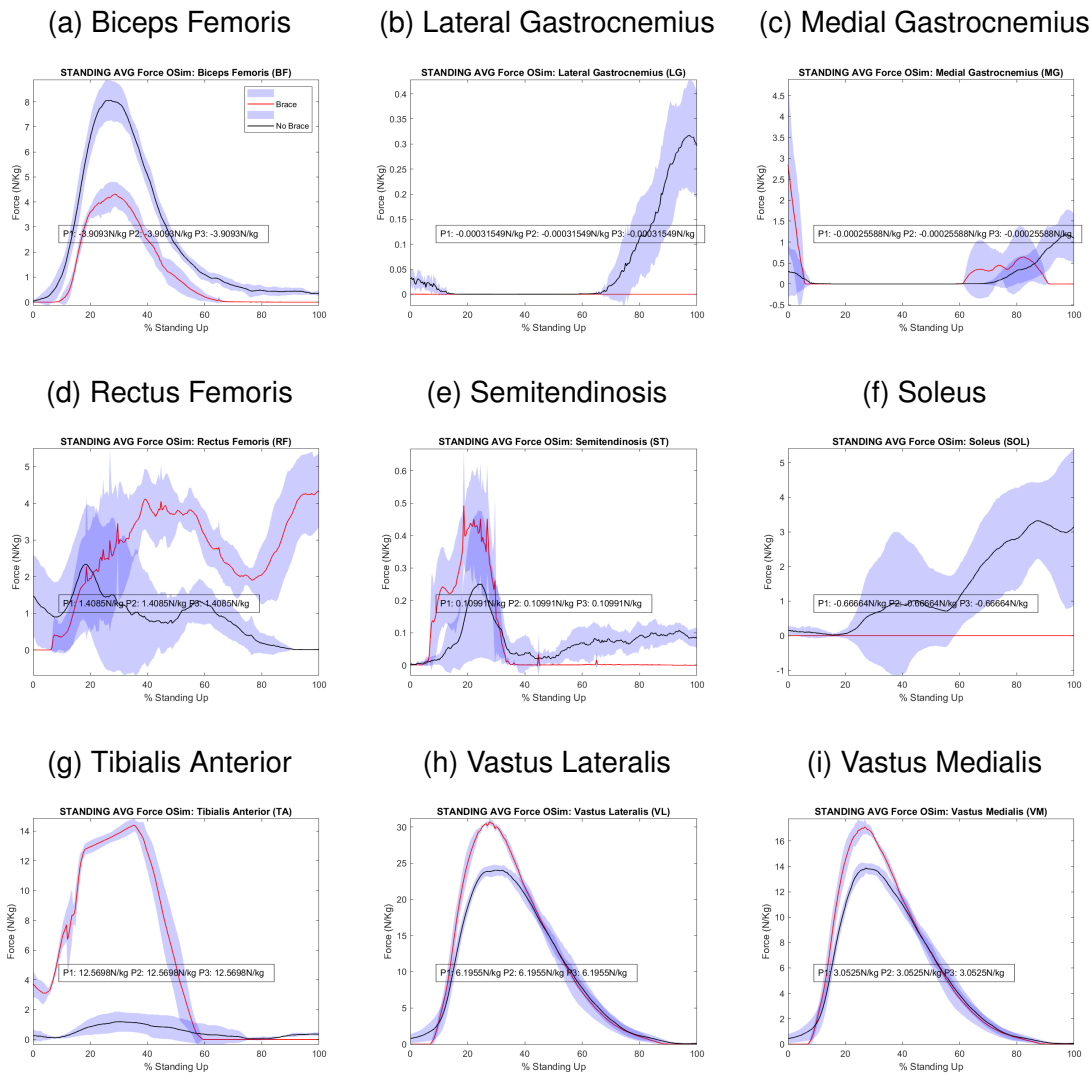

Figure 3.28: Static Optimization results for standing up trials. Right leg muscle forces plots normalized to body weight in N/Kg.

Knee Contact Forces (KCF) and CCI

The peak KEM is lower for the brace trials (0.28 Nm/kg reduction); this is in most part caused by the external extension moment applied by the brace, where it is assumed that the external torque is transmitted to the joint at 100% efficiency. However, this does not cause a reduction in peak KCF (Fig. 3.29), as the muscle forces

pattern changes. Table 3.3 shows the muscle force variations at peak KCF; increased force at peak KCF for VL, VM and RF are in agreement with increased peak KCF.

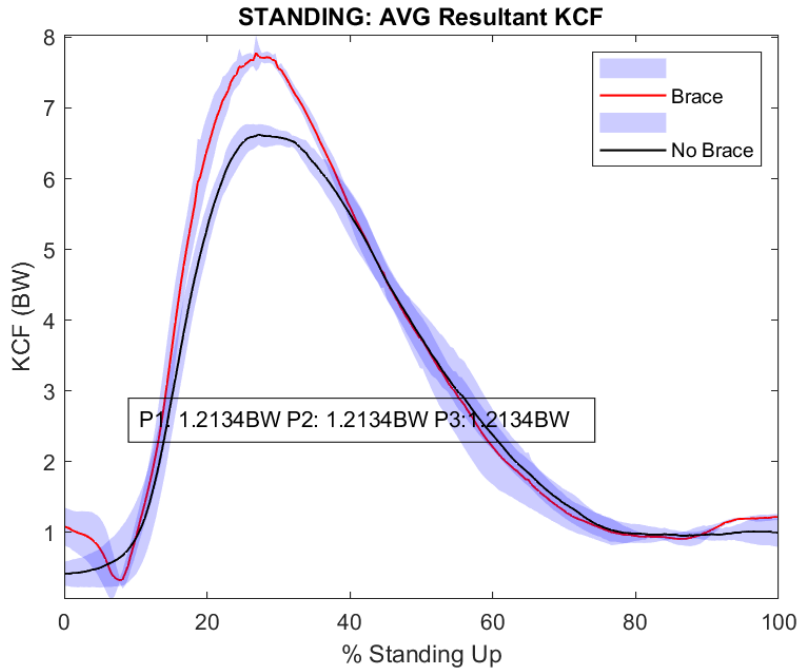

Figure 3.29: Average tibiofemoral Knee Contact Forces (KCF) during the standing up trials.

Table 3.3: Muscle activity changes at peak KCF.

Muscle	**P (↑)**	KCF Contributor?
BF	$\downarrow -3.91\ N/kg$	YES
LG	0	YES
MG	0	YES
RF	$\uparrow 1.41\ N/kg$	YES
ST	0	YES
SOL	$\downarrow$	NO
TA	$\uparrow$	NO
VL	$\uparrow 6.20\ N/kg$	YES
VM	$\uparrow 3.05\ N/kg$	YES

Peak KCF increases while wearing the brace by about 1.21 BW. This increase

reflects the total KCF magnitude due to limitations in musculoskeletal modeling, the EMG co-contraction pattern, as defined by Rudolph et al. (2000), can be used as an indicator of the distribution of this force between the medial and lateral condyles. The co-contraction intensity and duration are reduced for the medial side of the knee and slightly increased for the lateral side while wearing the knee brace (Fig. 3.30); it must be noted, however, that a possible interference with the VL EMG transducer was reported after data collection.

(a) Medial: VM - MG

(b) Medial: VM - ST

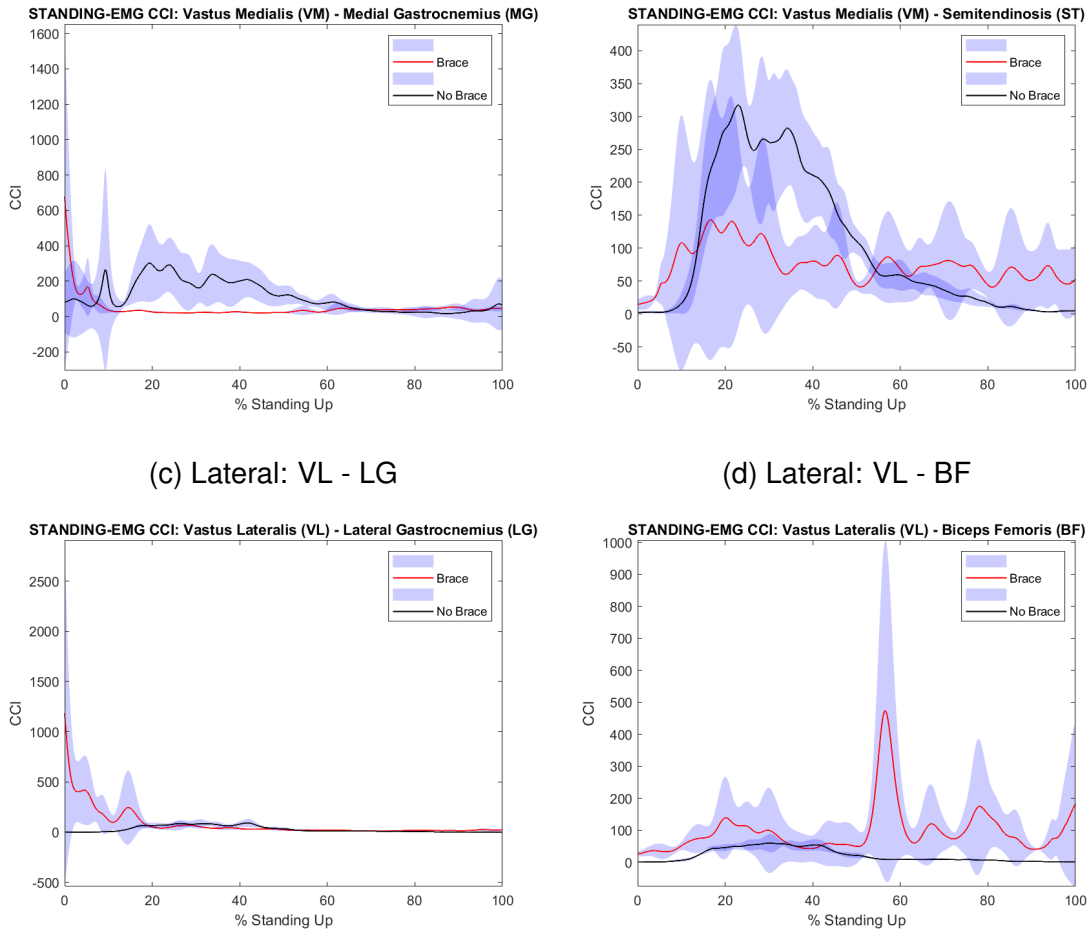

(c) Lateral: VL - LG

(d) Lateral: VL - BF

Figure 3.30: CCI curves for the standing up trials.

3.3.3 Stepping Up

Kinematics

Results from IK for the Stepping Up trials are shown in Fig. 3.31, 3.32 and 3.33; these results are discussed in section 3.4.3.

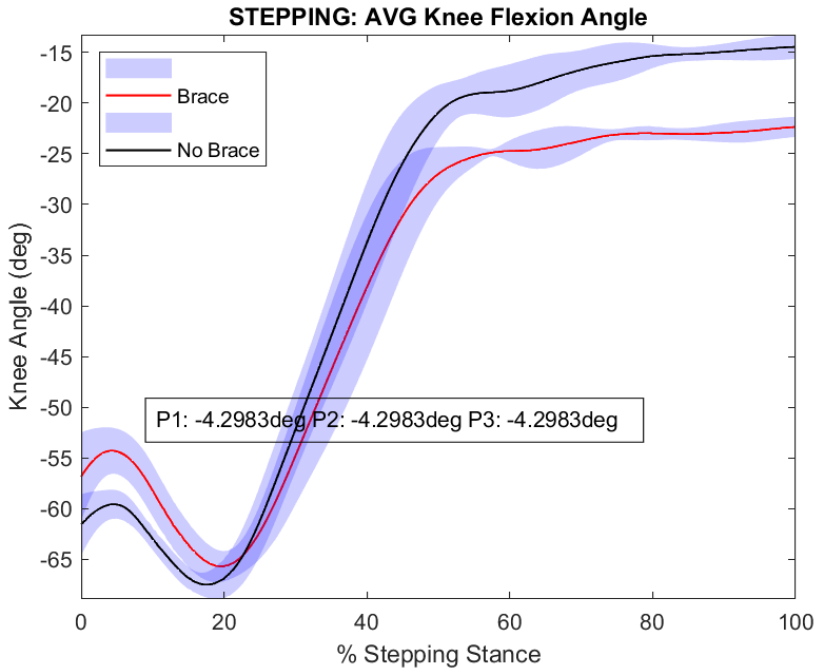

Figure 3.31: Average Knee Flexion Angle (KFA) during the stepping up trials (+ extension, - flexion). The KFA change effect caused by the knee brace at the peak KCF is indicated in the plot.

The KFA range is limited by the brace. At the beginning of the phase, the knee is more flexed in the no brace trials (Fig. 3.31), however, when the KFM starts rising (around 20% in Fig. 3.36), the two KFA are very similar. This does not imply the same posture between conditions, as the ankle is less dorsiflexed and the hip is more flexed as this point for the brace trials (Fig. 3.33 and 3.32).

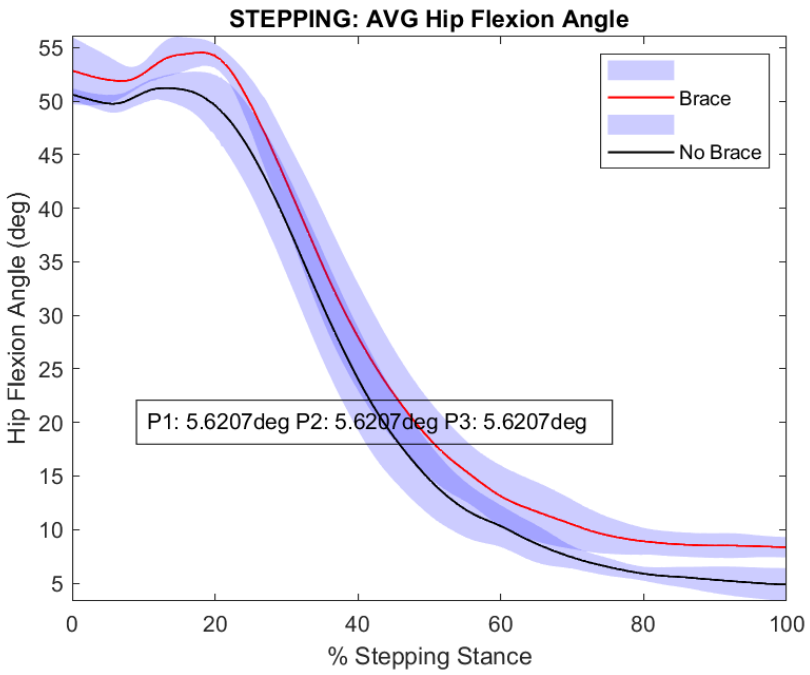

Figure 3.32: Average Hip Flexion Angle (HFA) during the stepping up trials. The HFA change effect caused by the knee brace at the peak KCF is indicated in the plot.

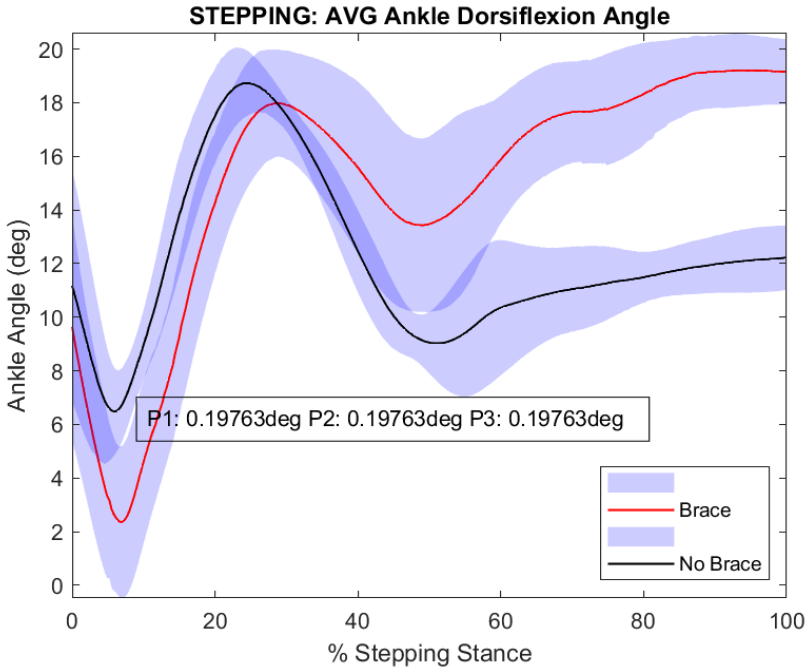

Figure 3.33: Average Ankle Dorsiflexion Angle during the stepping up trials. The ADA change effect caused by the knee brace at the peak KCF is indicated in the plot.

Other kinematic changes observed in the brace trials are a more dorsiflexed ankle towards the end of the range and a more flexed hip during the entire range (Fig. 3.33 and 3.32).

Joint Moments

HFM was not affected below 60% of the phase (Fig. 3.34). Towards the end of the phase, a smaller hip extension moment is observed for the Brace trials, this could be a consequence of the higher HFA observed at the final pose for the Brace trials.

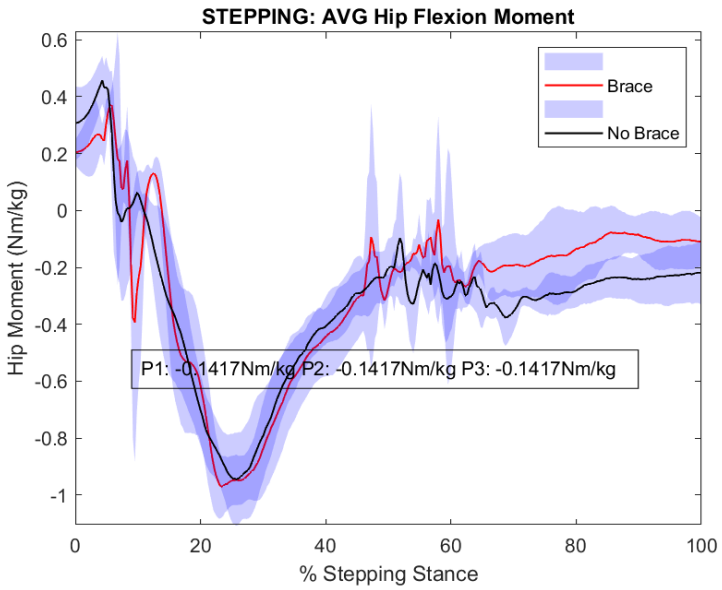

Figure 3.34: Hip Flexion Moment (HFM) during the stepping up trials. The change caused by the knee brace at the peak KCF is indicated in the plot.

Although high variation is observed, a higher average ankle plantarflexion moment is observed at the end of the phase for the No Brace trials in Fig. 3.35.

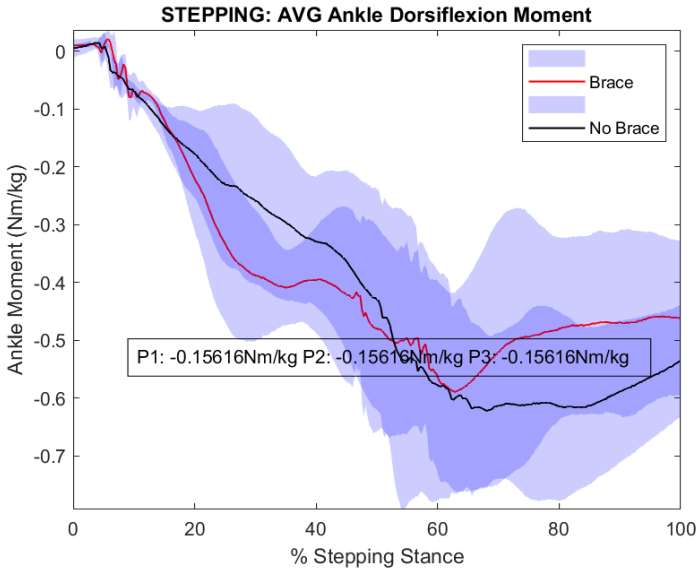

Figure 3.35: Ankle Dorsiflexion Moment (ADM) during the stepping up trials. The change caused by the knee brace at the peak KCF is indicated in the plot.

The KFM is smaller for the brace trials until the KFA starts settling, at about 50% of the phase (Fig. 3.36 and 3.31).

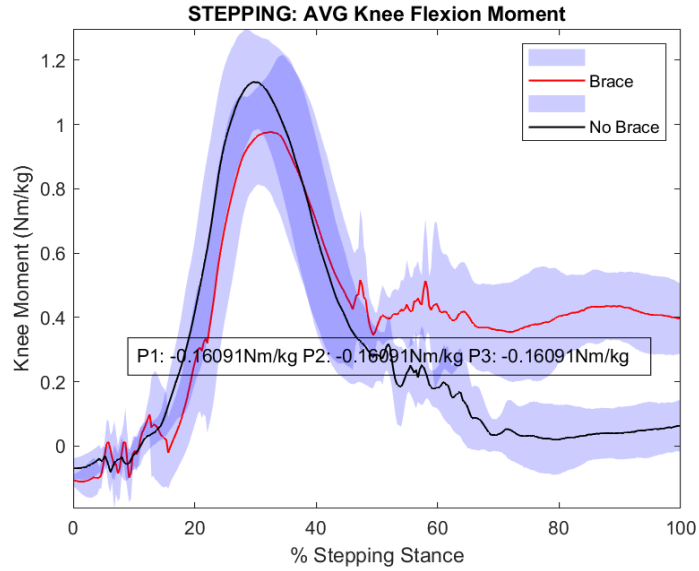

Figure 3.36: Knee Flexion Moment (KFM) during the stepping up trials. The change caused by the knee brace at the peak KCF is indicated in the plot.

From 50% up to the end of the phase, the knee remains more flexed for the brace trials due to the range of motion reduction while wearing the device; this higher flexion demands a higher knee extension moment to support the final pose, since at this smaller knee angle the brace does not provide significant external assistance (Fig. 3.37), this moment needs to be provided by the knee extensors.

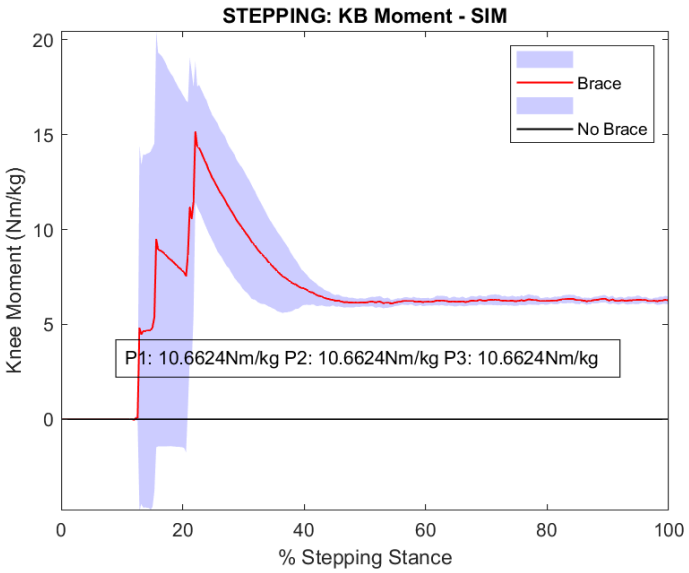

Figure 3.37: External knee brace moment as simulated for the Stepping Up trials.

The increased knee extension moment is reflected in a higher OSim force of RF, VM and VL during this part of the phase for the brace condition (Fig 3.39). Similarly, EMG data shows higher activity for RF, VL and VM after 50% of the phase for the brace condition (Fig. 3.38); a possible brace interference was observed during data collection for the VL EMG transducer, however, EMG data for VM and RF was not interfered and a reduction is observed in the indicated range.

The BF and ST are slightly more active at the beginning of the phase in the brace trials; this could be caused by the external torque applied by the brace even

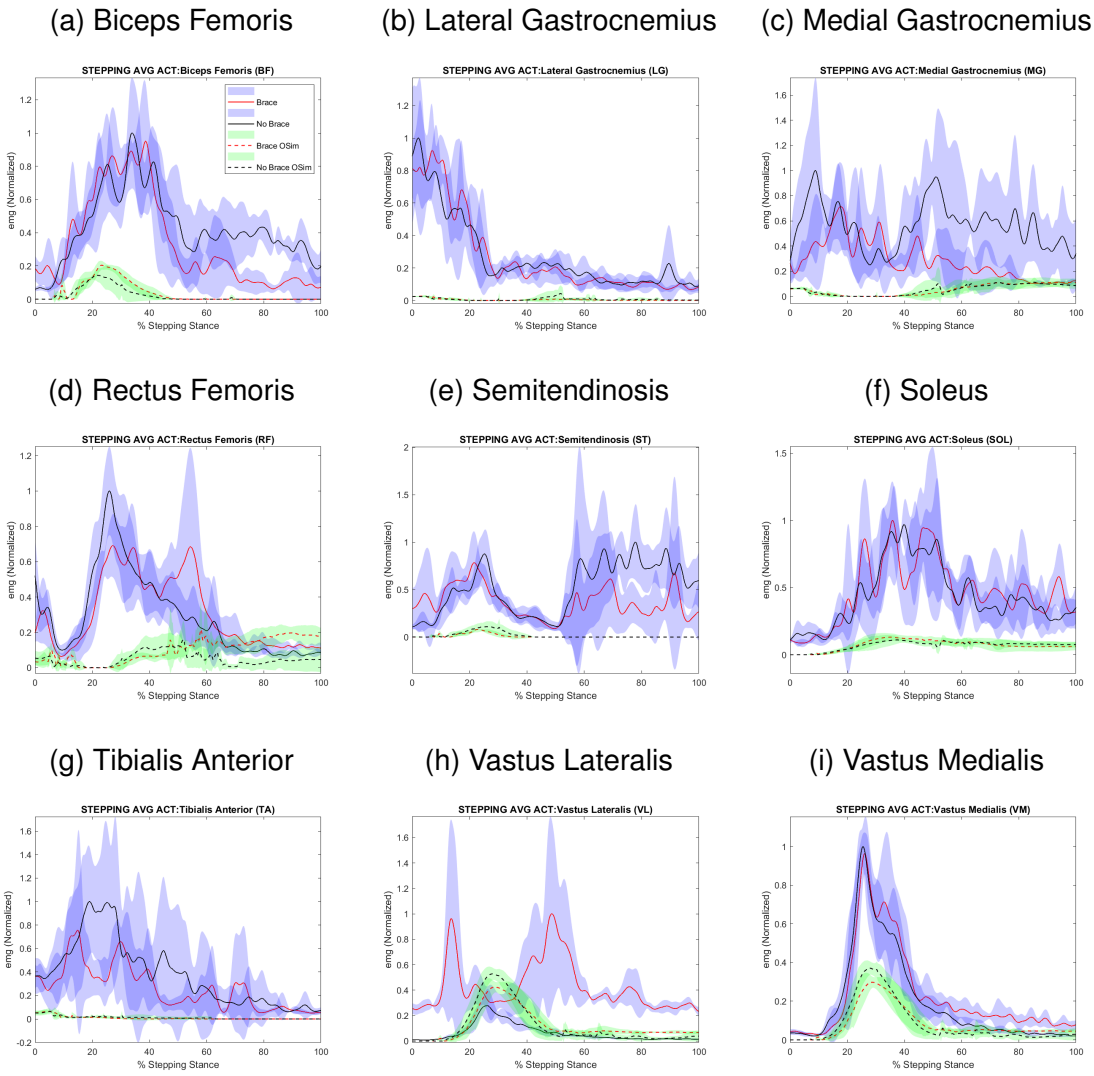

Figure 3.38: EMG envelope and OSim activation for right leg muscles during the stepping up trials.

before the KEM starts rising. This could also explain a higher medial and lateral co-contraction observed in the brace trials before the knee starts extending (before 20%), see Fig. 3.40.

Static Optimization

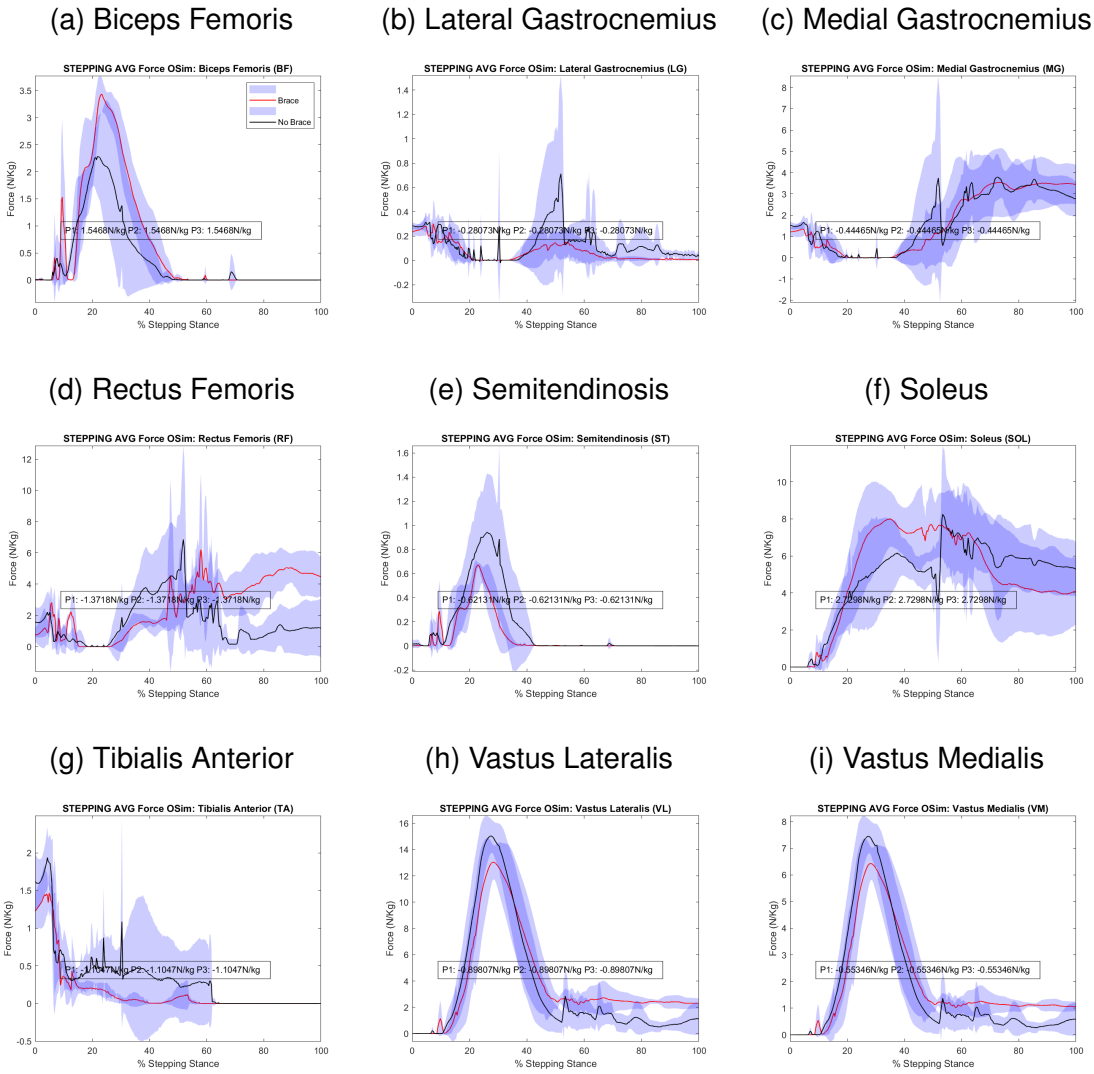

Figure 3.39: Static Optimization results for stepping up trials. Right leg muscle forces plots normalized to body weight in N/Kg.

A slight reduction in peak KCF is observed at around 30% (Fig. 3.41), however, significance may be questionable due to the small sample size and the relatively high variation. This is in agreement with CCI results (Fig. 3.40); VM – MG shows a reduction for the brace trials at peak KCF, VM – ST shows no variation, lateral

muscles CCI should be reevaluated due to the interference reported for the VL EMG transducer.

The CCI plots for the Stepping Up trials are shown in Fig. 3.40.

(a) Medial: VM - MG

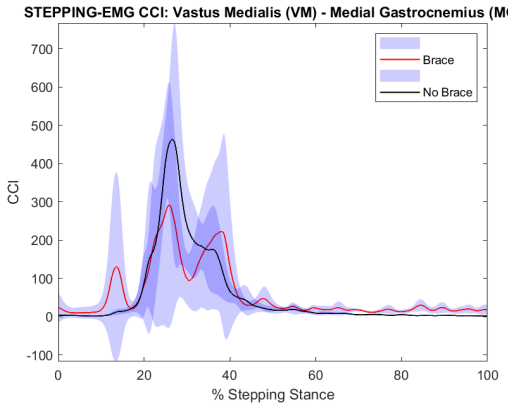

(b) Medial: VM - ST

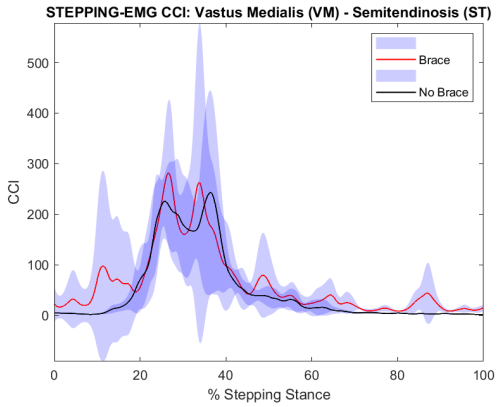

(c) Lateral: VL - LG

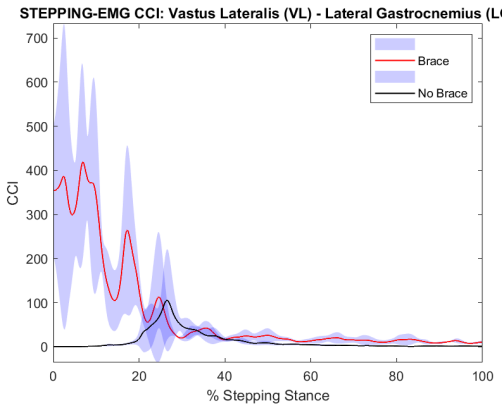

(d) Lateral: VL - BF

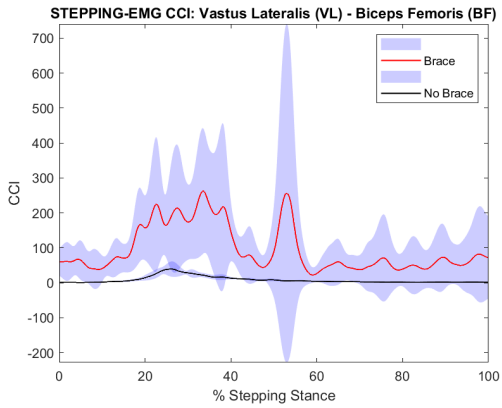

Figure 3.40: CCI during the stepping up trials.

As expressed in Table-3.4, taken from Fig. 3.39 at peak KCF, a reduction in OSim muscle force is observed for RF, ST, VL and VM. This goes in agreement with CCI reduction; the increased BF OSim force value would potentially point towards an increased CCI for the lateral muscles.

The KCF plots are shown in Fig. 3.41. Table 3.4 indicates the muscle activity changes at the three peak KCF.

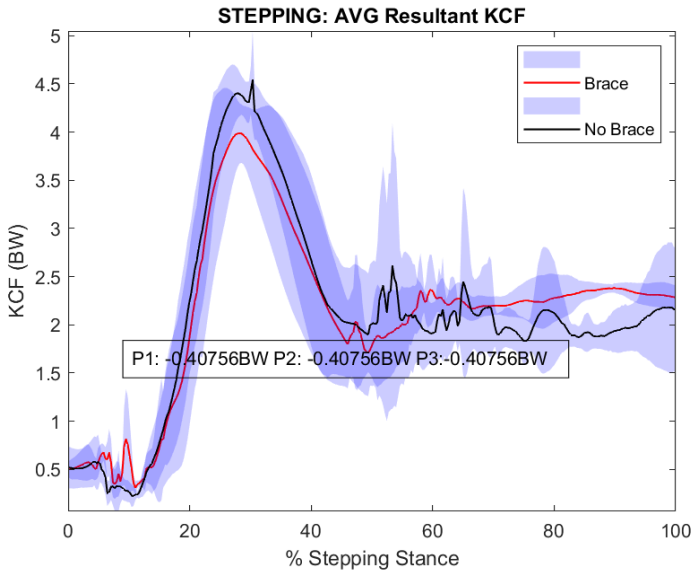

Figure 3.41: Tibiofemoral Knee Contact Forces (KCF) during the stepping up trials.

Table 3.4: Muscle activity changes at peak KCF for the Stepping Up trials.

Muscle	**P (↓)**	KCF Contributor?
BF	$\uparrow 1.55\ N/kg$	YES
LG	0	YES
MG	0	YES
RF	$\downarrow -1.37\ N/kg$	YES
ST	$\downarrow -0.62\ N/kg$	YES
SOL	$\uparrow$	NO
TA	$\downarrow$	NO
VL	$\downarrow -0.90\ N/kg$	YES
VM	$\downarrow -0.55\ N/kg$	YES

Although a higher KFM and higher knee extensors activity is observed towards the end of the phase (Fig. 3.38 and 3.39), the KCF for this part of the phase remains similar between conditions (Fig. 3.41); nevertheless, KCF is slightly higher for the brace condition at the end of the phase. The changes in KFM and mus-

cle activity towards the end of the phase might be directly related to the changes and kinematics; designing to allow preservation of the natural kinematics would potentially mitigate this problem.

3.4 Discussion

3.4.1 Walking Trials

The reduction in KCF found for this task seems to be due to alterations in kinematics and not due to external torque assistance. Further modifications are needed in order to apply assistive torque at small flexion angles (where the peak KCFs occur). The alterations in kinematics caused a reduced KFM and this was achieved by a reduced activity in hamstrings and calf (Table 3.2).

It was also found that the range of motion is limited with the brace. Brace and no brace KFA curves meet at midswing but both flexion and extension peaks are smaller for the Brace condition.

3.4.2 Standing Up Trials

The external moment timing seems to be appropriate as the KEM was effectively reduced at its peak (Fig. 3.25). However, it is necessary to model medial and lateral knee condyles independently in order to further understand the KCF distribution variations and CCI changes. Co-contraction duration has been associated with medial knee OA progression (Hodges et al., 2016) and co-contraction intensity

has been associated with peak KCF (Trepczynski et al., 2018). Improvement in musculoskeletal modeling would allow to observe medial and lateral condyles KCF independently and would help explain the observed KCF increase. Tibial rotations should also be considered in future studies to observe if it plays any role in KCF distribution, muscle activation patterns and CCI for this task.

3.4.3 Stepping Up Trials

The knee brace effectively reduced the KFM and a small reduction effect on KCF and CCI was observed, however, the brace torque settles after 40% of the phase, while the KFA starts settling after 50%. Adjusting the effective range of the brace could provide assistance beyond 40% and help with the last portion of the phase before the KFA settles. Engagement control would provide the manipulation capabilities required to achieve this.

3.5 Conclusions

The assistive device showed to have different behavior requirements for each task. For Walking, high moment is required for small KFA, whereas small moment is required for high KFA, especially while flexing the knee. For the Stepping Up and Standing Up task, high external moment is required for high KFA and low external moment is required for low KFA. During resting periods and during knee flexion, no extension moment should be applied by the device; assistive external moment applied during these periods can cause increased muscle contraction, increasing

knee moment and KCF. Capability to control moment engagement timing is recommended to solve this problem.

The device limited the range of motion of the knee joint and overall affected joint kinematics during the tasks. While an external assistive device can always alter kinematics, care must be taken in order to avoid kinematic changes that increase knee loading or considerably alter other joints kinetics.

Muscle activation patterns were also affected by the device, as the Standing Up task showed a redistribution of medial to lateral knee muscle CCI despite the absence of frontal plane assistance moment. Musculoskeletal modeling should be improved to allow for separate analysis of medial and lateral knee joint condyles loading, in order to examine how these muscle activation pattern changes affect knee joint load distribution.

Chapter 4

A Clutch-Based Energy Storage and Release Assistive Knee Brace

4.1 Introduction

Clutching mechanisms have been recently used as an approach for energy storage in lower limb orthoses, particularly to release the stored energy in synergy with the concentric contraction of the calf muscles during gait (Wang et al., 2020, 2019; Yandell et al., 2019), reporting up to 17% reduction in Soleus EMG activity, and over 11% reduction in Gastrocnemius force. The functioning principle of these energy storage mechanisms relies on the detection of the phases of the gait cycle, in order to release the energy during plantarflexion and absorb the energy during dorsiflexion in the stance phase. A similar approach, applied to the knee joint, has been implemented to conceptualize, design, and prototype our clutch-based

energy storage and release assistive knee brace KB-3.0.

This chapter details the design process, device specifications, and system integration of our assistive device. A comparison of capacity, power consumption, and weight is done using the existing literature as a point of reference.

4.2 Clutching Mechanism Principle

When an elastic element is added to a joint with the purpose of storing energy as a function of the coordinate of that joint, the energy storage and release will be dictated by the position of that joint. As a consequence, the maximum energy storage and delivery lie at the highest coordinate value. If we consider a simplified knee joint and add a torsional spring, the maximum energy storage will be at the maximum knee flexion angle (KFA), and the energy will be delivered as the joint moves back to smaller KFA values (Fig. 4.1). However, in our preliminary study (see Chapter 3), we determined that this was not the desired behavior for providing assistance during walking, sit and stand, and stair ascent, because peak knee contact forces (KCF) did not occur at the same time as peak KFA.

In order to store the elastic energy and deliver it at the desired state, we can add a clutching element to act as an ON/OFF switch for the spring, allowing or preventing interaction with the joint to which it is assigned. Under this principle, the torsional spring can store energy during knee flexion, disengage from the system to keep the energy stored, and reengage at a later angle, delivering the maximum energy at angles other than the maximum KFA (Fig. 4.2).

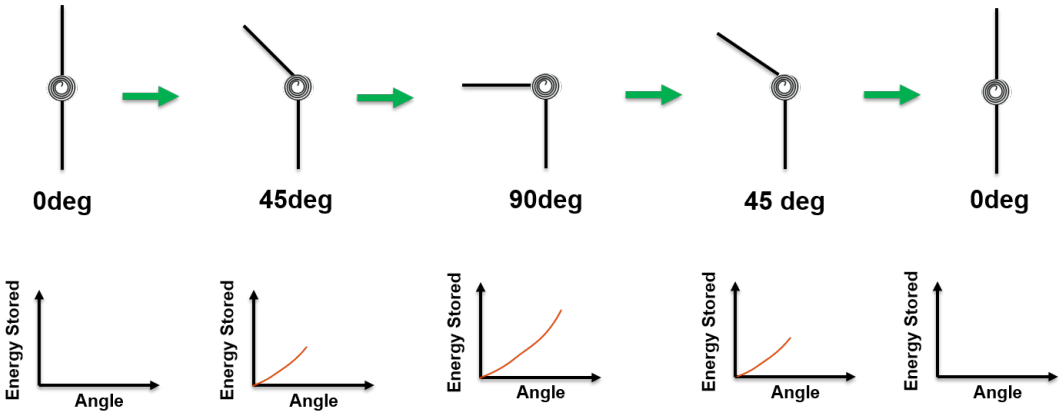

Figure 4.1: Direct torsional spring on a rotational joint. The maximum stored energy is always at the maximum coordinate value.

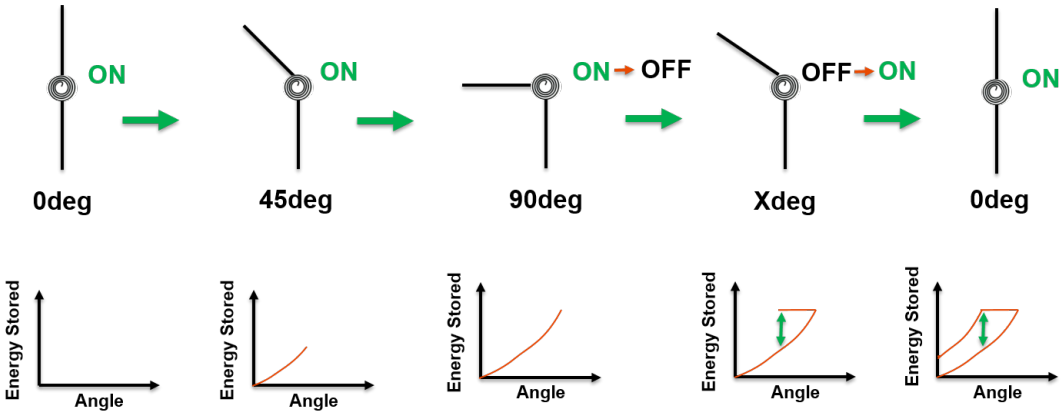

Figure 4.2: Torsional spring with ON/OFF clutching mechanism on a rotational joint. The maximum stored energy can be delivered at arbitrary angles other than the maximum coordinate value.

4.3 Mechanical Design

4.3.1 Overview

Our prototype is built on a Breg DUO knee brace frame. To achieve the clutching effect, our design has two electromagnetic brakes (SEPAC SSB-172-24- M08) con-

nected to elastic elements through respective rotational shafts, and these shafts interconnected through a stiff but flexible Vectran cable to transmit the assistive moment, using a pulley as the pivot for the moment arm. As observed in Fig. 4.3, Brake 2 is connected to an elastic band capable of building up high torques as the knee flexes, while Brake 1 is connected to a low stiffness torsion spring, used to avoid slack on the force-transmitting cable. The clutching behavior is achieved through a combination of ON/OFF states of the electromagnetic brakes, allowing either the high force elastic band or the low stiffness torsion spring to transmit power through the Vectran cable. The allowed states and their corresponding outcome during practical use are shown in Table 4.1.

Table 4.1: Break clutching states and the resulting behavior for the clutch-based knee brace.

Break 1	**Break 2**	**Behavior**
Engaged	Dissengaged	Absorb/ Deliver Energy: Elastic band engaged and transmitting force trough the cable.
Dissengaged	Engaged	Energy storage: The elastic band is held at a constant length while the torsional spring avoids slack in the cable.
Engaged	Engaged	Knee flexion locked: Used for device setup and stiffness adjustment.

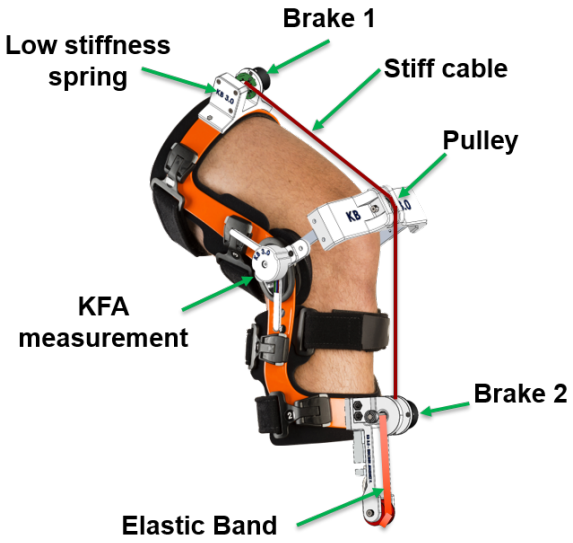

Figure 4.3: Torsional spring with ON/OFF clutching mechanism on a rotational joint. The maximum stored energy can be delivered at arbitrary angles other than the maximum coordinate value.

4.3.2 Energy Storage

Energy storage is dictated by the capacity of the elastic band used and is retained by engaging Brake 2 in Fig. 4.3. As shown in Fig. 4.4, when knee flexion occurs, and the cable is pulled, the shaft is rotated, releasing Vectran cable while coiling the elastic band.

Because the initial length of the elastic band (l_0) is reduced with each turn, the strain in the material is further increased, achieving a higher force for an equivalent total displacement (i.e. knee flexion angle KFA). The magnitude of this force can be estimated as follows.

Suppose we have an elastic cable of length L_1^0 fixed to the ground and attached to a rotating shaft, as shown in Fig. 4.5, and let's assume that the cable is made of

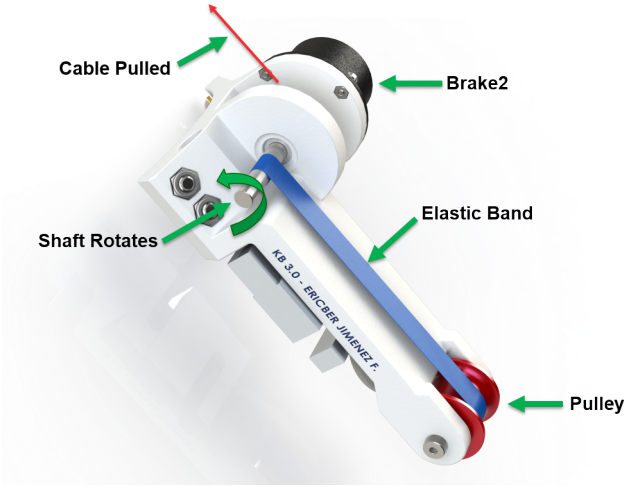

Figure 4.4: When knee flexion occurs, the Vectran cable is pulled, rotating the shaft and coiling the elastic band around it.

a material with elastic constant K in units of Force/Strain.

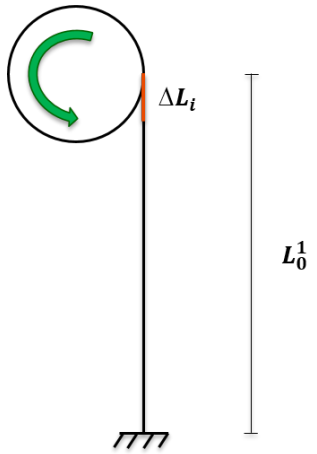

Figure 4.5: Static diagram of an elastic cable subject to deformation by coiling around a shaft.

With each small rotation, a length of ΔL_i is coiled around the shaft, this small length accounts in part for the original length as well as for the elastic deformation caused by the small rotation. Therefore, the effective original length L_1^0 changes as a function of the strain ϵ_1 as $L_2^0 = L_1^0/(1+\epsilon_1)$. More generally:

$$L_i^0 = \frac{L_{i-1}^0}{1 + \epsilon_{i-1}} \tag{4.1}$$

Where i represents an arbitrary instant. Given the effective length L_i^0, the new strain can be obtained as:

$$\epsilon_i = \frac{\Delta L_i}{L_i^0} \tag{4.2}$$

And finally, the change in force at an instant i can be obtained as:

$$\Delta F_i = K\epsilon_i \tag{4.3}$$

In practice, however, we care more about the knee flexion angle than about the displacement in the cable to define the kinematics. In order to represent Eq.4.3 in terms of the knee flexion angle, we need to consider the geometry and mechanism of the knee brace frame (Fig. 4.6).

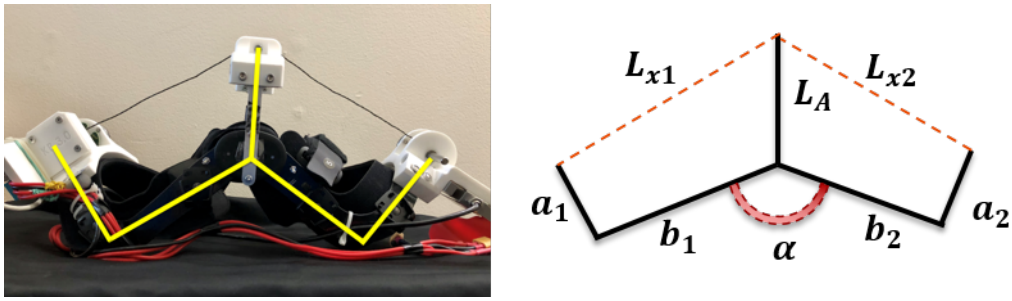

Figure 4.6: Frame geometry for estimation of cable extension as a function of the knee flexion angle.

Approximating the joint mechanism as a rotating joint, and making the knee flexion angle $KFA = \alpha - 180$, we estimate the length of the cable to be:

$$L = L_{x1} + L_{x2} \tag{4.4}$$

Where:

$$L_{x1} = \sqrt{L_A^2 + b_1^2 + a_1^2 - 2L_A\sqrt{b_1^2 + a_1^2} * d_1 cos\left(\frac{KFA}{2} + atan\left(\frac{b_1}{a_1}\right)\right)} \tag{4.5}$$

$$L_{x2} = \sqrt{L_A^2 + b_2^2 + a_2^2 - 2L_A\sqrt{b_2^2 + a_2^2} * d_2 cos\left(\frac{KFA}{2} + atan\left(\frac{b_2}{a_2}\right)\right)} \tag{4.6}$$

To validate our assumptions and estimations, Fig. 4.7 shows a plot comparing the theoretical force reading at the elastic band as a function of the knee flexion angle, determined with Eq. 4.3 and Eq. 4.4, with the direct force readings from a load cell and the theoretical force produced by an equivalent elastic band under the same cable displacement but without coiling. As observed, the direct reading is in agreement with the theoretical prediction; moreover, the final force reading is approximately 12 N higher than the no-coiling equivalent model, justifying our design approach. The differences between our coiling estimation and the direct force reading can be attributed to factors such as friction, imperfect modeling of the brace articulation, and variations in mechanical properties.

Once the force F across the cable is known, the effective extension moment, to which we will refer as Assistive Knee Brace Moment, can be determined as:

$$M = F(d_1 sin(\gamma_1) + d_2 sin(\gamma_2)) \tag{4.7}$$

Where

$$\gamma_1 = asin\left(\frac{L_A sin\left(\frac{KFA}{2} + atan\left(\frac{b_1}{a_1}\right)\right)}{L_{x1}}\right) \tag{4.8}$$

$$\gamma_2 = asin\left(\frac{L_A sin\left(\frac{KFA}{2} + atan\left(\frac{b_2}{a_2}\right)\right)}{L_{x2}}\right) \tag{4.9}$$

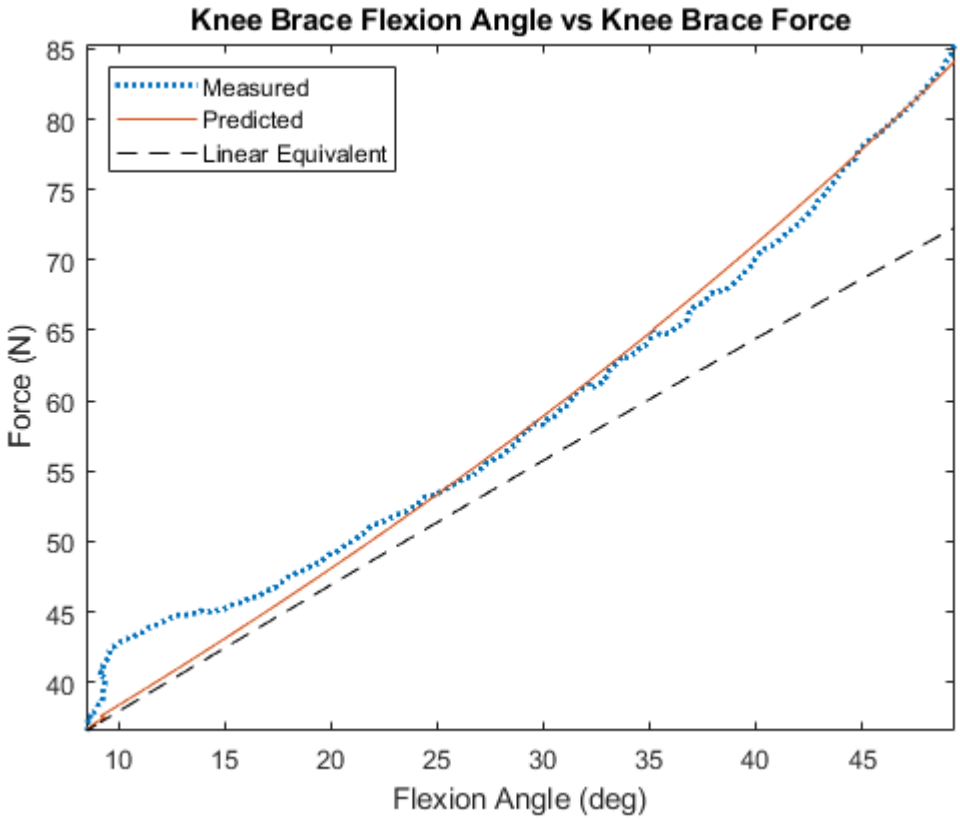

Figure 4.7: Knee Brace stored force reading as a function of the knee flexion angle KFA. Generated with an elastic constant of $K = 82.4$ N/(mm/mm). RMSE = 1.7 N.

4.4 System Architecture

The system architecture of the knee brace KB-3.0 can be represented by the diagram in Fig. 4.8. The high-level control system, data processing, and communication are executed from an Arduino Nano 33 BLE microcontroller. This module was selected due to its high processing speed (64 MHz clock), low noise Bluetooth communication capability, analog inputs, and SPI communication. Additionally, this module is very compact, as shown in Fig. 4.10, which allowed for a space-efficient design of the electronics and signal conditioning circuitry. The entire system is powered by a power bank of LiPo batteries, regulated to supply $+5.2$ V, $+5.4$ V -5 V, and $24V$ V. Fig. 4.9 shows the final device fully assembled. While a Renishaw RM08 magnetic encoder was originally implemented to measure knee brace flexion angle, it was not used during testing due to a failure in the circuit board; this reading, however, was replaced by marker-based flexion angle estimation with a motion capture system.

All connections are centralized in a printed circuit board (Fig. 4.10), and, since the IMU is also built into the Arduino microcontroller, the inertial measurements are also taken at that location.

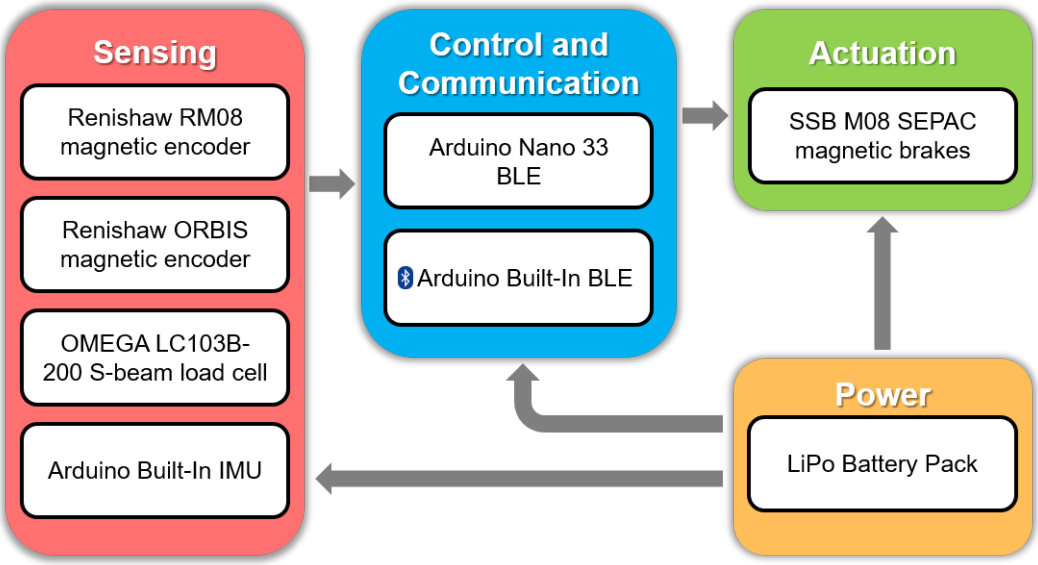

Figure 4.8: System architecture for KB 3.0

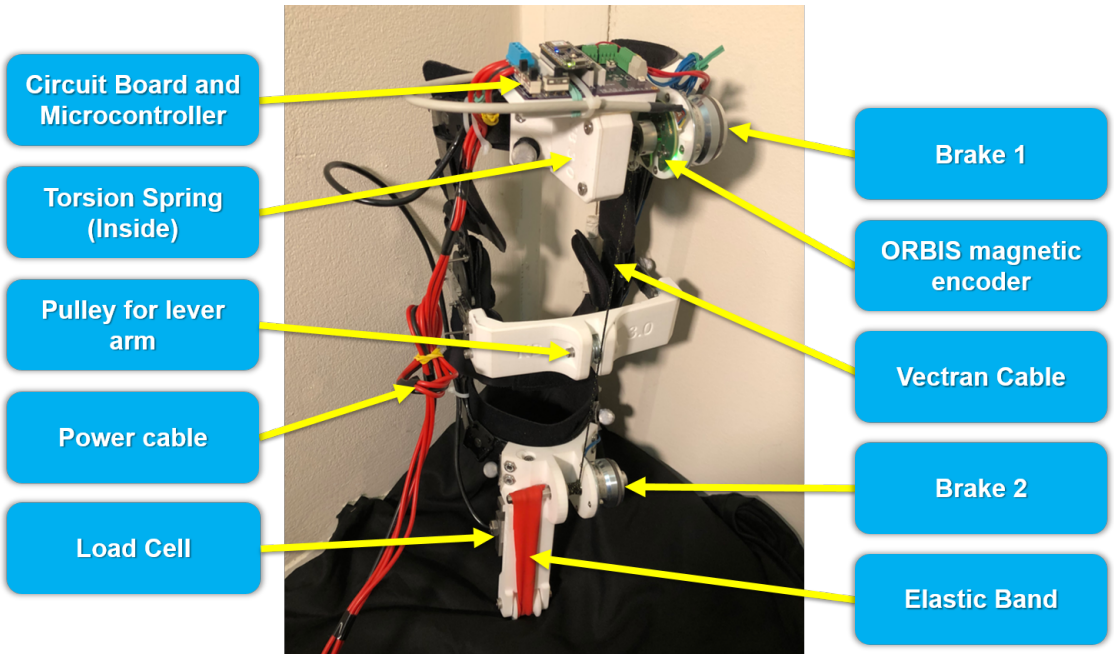

Figure 4.9: KB 3.0 fully assembled, knee brace flexion angle reading was excluded.

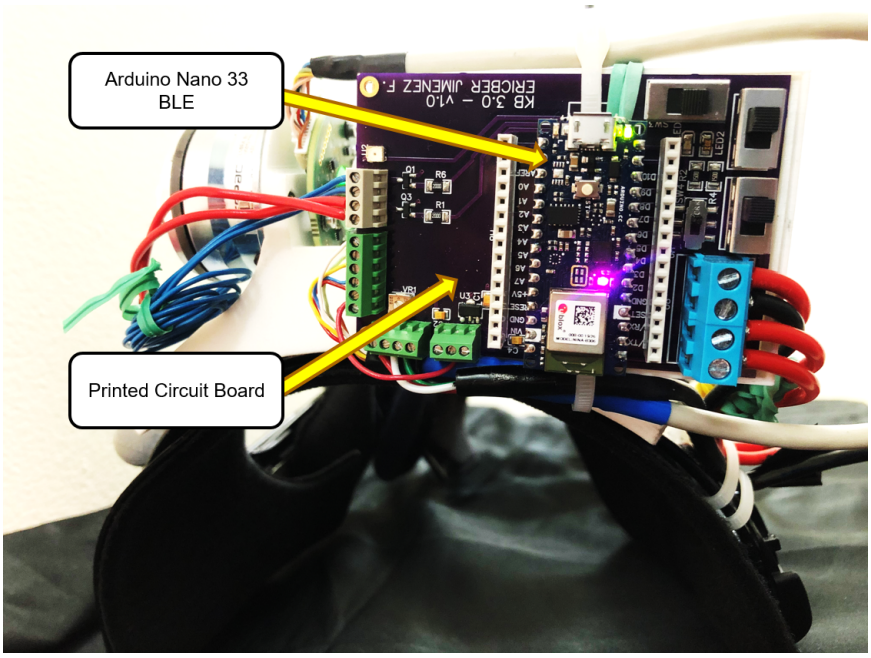

Figure 4.10: KB 3.0 circuit board, all connections and sensing signals are centralized.

4.5 Sensing and Calibration

4.5.1 Assistive Moment Measurement

In order to estimate the assistive knee brace moment, the readings from the load cell (Fig. 4.11) are taken, translated to the cable through proper calibration, and Eq. 4.7 is used. A **OMEGA LC103B-200 Stainless Steel S Beam Load Cell** was implemented. The load cell was powered with 5.4 V excitation voltage and the output signal was amplified using AD627 instrumentation amplifiers and RC low pass filtered at 10 Hz; this cutoff frequency was found to eliminate noise while allowing to capture the dynamics of the tasks being analyzed.

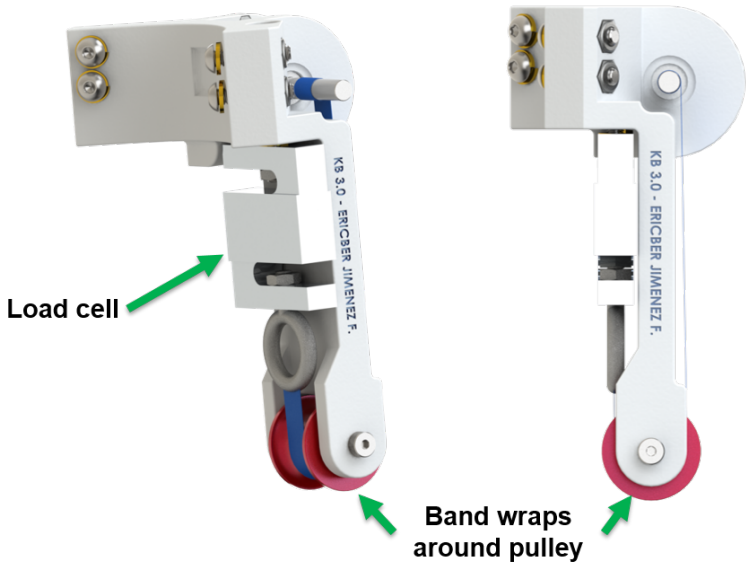

Figure 4.11: KB 3.0 load cell location, the elastic band wraps around the pulley and connects to load cell.

The load cell was calibrated under tension using discrete weights of 22.6 N, 44.8 N, 82.3 N, 135.1 N, 180.1 N, 221.5 N, and 266.6 N. These weights were previously calibrated using a Mark-10 force measurement unit Fig. 4.12. The calibration was executed including the pulley, in order to account for any variations introduced due to bending and bearing friction.

In Table 4.2, F_{Calib} represents the tension load value at which the load cell was statically held during data collection at the corresponding nominal force value. $\overline{R}_A$ represents the mean value of the samples read during the static calibration period for each nominal force value. σ_{R_A} represents the standard deviation corresponding to $\overline{R}_A$. F_A represents the force value obtained from the knee brace readings after adjusting with the model determined from the calibration. e is the reading error $(F_A - \overline{R}_A)$. $\%e$ is the percentage error (e/F_{Calib}). Fig. 4.13 shows the calibration

Figure 4.12: KB 3.0 Load cell calibration. The discrete weight were calibrated with a traceable load cell before being used to calibrate the knee brace load cell.

curve as determined by the measurements.

Table 4.2: Calibration data for the load cell in KB-3.0.

$\overline{R}_A$	$F_{Calib}(N)$	σ_{R_A}	F_A	e	$\%e$
57	22.6	0.77	22.9897	0.3897	1.72%
106	44.8	1.09	44.6722	-0.1278	-0.29%
190	82.3	0.81	81.8422	-0.4578	-0.56%
308	135.1	1.34	134.0572	-1.0428	-0.77%
415	180.1	1.85	181.4047	1.3047	0.72%
508	221.5	1.31	222.5572	1.0572	0.48%
605	266.6	1.61	265.4797	-1.1203	-0.42%

4.5.2 Torsion Spring

The torsion spring produces a force as a function of the rotation of the shaft attached to Brake 1 (Fig. 4.14). This force is estimated using a Renishaw ORBIS magnetic encoder and applying the corresponding force calibration. The readings

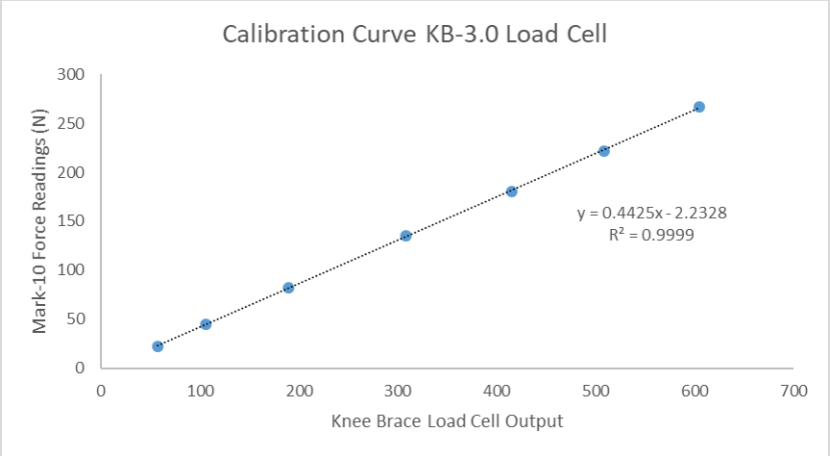

Figure 4.13: Calibration curve for KB-3.0. Data from Table 4.2.

from this multiturn encoder are obtained by the Arduino microcontroller via SPI communication. To obtain a calibration curve, the setup shown in Fig. 4.15 was implemented. The maximum force reading obtained for the range of rotation was 9 N; due to the small moment that this would produce, this force was neglected during data analysis.

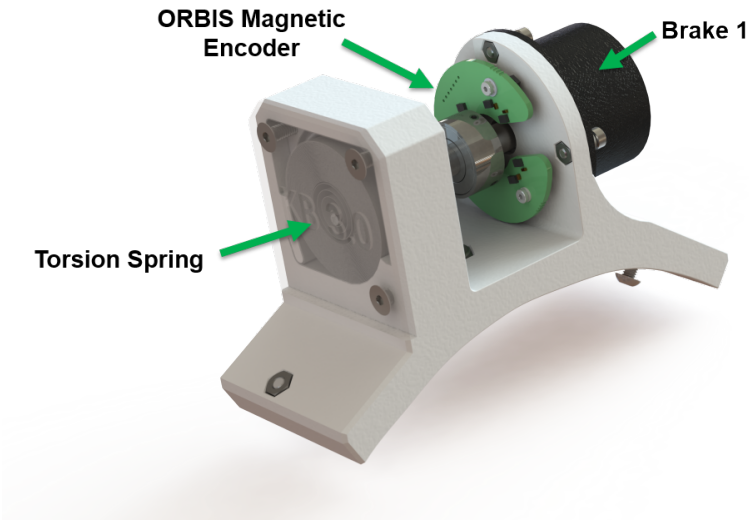

Figure 4.14: Torsion spring and ORBIS magnetic encoder assembly.

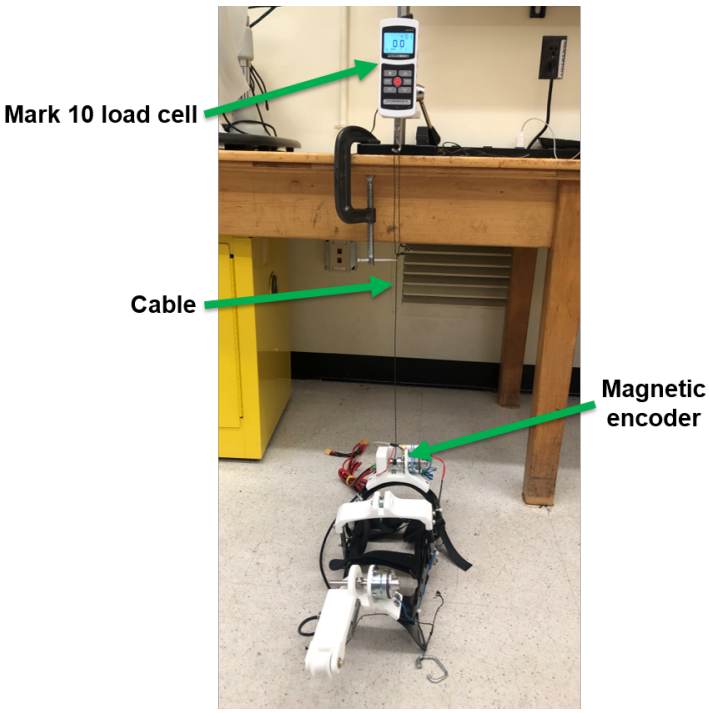

Figure 4.15: Torsion spring and ORBIS magnetic encoder calibration setup.

4.5.3 IMU

The Arduino Nano 33BLE used, has a built-in LSM9DS1 inertial measurement unit IMU. This data was implemented as input variables for the control system.

4.6 Control System

As determined in Chapter 3, the desired behavior of the knee brace is highly dependent on the task being executed and the stage of that task at any particular point in time. This knee brace was tested under four different tasks: Stair Ascent, Stair Descent, Stand-to-Sit-to-Stand, and Level Walking. For each one of these tasks, a finite state machine controller was designed, using the IMU as the source

of input variables for change of state, and using the ON/OFF commands for the brakes as output variables. Fig. 4.16 to 4.19 shows the finite state machine controller methodology implemented for each of the tasks considered.

4.6.1 Finite State Machine: SA

The finite state machine controller for the SA task was configured to be one-directional. The possible states were defined as follows:

- **Initial State:** Initial position with lower limbs in anatomical position. Elastic band not engaged.
- **First Swing:** The assisted limb swings forward. Elastic band not engaged.
- **First Stance:** Stance phase of the assisted limb on the floor before swinging towards the instrumented stairs. Elastic band not engaged.
- **Second Swing:** The assisted limb leaves the floor and swings towards the first step. Elastic band not engaged.
- **Step Up:** The assisted limb makes contact with the instrumented step and extends up. Elastic band engaged.
- **Final Pose:** The assisted knee is fully extended. Elastic band engaged.

The transition between states was determined by the angular velocity of the leg in the sagittal plane (GYRO) and the acceleration along the femur axis (ACC). The diagram of this controller is shown in Fig. 4.16.

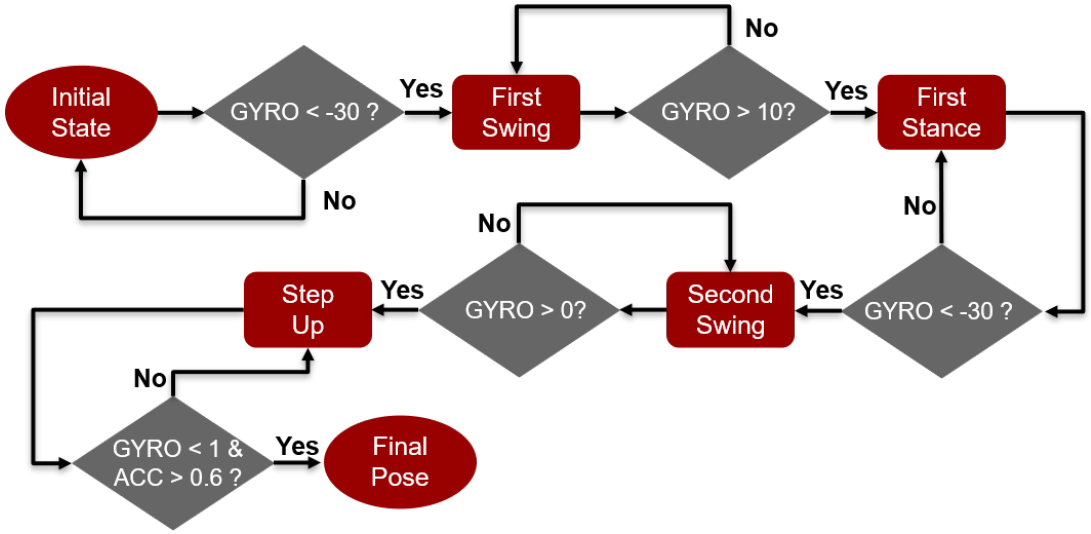

Figure 4.16: Finite state machine controller methodology for Stair Ascent (SA).

4.6.2 Finite State Machine: SD

The finite state machine controller for the SD task was also configured to be one-directional. The possible states were defined as follows:

- **Initial State:** Initial position on top of the first step, with lower limbs in anatomical position. Elastic band not engaged.
- **Descent:** The unassisted limb starts descending towards the floor while the assisted knee flexes. Elastic band engaged
- **Swing:** The assisted limb swings forward after the unassisted limb makes contact with the floor. Elastic band not engaged.

The transition between states was determined by the angular velocity of the leg in the sagital plane (GYRO) and the acceleration along the femur axis (ACC). The diagram of this controller is shown in Fig. 4.17.

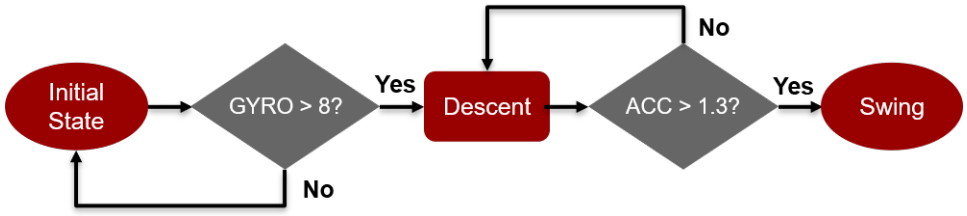

Figure 4.17: Finite state machine controller methodology for Stair Descent (SD).

4.6.3 Finite State Machine: STS

The finite state machine controller for the STS task was also configured to be one-directional. The possible states were defined as follows:

- **Initial State:** Initial position with lower limbs in anatomical position. Each foot on a different force plate. Elastic band not engaged.
- **Flexing:** The knees flex as the subject performs the sitting down motion. Elastic band engaged.
- **Seating:** Seating position. Elastic band not engaged.
- **Extending:** The knees extend as the subject stands up. Elastic band engaged.

The transition between states was determined by the angular velocity of the leg in the sagital plane (GYRO) and the acceleration along the femur axis (ACC). The diagram of this controller is shown in Fig. 4.18.

4.6.4 Finite State Machine: W

The finite state machine controller for the W task was configured to be cyclic. The possible states were defined as follows:

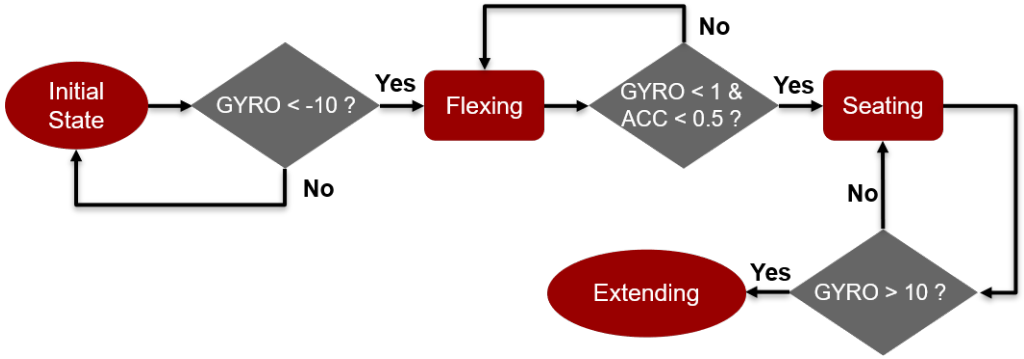

Figure 4.18: Finite state machine controller methodology for Stand-to-Sit-to-Stand (STS).

- **Initial State:** Initial position with lower limbs in anatomical position. Elastic band not engaged.
- **Swing:** The assisted limb swings forward. Elastic band not engaged.
- **Early Stance:** Early stance phase of the assisted limb after contact with the floor. Elastic band engaged.
- **Mid Stance:** Mid stance phase of the assisted limb after early stance. Elastic band engaged.
- **Late Stance:** Late stance phase of the assisted limb after contralateral contact with the floor. Elastic band not engaged.

4.7 Communication and System Integration

For experimental purposes, the knee brace KB-3.0 was given the capability to be integrated with a Qualisys motion capture system and a Delsys Trigno EMG measurement system. To synchronize the three systems, an external trigger signal is sent to the Delsys Trigno system via a microcontroller commanded from a user

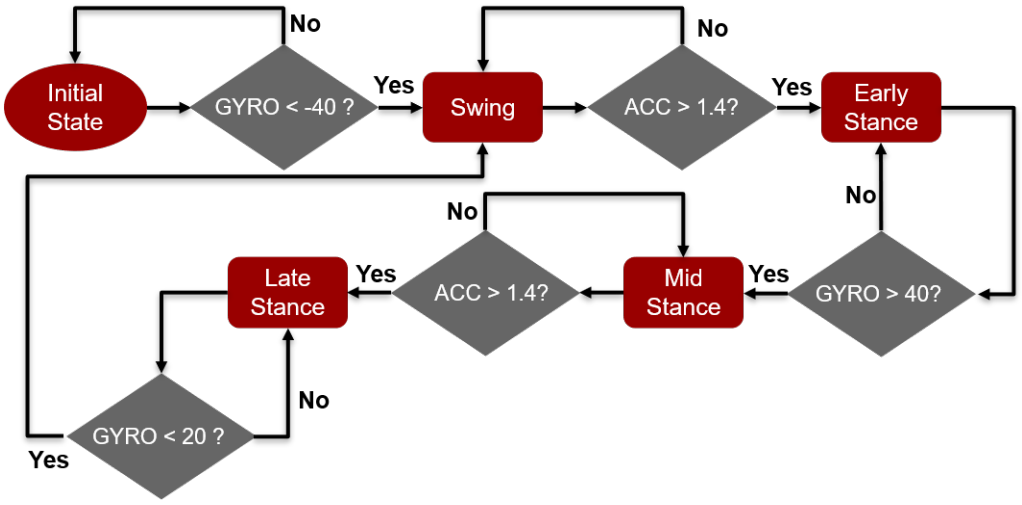

Figure 4.19: Finite state machine controller methodology for Level Walking (W).

interface and this triggers the Qualisys system and the knee brace KB 3.0 for data collection (Fig. 4.20). Each data collection trial has a predetermined collection time, and data is fetched and saved after the time has elapsed. In order to quantify the trigger delay in KB 3.0 with respect to the motion capture system, the knee brace was set to emit infrared light detectable by the Qualisys cameras in active marker mode; a total of 10 trials were taken, and the time interval between the first frame captured and the first frame containing the infrared signal was measured. The delay was measured at 109 ± 12 ms.

The knee brace communicates with a user interface developed as a Visual Studio C# .NET Windows Form Application (Fig. 4.21). The user interface has the following functionalities:

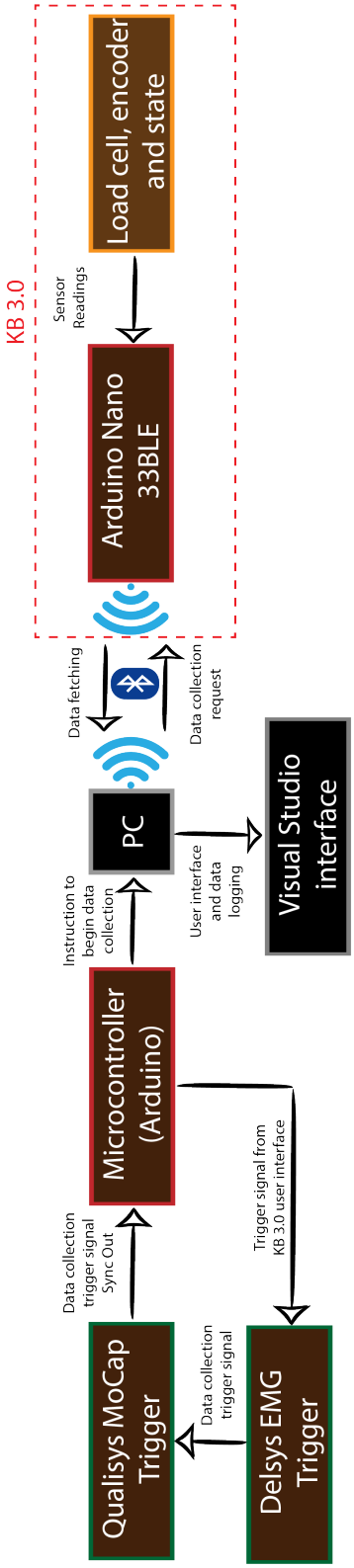

Figure 4.20: System integration diagram for KB-3.0.

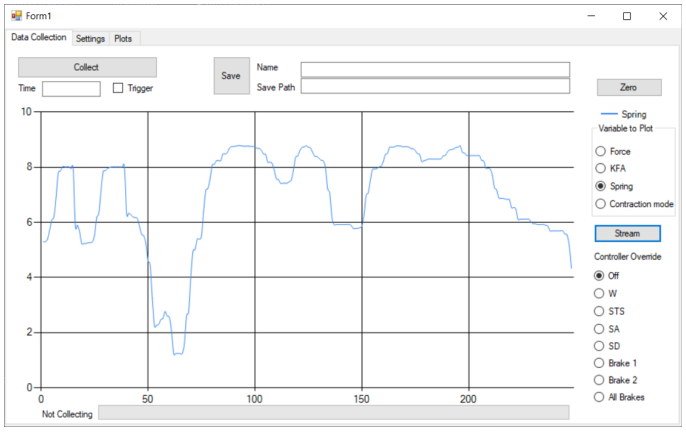

Figure 4.21: KB-3.0 Data Collection User Interface.

- **Settings:** This tab has the options to connect a bluetooth module to the software, enable a trigger COM port, and configure the trigger to send and receive or just receive the trigger signal.
- **Collect button:** This starts data collection; a bluetooth device must be connected to the software beforehand.
- **Save button:** This will save the last collected dataset to the path specified in "Save Path" under the name specified in "Name".
- **Zero:** Used to zero the load cell and encoder readings to correct the baseline reading.
- **Time (s):** Sets the time to collect data for the current trial.
- **Stream:** Streams data from the knee brace in real time. The variable selected will be plotted.
- **Controller override:** Sets the controller mode to be implemented according to the task to be executed.

4.8 Prototype Specifications

This prototype has been designed to be a low-power high-torque implementation. The maximum assistive moment will depend on the mechanical properties of the elastic band used, however, the electromagnetic brakes torque limit would only allow the knee brace to go up to 62 Nm, according to our design parameters.

In application, however, the maximum assistive moment that can be tolerated by a subject is highly dependent on the knee brace frame and strapping system. The maximum external moment applied during our experiments and system evaluation was 23 Nm during the STS task. The engagement and disengagement times were averaged at 6 ms and 85 ms respectively; this indicates that our device can be suitable for implementations involving dynamic tasks with a maximum engagement frequency of 11.76 Hz.

The total weight of the device was measured at 2.80 kg. However, in a non-experimental setting, the load cell can be removed because this variable is not used for control purposes, and this would reduce the total weight to 2.58 kg.

While the device was powered using LiPo batteries, no high current peaks were detected. The maximum power consumption depends on the control system being implemented; for the worst-case scenario, with both brakes engaged, the maximum power consumption was measured at 19.68 W. Table. 4.3 serves as a comparison of our device against recent knee exoskeletons.

Table 4.3: Comparison of KB-3.0 with experimental and commercially available exoskeleton and active orthoses. LW = Level walking, STS = Sit-to-stand, SA = Stairs ascend, SD = Stairs descend, R = Running, N/R = Not reported, FSM = Finite State Machine

Reference	**Task**	**Type**	**Max Torque**	**Max Speed**	**Control**	**Mechanism**	**Weight**	**Power**
KB 3.0	STS/ SA/ SD/ W	Hybrid	23Nm	>User-limited	FSM	Clutch-Cable	2.58kg	19.68 W
(Shepherd & Rouse, 2017)	STS	Active	80Nm	>3.5 rad/s	Impedance	Rotational	1.8kg	200W motor
(Liao et al., 2015)	LW, SA, SD	Active	18Nm	N/R	Impedance	Rolling	N/R	N/R
(Dollar & Herr, 2008a)	R	Semi-Act	47.5Nm	N/R	Position	Rot. + Linear	2.5 kg	2W controller 200W motor Approx 115W peak demand
(Witte et al., 2017)	LW	Active	62.2Nm	N/R	Torque	Rotational	0.76kg	N/R
(Horst, 2009)	LW, SA , SD , STS	Active	34 Nm	>1.75rad/s	N/R	Rot./ Flex CVA	2.2 kg	70W
(Jun et al., 2015)	Bench testing	Semi-Act	0.6 Nm	User	N/R	Beam bending	0.6kg/ 1.5kg	N/R

4.9 Discussion

An experimental clutch-based assistive knee brace has been developed with the goal of providing knee extension assistance during stair ascent (SA), stair descent (SD), Stand-to-Sit-to-Stand (STS), and level walking (W). The biomechanic effects of this device under these four tasks are studied in Chapter 5. When compared with recent experimental and commercially available knee exoskeletons and active orthoses, we can point out the following:

- KB 3.0 is designed to be evaluated under four different tasks; this is the first time, to our knowledge, that a non-active knee assistance device has been designed with such versatility. Dollar & Herr (2008a) for instance, only evaluated for level walking, while Jun et al. (2015) limited the evaluation to bench testing.

- While KB 3.0 is slightly heavier than most knee exoskeletons in the literature (Table 4.3), the design is over-dimensioned since the brakes never get close to their maximum torque capacity. Our design can be optimized to reduce extra weight by selecting smaller magnetic brakes and lighter materials.

- KB-3.0 has a maximum torque of 23 Nm, as reached during experimentation, this torque can be increased if propper frame structure and strapping are used. This maximum torque is higher than that achieved by Liao et al. (2015) with an active exoskeleton, and is about 49 % the capacity reached by Dollar & Herr (2008a), while consuming about 10 % of the electric power (Table 4.3).

Evidently, our novel design seems to be a suitable low-power, moderate-to-high torque alternative for knee assistive devices. One important limitation during the experimental phase was the effectiveness of the strapping system to minimize soft-tissue motion. This must be further improved in future designs.

Chapter 5

Biomechanic Effects of a Clutch-Based Assistive Knee Brace During Daily Life Activities

5.1 Introduction

Traditional valgization Knee Bracing has been proposed and implemented as an alternative to unload the medial compartment in knee OA patients. However, the literature is inconclusive on whether these traditional knee braces achieved the desired tibiofemoral contact force reduction effect (Hall et al., 2019). While powered knee exoskeletons have been designed to enhance knee moment production or assist on physical impairments and rehabilitation (Horst, 2009), no exoskeleton was found in the literature to have been evaluated in terms of the tibiofemoral

contact forces. Moreover, no clutching design approach has been evaluated.

The main objective of this research was to develop a novel clutch-based assistive knee bracing approach and evaluate its biomechanic effects at the knee joint. More specifically, this research was focused on investigating the effect of the level of assistance of the knee brace on the tibiofemoral contact forces under four tasks: Stair Ascent (SA), Stair Descent (SD), Stand-to-Sit-to-Stand (STS), and Level Walk (W). A testing protocol was developed and adapted to each task.

5.2 Methods

5.2.1 Overview

The study was divided into four tasks: Stair Ascent (SA), Stair Descent (SD), Stand-to-Sit-to-Stand (STS), and Level Walk (W). These tasks were performed under different conditions of external knee brace assistance until a total of 20 successful repetitions were achieved. However, some trials were discarded during post-processing; the criteria to discard a trial in post-processing were as follows:

- The trial showed unrealistic kinematics due to missing marker trajectories that could not be filled.
- The EMG output for at least one transducer was empty or null.
- Musculoskeletal simulation optimization failure.

The variables observed as a result of the musculoskeletal analysis were:

- Peak medial, lateral, and total knee contact force (KCF) magnitude.

- Peak knee flexion angle (KFA) and knee flexion moment (KFM).
- Peak hip flexion angle (HFA) and hip flexion moment (HFM).
- Peak angle dorsiflexion angle (ADA) and ankle dorsiflexion moment (ADM).
- Co-Contraction index (CCI) at peak KCF.

For this evaluation study, the following hypotheses were tested:

- **H1:** External assistive moment magnitude will show an inverse relationship with peak medial KCF for SA, SD, STS, and W tasks.
- **H2:** External assistive moment magnitude will exhibit a direct relationship with lateral CCI and an inverse relationship with medial CCI.
- **H3:** The external assistive moment will reduce peak KFM, and KFA in the assisted knee during the level walking trials.
- **H4:** Peak ADM and HFM magnitude for the assisted limb will exhibit a direct relationship with the external assistive moment for for SA, SD, STS, and W tasks.

5.2.2 Equipment And Setup

Biomechanics data was collected at the Musculoskeletal & Orthopedic Biomechanics Lab (MOBL) at UMass Amherst. Motion data was captured by an 11-camera Qualisys MoCap system at 240 fps; passive reflective markers were used. A whole-body and knee brace marker set was implemented (Fig. 5.1); this allowed to account for soft tissue artifacts in the knee brace angle readings with respect to the knee angle. The markerset used is detailed in Table 5.1.

(a) Brace Marker Set. (b) No Brace Marker Set.

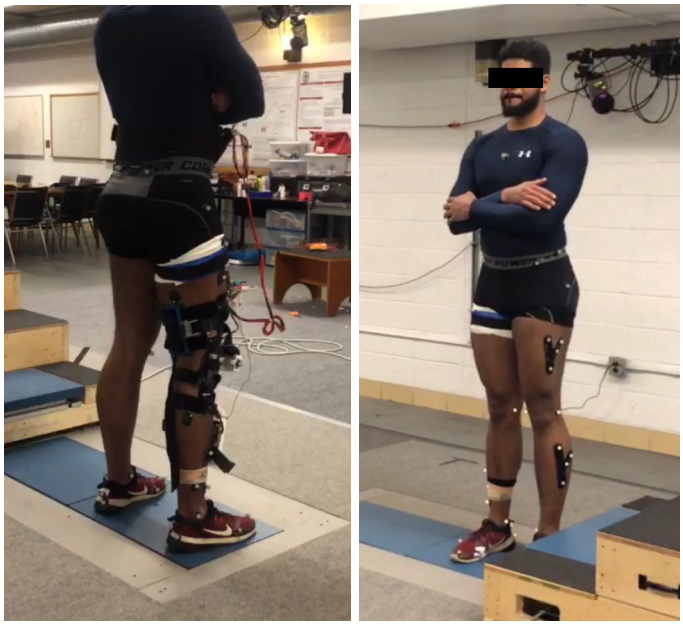

Figure 5.1: Marker Set used for data collection.

Table 5.1: Description of marker set implemented.

Markers	Description	Notes
TOR	Torso	-
RASI, LASI, RPSI, LPSI	L/R, A/P Asis	-
RGRT, LGRT	L/R Greater Trochanter	-
RTHUP, RTHUA, RTHLP, RTHLA	R Thigh cluster	-
LTHUP, LTHUA, LTHLP, LTHLA	L Thigh cluster	-
RLCO, RMCO	Right Knee condyles	No Brace trials
LLCO, LMCO	Left Knee condyles	-
RSHUP, RSHUA, RSHLP, RSHLA	R Shank cluster	-
LSHUP, LSHUA, LSHLP, LSHLA	L Shank cluster	-
RLMA, RMMA	Right Malleoli	-
LLMA, LMMA	Left Malleoli	-
RHLA, RHMD, RHPR	Right Heel	-
LHLA, LHMD, LHPR	Left Heel	-
R1MH, R5MH, RTOE	Right Metatarsal and Toe	-
L1MH, L5MH, LTOE	Left Metatarsal and Toe	-
B-UL, B-UM, B-LL, B-LM, B-AL, B-AM, B-PL, B-PM	Knee Brace	Brace trials

Ground reaction forces were recorded at $2,400$ Hz using AMTI force plates. Surface EMG signals were recorded at $2,000$ Hz using a wireless Delsys Trigno system synchronized with the MoCap system. EMG signals were collected for eight right lower limb muscles; Semitendinosus (ST), Biceps Femoris (BF), Vastus Medialis (VM), Rectus Femoris (RF), Soleus (SOL), Medial Gastrocnemius (MG), and Lateral Gastrocnemius (LG). All EMG placements were done following the SENIAM guidelines.

During the Walking trials, mechanical interference between the knee brace and the VL transducer war reported. VL signals turned out to be considerably higher in magnitude as compared to the rest of the transducers, and no consistent behavior was observed for the EMG envelope curve. For this reason, VL EMG data were deemed not reliable for the level walking trials.

Simultaneously, torque data from the instrumented knee brace was be recorded and transferred wirelessly to a laptop computer.

5.2.3 Testing Protocol

Due to human subject research limitations, one subject was selected for this study. Each task executed is described as follows.

Stair Ascent

The subject starts walking towards a set of instrumented stairs; an SA trial starts when the assisted limb (green dotted in Fig. 5.2) leaves the force FP1 and ends

when the unassisted leg reaches the second step above FP3.

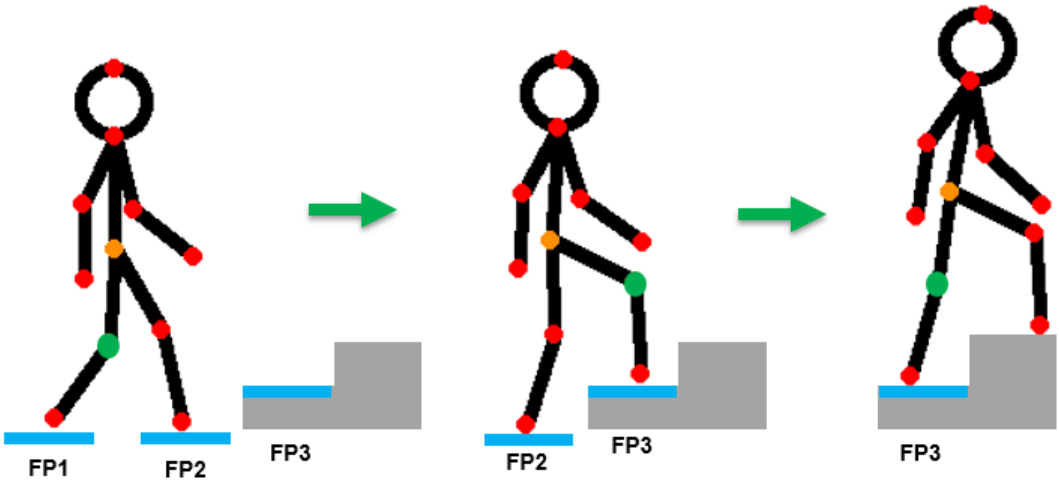

Figure 5.2: SA trials representation. FPx represent forceplates. The green dot represents the assisted knee.

For SA, two levels of KB-3.0 external assistance were tested. Each level is characterized based on the preload stored in the elastic band prior to the trial, and the stiffness of the elastic band used. The description of the assistance levels, as well as the number of trials that were fully processed, is summarized in Table 5.2.

Table 5.2: SA Trials description. N represents the number of trials.

Assistance Level	Preload (N)	Stiffness ($N/(mm/mm)$)	N
No Brace	-	-	10
Low	40 ± 5	44	10
High	80 ± 5	82	10

Stair Descent

For SD, the subject starts standing on the instrumented steps. An SD trial starts when the unassisted limb leaves the force plate FP3, and ends when the assisted

limb comes in contact with FP1 (Fig. 5.3). The description of the assistance levels, as well as the number of trials that were fully processed, is summarized in Table 5.3.

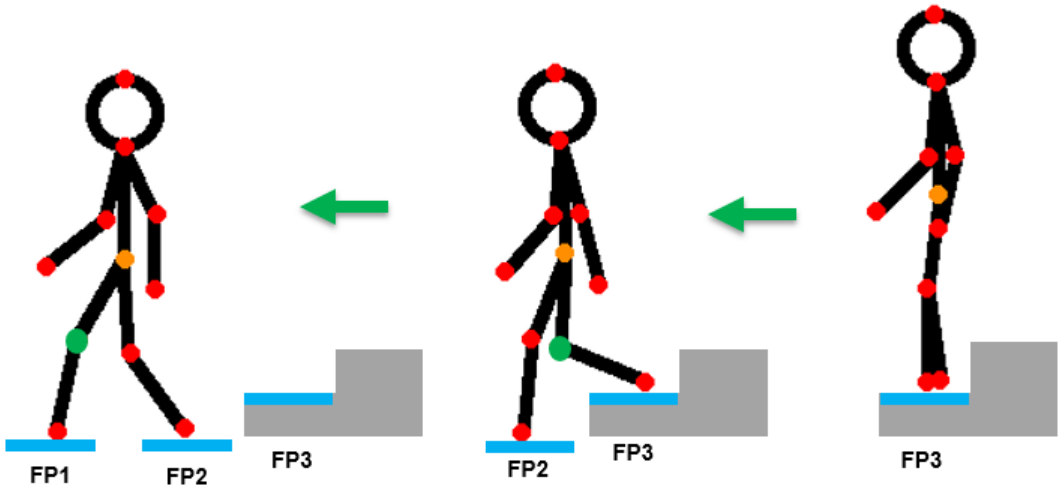

Figure 5.3: SD trials representation. FPx represent force plates. The green dot represents the assisted knee.

Table 5.3: SD Trials description. N represents the number of trials.

Assistance Level	Preload (N)	Stiffness ($N/(mm/mm)$)	N
No Brace	-	-	14
Low	40 ± 5	44	14
High	50 ± 5	82	14

Stand-to-Sit-to-Stand

For STS, The subject starts standing with each foot placed on a different force plate. An STS trial starts when the subject starts the motion to sit down on a small bench placed on top of a third force plate. The subject sits down and stands back up; the trial ends when the subject reaches a full standing position again (Fig. 5.4).

The description of the assistance levels, as well as the number of trials that were fully processed, is summarized in Table 5.4.

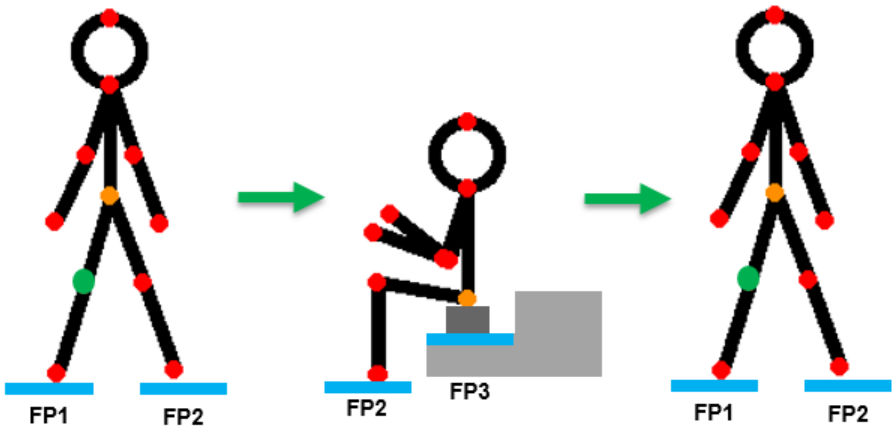

Figure 5.4: STS trials representation. FPx represent force plates. The green dot represents the assisted knee.

Table 5.4: STS Trials description. N represents the number of trials.

Assistance Level	Preload (N)	Stiffness ($N/(mm/mm)$)	N
No Brace	-	-	6
Low	20 ± 5	44	6
High	30 ± 5	74	6

Level Walking

For W, the subject level walking trials at preferred speed. The full gait cycle was analyzed. The description of the assistance levels, as well as the number of trials that were fully processed, is summarized in Table 5.5.

Table 5.5: W Trials description. N represents the number of trials.

Assistance Level	Preload (N)	Stiffness ($N/(mm/mm)$)	N
No Brace	-	-	4
Low	50 ± 5	44	4

Workflow

The work-flow of data collection is summarized by the diagram in Fig. 5.5. To begin preparation, the whole body marker set was placed on the subject. This was followed by a static trial to obtain data for musculoskeletal model scaling. Subsequently, the EMG sensors were placed, and one maximum voluntary isometric contraction MVIC trial was executed to obtain normalization values for EMG signals (Fig. 5.6); the isometric contractions were performed at different joint angle combinations, and the maximum reading for each muscle was taken after processing the EMG signal. Following this, the No Brace SA and SD trials were executed, followed by Brace SA and SD trials. After rearranging the force plate setup, the No Brace STS and W trials were executed, followed by the Brace STS and W trials. No informed consent was needed, as the UMass Amherst Institutional Review Board deemed this study as "No Human Subject Research".

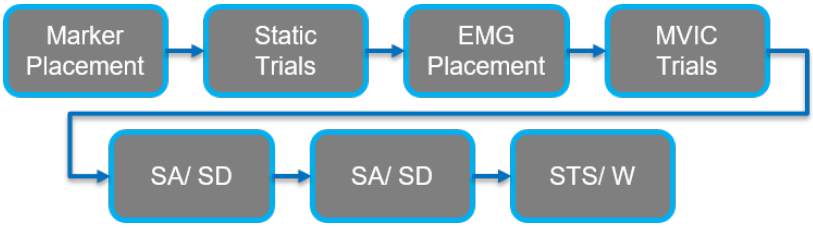

Figure 5.5: STS trials representation. FPx represent force plates. The green dot represents the assisted knee.

(a) MVIC Calf.

(b) MVIC Hamstrings.

(c) MVIC Quadriceps.

Figure 5.6: Maximum voluntary isometric contractions.

5.2.4 Data Processing

The data processing workflow subject is illustrated in Fig. 5.7. After collecting experimental data, the motion and GRF files were trimmed, gap-filled, and converted to OpenSim ".trc" and ".mot" formats (Delp et al., 2007). Subsequently, the data obtained from the instrumented knee brace was corrected for triggering delay to obtain a good synchronization with the MoCap data. These variables were inputted into a MATLAB-OpenSim script to run Inverse Kinematics, Inverse Dynamics, Static Optimization, and Analyze Tool for joint reactions.

The EMG data was band-pass filtered at 20 - 500 Hz, full-wave rectified, and the linear envelope was generated with a 10 Hz low pass filter. EMG-based Co-Contraction index calculation was adopted from D. Kim & Hwang (2018) (Eq. 5.1), and was calculated centered at each peak KCF location within a window of 300 ms.

Unlike the method implemented in Chapter 3, adopted from Rudolph et al. (2000), this new approach takes into account the activation levels of agonist and antagonist muscles before and after the time point of interest and outputs a single co-contraction value for the time window defined around the point of interest. In our case, the points of interest were the locations of peak knee contact forces.

$$CCI = 2\sum_{i=1}^{N} \frac{min[EMG_1(i), EMG_2(i)]}{EMG_1(i) + EMG_2(i)} \times 100 \tag{5.1}$$

While this approach focuses on the co-contraction during the peak KCF values instead of a time-wise co-contraction curve, this method still showed some limitations. Since the numerator in Eq. 5.1 is always taken as the minimum activation value between the agonist and antagonist muscle groups, increased activation in the more active muscle group will not reflect a higher CCI. Instead, a smaller value for the function will be determined due to a higher denominator value, leading to an inverse relationship between CCI and absolute activation of the more active muscle group. Since not all muscles have equal contribution to KCF due to muscle contraction, CCI might not necessarily be a surrogate for KCF distribution between medial and lateral condyles.

Statistical Evaluation

Our hypotheses were tested with a one-way ANOVA, applied independently to each outcome variable, for the SA, SD, and STS tasks. For the W task, a paired t-test was applied. Statistical Significance was defined as $p<0.05$. Where significant

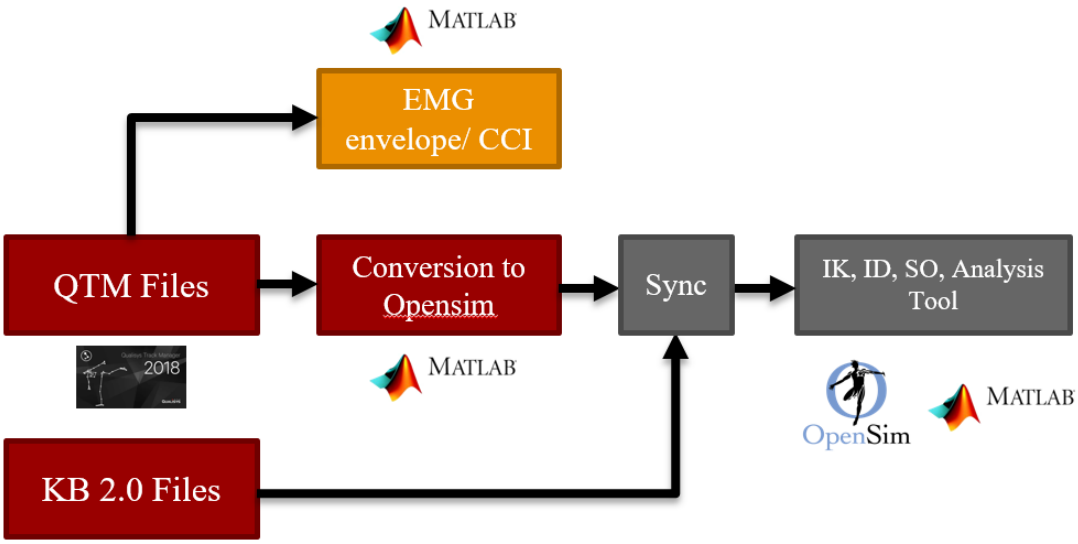

Figure 5.7: Data processing workflow for KB3.

effect was detected for the ANOVA, a Tukey test was applied as a post-hoc analysis to obtain pair comparisons.

5.2.5 Musculoskeletal Model

The OpenSim model implemented was based on the mediolateral knee model developed by Lerner et al. (2015). This model allowed for independent estimation of medial and lateral knee contact force. This model was modified to include the kinematics of the knee brace KB-3.0 (Fig. 5.8). This allowed for knee brace angle determination based on marker data. The external assistive knee brace moment was included in the static optimization simulations.

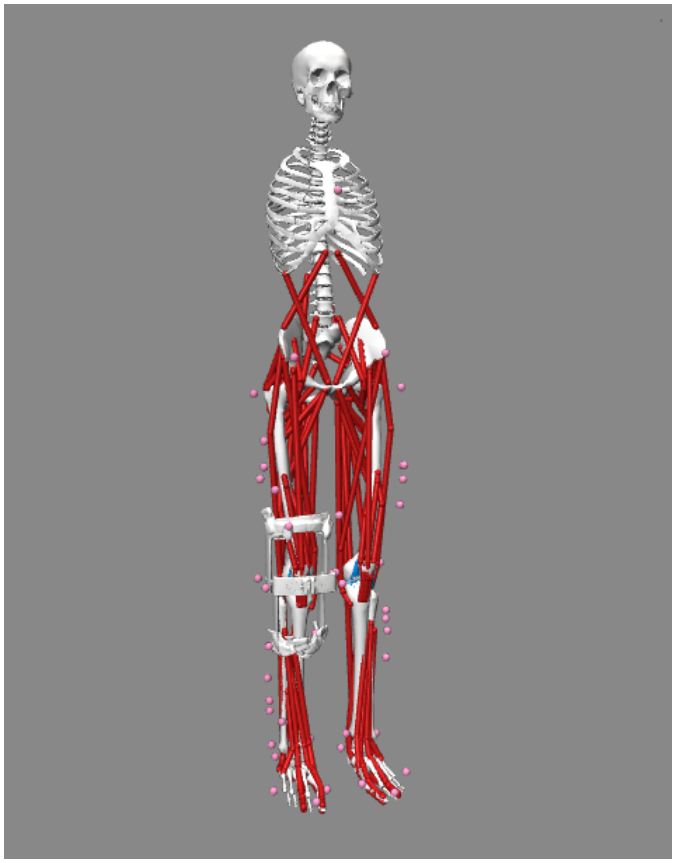

Figure 5.8: Musculoskeletal model implemented for the Brace trials.

5.3 Results

5.3.1 Stair Ascent (SA)

The result variables for each condition for the SA task are summarized in Table. 5.6. Statistically significant results are highlighted.

Figure 5.9 shows the medial and lateral KCF curves for all three conditions of the SA task, and statistically significant changes in peak KCF are shown.

The plots reveal two peak KCF locations, one at about 60 %, after the knee has started to extend during the step up, and one towards the end of the trial, when the

(a) SA: Medial KCF.

(b) SA: Lateral KCF.

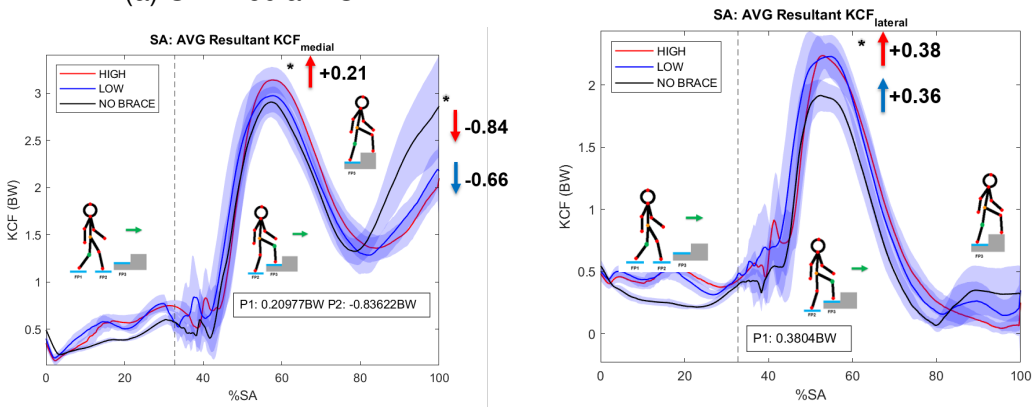

Figure 5.9: Medial and lateral KCF for SA. The dashed line represents the transition point between leg swing and step up.

knee is fully extended (Fig. 5.11). The first peak presented a statistically significant increase in medial KCF for the high assistance condition, and an increase and a statistically significant increase for the lateral KCF for both levels of assistance. The second peak exhibited a reduction in KCF for the medial condyle; no difference was detected between levels of assistance.

Table 5.6: Resulting tibiofemoral contact forces, lower limb kinematics and kinetics for SA task. P1 = Peak 1, P2 = Peak 2.

Assistance Level	**High (H)**		**Low (L)**		**No Brace (N)**		**Post-Hoc**				
Prameter	**Mean**	**SD**	**Mean**	**SD**	**Mean**	**SD**	**p-value**	**H-N**	**L-N**	**H-L**	**Cohen's f**
Medial KCF P1 (BW)	3.16	0.14	3.01	0.16	2.95	0.14	**0.0103**	**0.21**	0.06	0.15	0.60
Medial KCF P2 (BW)	1.99	0.15	2.17	0.22	2.83	0.52	**1.82E-05**	**-0.84**	**-0.66**	-0.18	1.07
Lateral KCF P1 (BW)	2.34	0.09	2.32	0.16	1.96	0.13	**3.34E-07**	**0.38**	**0.36**	0.02	0.75
Lateral KCF P2 (BW)	-	-	-	-	-	-	-	-	-	-	-
Total KCF P1 (BW)	5.36	0.17	5.23	0.29	4.82	0.16	**1.46E-05**	**0.54**	**0.41**	0.13	1.07
Total KCF P2 (BW)	1.98	0.20	2.31	0.41	3.16	0.69	**2.33E-05**	**-1.18**	**-0.85**	-0.33	1.04
VL-BF CCI P1	44.1	11.65	21.27	9.69	38.52	13.45	**0.0005**	**5.58**	-17.25	**22.83**	0.83
VL-BF CCI P2	46.35	14.09	11.66	5.08	34.75	7.70	**5.6E-08**	**11.60**	**-23.09**	**34.69**	1.48
VL-LG CCI P1	19.66	15.91	19.42	12.09	39.416	18.27	**0.0107**	**-19.76**	**-20.00**	0.24	0.60
VL-LG CCI P2	32	18.97	36.19	11.09	48.33	8.93	**0.0342**	**-16.33**	-12.14	-4.19	0.51
VM-ST CCI P1	30.62	14.8	43.28	12.79	35.37	10.33	0.1004	-4.75	7.91	-12.66	0.41
VM-ST CCI P2	46.99	8.94	41.88	10.57	33.28	7.76	**0.0085**	**13.71**	8.60	5.11	0.62
VM-MG CCI P1	7.24	4.18	12.12	9.42	32.64	18.05	**0.0001**	**-25.40**	**-20.52**	-4.88	0.92
VM-MG CCI P2	23.13	6.61	30.05	20.95	29.4	4.15	0.4272	-6.27	0.65	-6.92	0.24
Peak KFA (deg)	-70.91	2.54	-72.4	3.79	-87.38	1.77	**2.09E-13**	**16.47**	**14.98**	1.49	2.63
Peak KFM (Nm/kg)	1.39	0.06	1.39	0.11	1.35	0.07	0.525	0.04	0.04	0	0.23
Peak ADA (deg)	24.52	1.21	20.71	2.38	21.51	1.06	**7.90E-06**	**3.01**	-0.80	**3.81**	0.99
Peak ADM (Nm/kg)	-1.28	0.18	-1.33	0.26	-1.16	0.17	0.208	-0.12	-0.17	0.05	0.34
Peak HFA (deg)	55.55	2.21	59.57	2.27	57.21	1.35	**0.0005**	-1.66	**2.36**	**-4.02**	0.83
Peak HFM (Nm/kg)	-1.11	0.09	-1.09	0.24	-0.82	0.10	**0.0003**	**-0.29**	**-0.27**	-0.02	0.83

While the kinematics were affected during the swing phase, showing a reduced knee flexion range for both assistance levels and a more plantarflexed motion for the high assistance level, the curves show no significant difference during most part of the stepping up phase (Fig. 5.11). At the end of the task, however, the end position tends to show a more flexed hip and knee, and a more dorsiflexed ankle. The hip was the only joint that showed an increase in peak moment production; the extension moment was higher for the assisted conditions during the stepping up portion of the task.

The VL-BF co-contraction index (Fig. 5.10) was higher for the first peak, while the VL-LG showed a significant reduction for that same peak; similarly for the second peak, where VL-LG decreased by 16.33 while VL-BF increased by 11.60. The higher assistance also showed an increased VL-BF CCI as compared with the low assistance condition. Medial CCI decreased by 25.40 for the assisted condition during the first peak but increased by 13.71 during the second peak KCF.

(a) SA: VL-BF CCI.

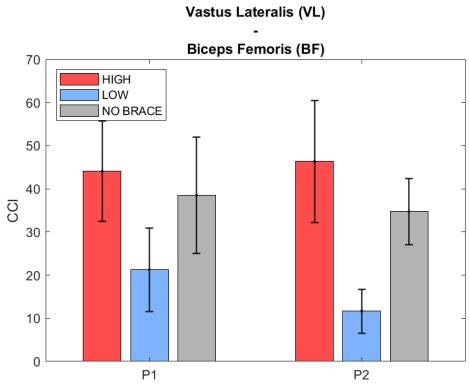

(b) SA: VL-LG CCI.

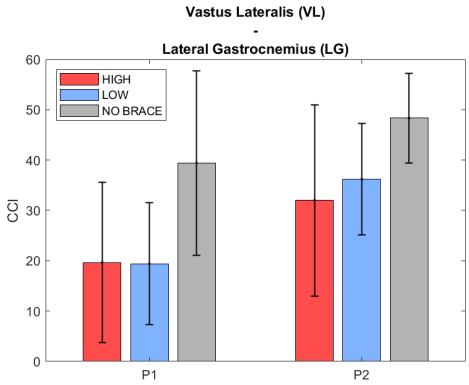

(c) SA: VM-ST CCI.

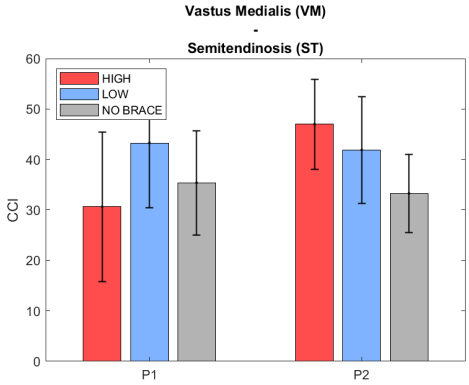

(d) SA: VM-MG CCI.

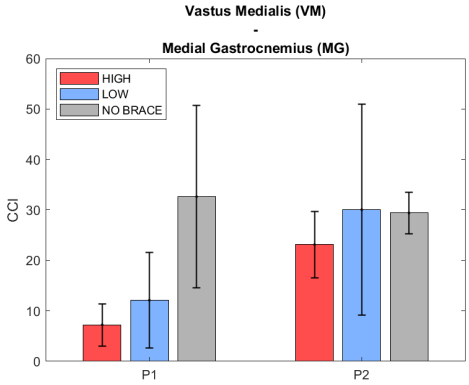

Figure 5.10: Co-Contraccion Index for SA task.

Figure. 5.12 shows the muscle activity as predicted by OpenSim static optimization simulations. The BF, ST, VM, and VL were predicted to increase the force production for the assisted conditions during the first KCF peak. Towards the end, however, the soleus shows increased activity, while MG and LG reduce force production as compared to the no brace condition.

(a) SA: KFA.

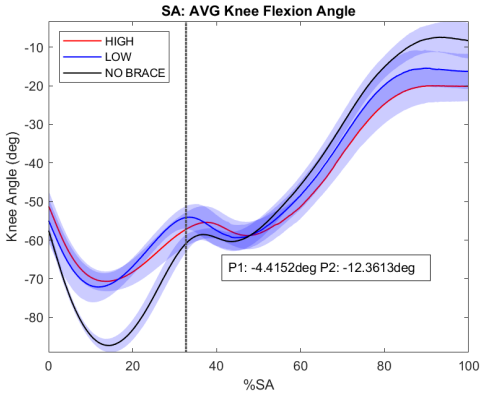

(b) SA: KFM.

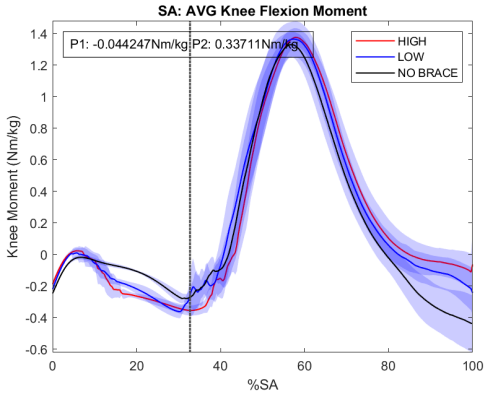

(c) SA: HFA.

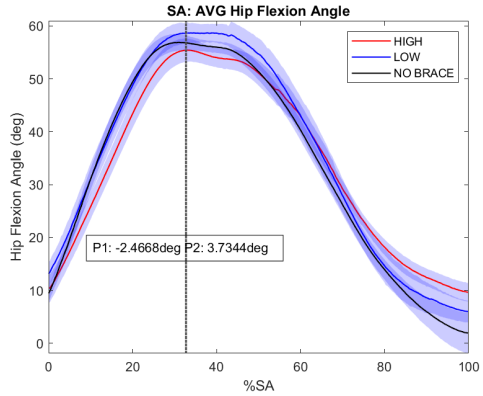

(d) SA: HFM.

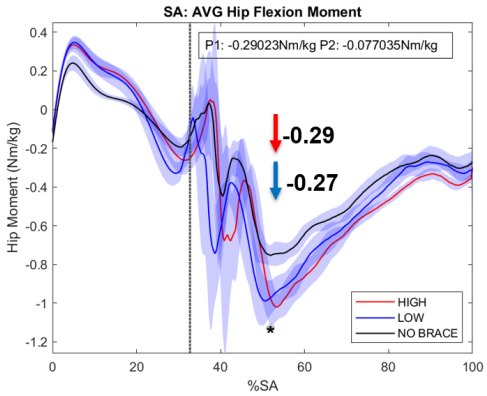

(e) SA: ADA.

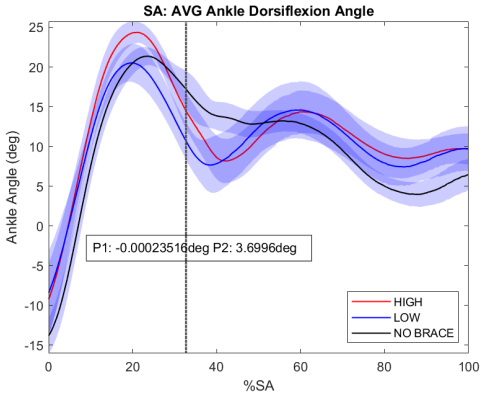

(f) SA: ADM.

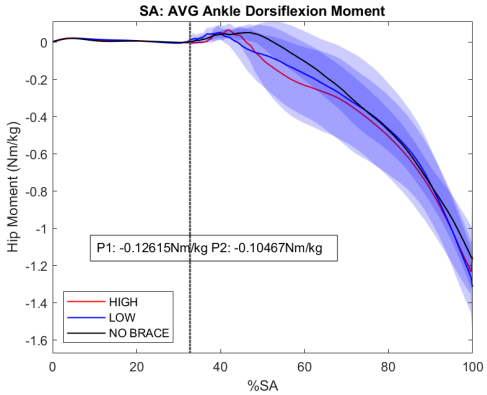

Figure 5.11: Knee, hip, and ankle kinematics and kinetics for SA. The dashed line represents the transition point between leg swing and step up. KFA/KFM = Knee Flexionn Angle/ Moment. HFA/HFM = Hip Flexion Angle/ Moment. ADA/ADM = Ankle Dorsiflexion Angle/ Moment.

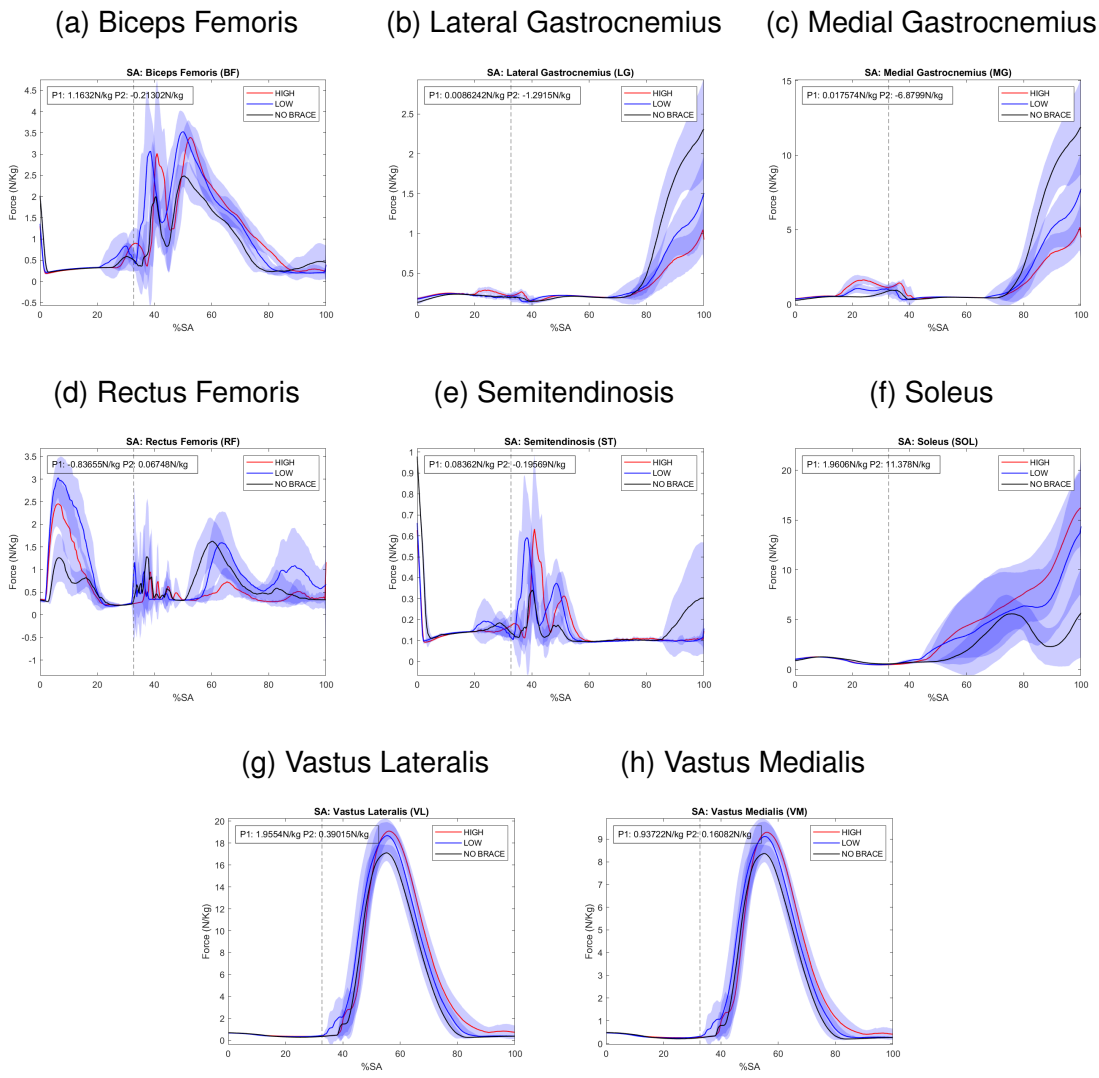

Figure 5.12: Static Optimization results for SA trials. Right leg muscle forces plots normalized to body weight in N/Kg.

The musculoskeletal simulation used an approximation to apply the measured external assistance. The comparison between the measured external knee brace moment and the simulated approximation is shown in Fig. 5.13.

(a) Measured KB-3.0 Moment. (b) Approximated KB-3.0 Moment.

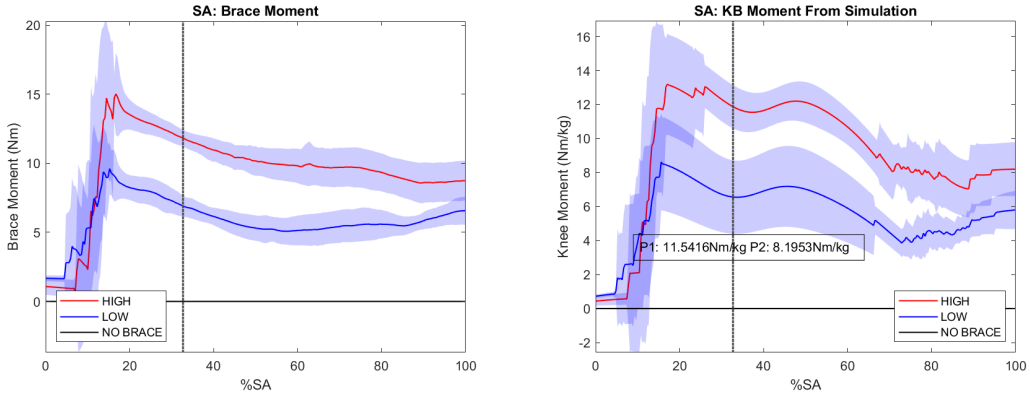

Figure 5.13: Comparison between the KB-3.0 measured external moment and the approximation curved used in the musculoskeletal simulation

5.3.2 Stair Descent (SD)

The result variables for each condition for the SA task are summarized in Table. 5.7. Statistically significant results are highlighted. The only statistically significant KCF change due to the external assistance is a 0.41 BW reduction in medial KCF. As shown in Fig. 5.14 for this task, there is one single KCF peak that occurs during the later portion of the step down eccentric contraction phase (before the contralateral limb makes contact with the floor). Most importantly, this significant reduction is due to the low assistance level; the high assistance condition did not show a statistically significant change in KCF.

Table 5.7: Resulting tibiofemoral contact forces, lower limb kinematics and kinetics for SD task. P1 = Peak 1.

Assistance Level	**High (H)**		**Low (L)**		**No Brace (N)**		**Post-Hoc**				
Prameter	**Mean**	**SD**	**Mean**	**SD**	**Mean**	**SD**	**p-value**	**H-N**	**L-N**	**H-L**	**Cohen's f**
Medial KCF P1 (BW)	2.76	0.19	2.66	0.27	3.07	0.58	**0.0219**	-0.31	**-0.41**	0.10	0.45
Medial KCF P2 (BW)	-	-	-	-	-	-	-	-	-	-	-
Lateral KCF P1 (BW)	1.45	0.25	1.38	0.32	1.54	0.40	0.4431	-0.09	-0.16	0.07	0.20
Lateral KCF P2 (BW)	-	-	-	-	-	-	-	-	-	-	-
Total KCF P1 (BW)	4.15	0.40	3.92	0.65	4.55	0.97	0.0725	-0.40	-0.63	0.23	0.37
Total KCF P2 (BW)	-	-	-	-	-	-	-	-	-	-	-
VL-BF CCI P1	36.29	15.85	39.49	13.25	44.84	8.34	0.2189	-8.55	-5.35	-3.20	0.27
VL-BF CCI P2	-	-	-	-	-	-	-	-	-	-	-
VL-LG CCI P1	16.3	13.11	13.53	10.67	13.56	5.79	0.7200	2.74	-0.03	2.77	0.13
VL-LG CCI P2	-	-	-	-	-	-	-	-	-	-	-
VM-ST CCI P1	31.11	19.91	38.06	17.4	30.84	15.17	0.4755	0.27	7.22	-6.95	0.19
VM-ST CCI P2	-	-	-	-	-	-	-	-	-	-	-
VM-MG CCI P1	32.06	13.82	27.6	11.04	25.04	11.81	0.3018	7.02	2.56	4.46	0.24
VM-MG CCI P2	-	-	-	-	-	-	-	-	-	-	-
Peak KFA (deg)	-72.77	7.29	-76.16	6.42	-81.45	11.43	**0.0376**	**8.68**	5.29	3.39	0.41
Peak KFM (Nm/kg)	1.02	0.14	0.96	0.19	1.01	0.18	0.4058	0.01	-0.05	0.06	0.15
Peak ADA (deg)	43.13	3.66	45.1	2.16	45.7	3.13	0.0786	-2.57	-0.60	-1.97	0.36
Peak ADM (Nm/kg)	-1.29	0.06	-1.22	0.09	-1.24	0.05	**0.0187**	-0.05	0.02	**-0.07**	0.43
Peak HFA (deg)	29.63	2.21	31.06	3.07	30.56	3.03	0.3971	-0.93	0.50	-1.43	0.21
Peak HFM (Nm/kg)	-0.33	0.08	-0.43	0.09	-0.47	0.12	**0.0019**	**0.14**	0.04	**0.10**	0.60

(a) SD: Medial KCF. (b) SA: Lateral KCF.

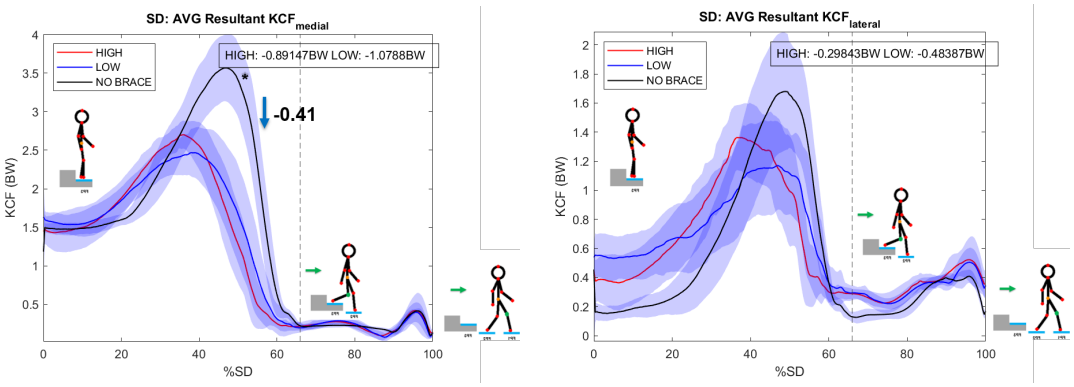

Figure 5.14: Medial and lateral KCF for SD. The dashed line represents the transition point between leg swing and step up.

No statistically significant differences were found for medial or lateral CCI, rejecting our hypothesis (Fig. 5.15). However, Fig. 5.17 suggests that some muscle force reduction may occur nonetheless, showing a reduction of up to 4.3 N/kg in quadriceps force production at the peak KCF.

While, as hypothesized, the hip joint was more loaded during the high assistance condition, this higher HFM occurred after the step down eccentric contraction (Fig. 5.16). During the eccentric contraction phase,the HFM remains the same across all conditions. As expected, however, the maximum KFA was limited by the knee brace during the knee brace condition, showing a reduction of $8.68°$ between the high assistance level and the no brace condition.

(a) SD: VL-BF CCI.

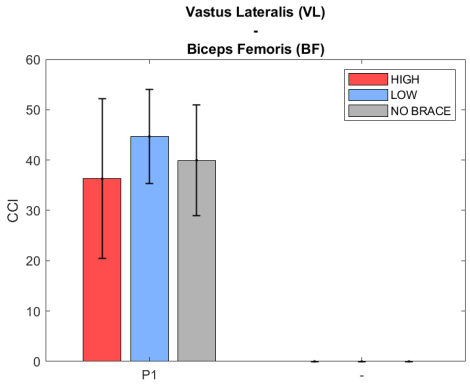

(b) SD: VL-LG CCI.

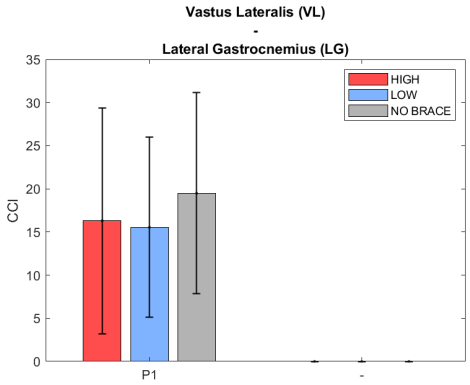

(c) SD: VM-ST CCI.

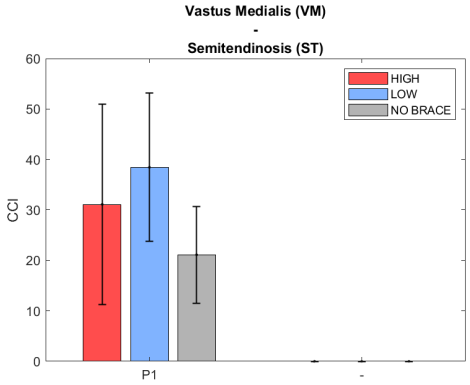

(d) SD: VM-MG CCI.

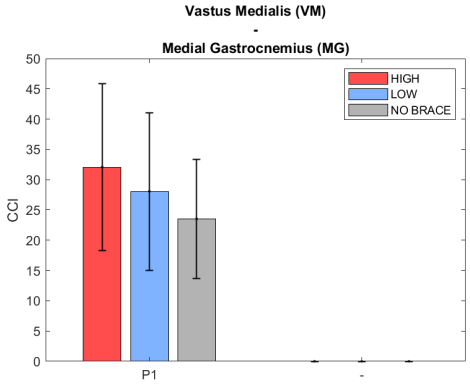

Figure 5.15: Co-Contraccion Index for SD task.

Figure. 5.12 shows the muscle activity as predicted by OpenSim static optimization simulations. The BF, ST, VM, and VL were predicted to increase the force production for the assisted conditions during the first KCF peak. Towards the end, however, the soleus shows increased activity, while MG and LG reduce force production as compared to the no brace condition.

(a) SD: KFA.

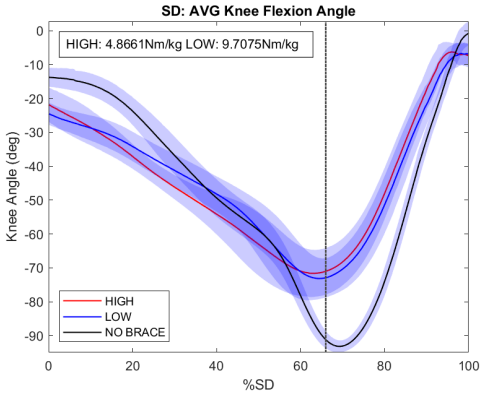

(b) SD: KFM.

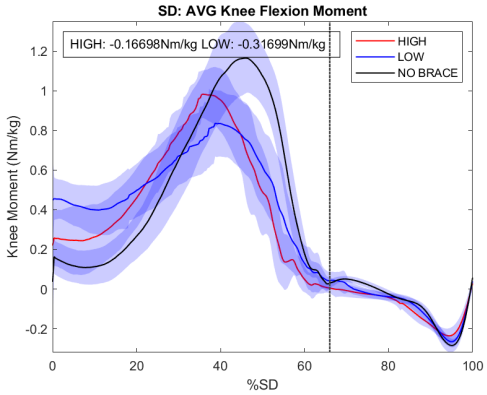

(c) SD: HFA.

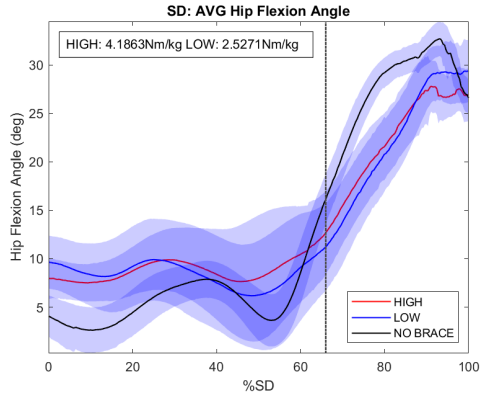

(d) SD: HFM.

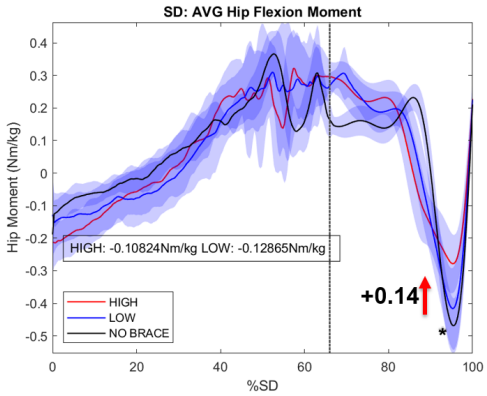

(e) SD: ADA.

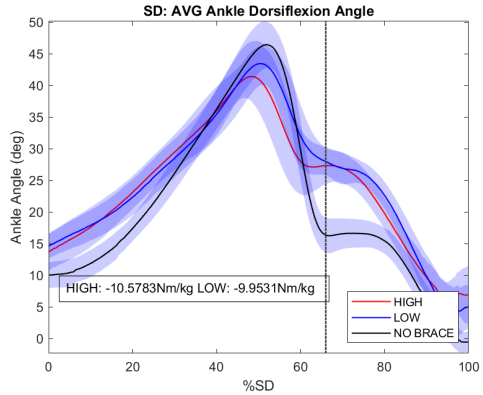

(f) SD: ADM.

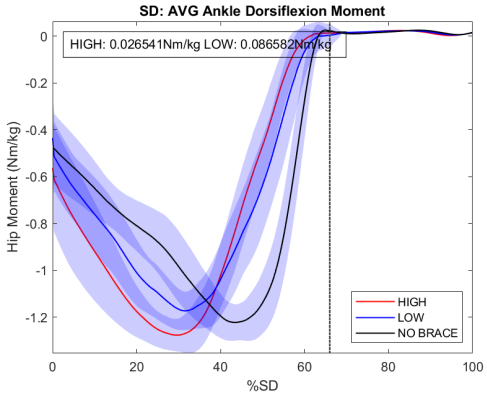

Figure 5.16: Knee, hip, and ankle kinematics and kinetics for SD. The dashed line represents the transition point between leg swing and step-up. KFA/KFM = Knee Flexion Angle/ Moment. HFA/HFM = Hip Flexion Angle/ Moment. ADA/ADM = Ankle Dorsiflexion Angle/ Moment.

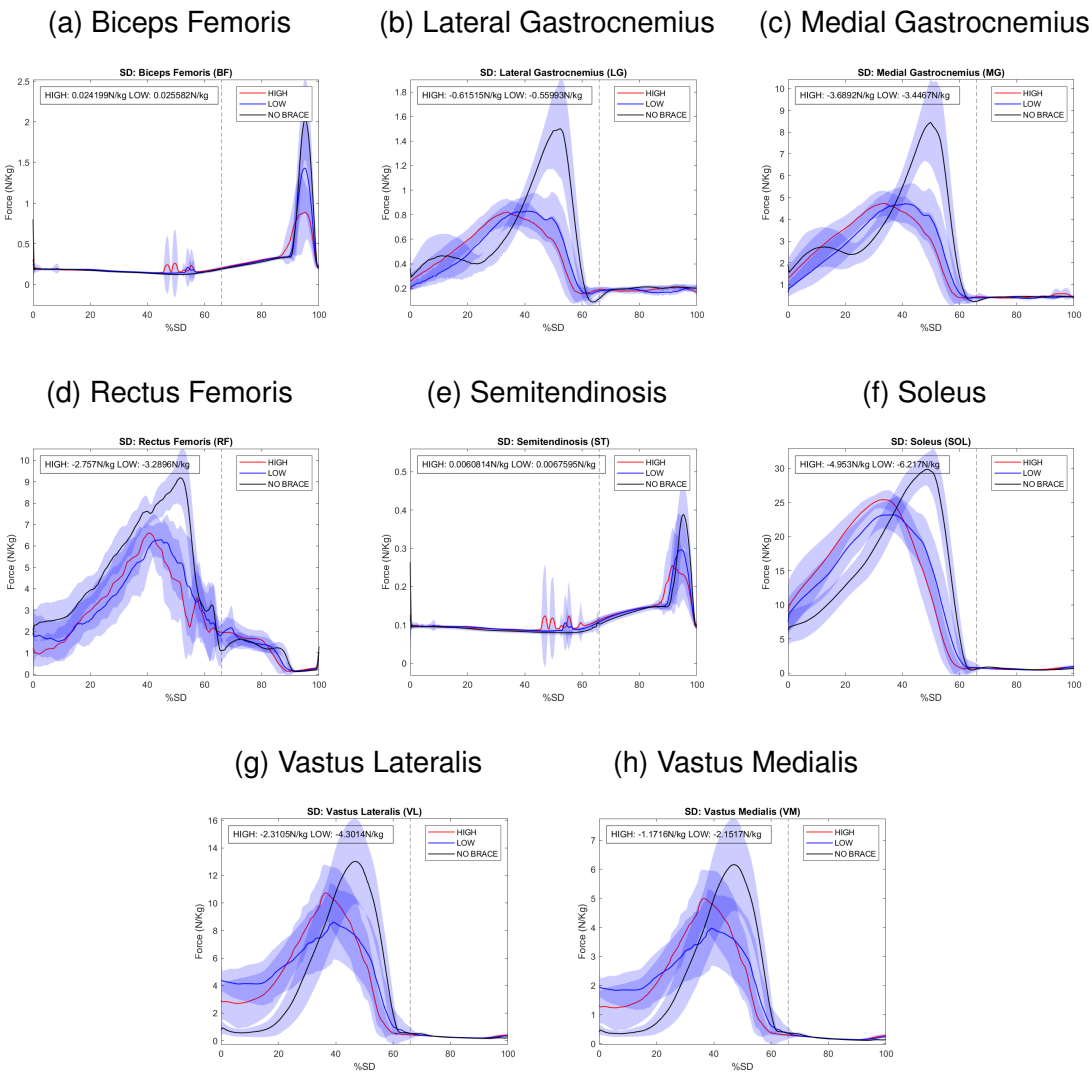

Figure 5.17: Static Optimization results for SA trials. Right leg muscle forces plots normalized to body weight in N/Kg.

The measured external assistance. The comparison between the measured external knee brace moment and the simulated approximation for the SD task is shown in Fig. 5.18. As we can observe, the assistive moment increases during eccentric contraction, until the energy release is triggered.

(a) Measured KB-3.0 Moment. (b) Approximated KB-3.0 Moment.

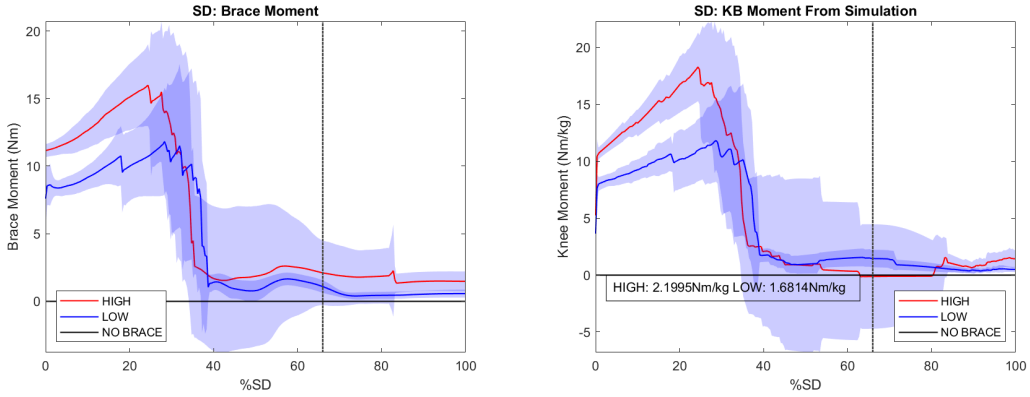

Figure 5.18: Comparison between the KB-3.0 measured external moment and the approximation curved used in the musculoskeletal simulation

5.3.3 Stand-to-Sit-to-Stand (STS)

The result variables for each condition for the STS task are summarized in Table. 5.8. Statistically significant results are highlighted.

Table 5.8: Resulting tibiofemoral contact forces, lower limb kinematics and kinetics for STS task. P1 = Peak 1, P2 = Peak 2.

Assistance Level	**High (H)**		**Low (L)**		**No Brace (N)**		**Post-Hoc**				
Prameter	**Mean**	**SD**	**Mean**	**SD**	**Mean**	**SD**	**p-value**	**H-N**	**L-N**	**H-L**	**Cohen's f**
Medial KCF P1 (BW)	1.28	0.13	1.66	0.48	3.12	0.26	**1.25E-07**	**-1.84**	**-1.46**	-0.38	2.45
Medial KCF P2 (BW)	2.90	0.29	3.41	0.28	4.10	0.17	**2.72E-06**	**-1.20**	**-0.69**	**-0.51**	1.95
Lateral KCF P1 (BW)	1.52	0.07	1.56	0.10	2.82	0.14	**1.04E-12**	**-1.30**	**-1.26**	-0.04	5.59
Lateral KCF P2 (BW)	2.41	0.10	2.70	0.21	3.01	0.14	**4.60E-05**	**-0.60**	**-0.31**	**-0.29**	1.56
Total KCF P1 (BW)	2.61	0.15	2.96	0.51	5.39	0.36	**1.93E-09**	**-2.78**	**-2.43**	-0.35	3.33
Total KCF P2 (BW)	4.77	0.34	5.58	0.52	6.41	0.18	**1.26E-06**	**-1.64**	**-0.83**	**-0.81**	1.79
VL-BF CCI P1	27.80	7.99	38.36	12.36	44.08	6.01	**0.0235**	**-16.28**	-5.72	-10.56	0.74
VL-BF CCI P2	34.09	2.61	39.76	2.79	32.91	9.99	0.1557	1.18	6.85	-5.67	0.48
VL-LG CCI P1	36.81	12.82	35.21	16.22	37.70	14.19	0.9554	-0.89	-2.49	1.60	0.06
VL-LG CCI P2	44.48	3.52	45.46	4.18	34.67	8.07	**0.0082**	**9.81**	**10.79**	-0.98	0.87
VM-ST CCI P1	27.75	8.39	23.85	15.11	42.50	12.74	**0.047**	-14.75	**-18.65**	3.90	0.65
VM-ST CCI P2	37.98	6.29	17.21	2.79	23.23	7.53	**6.25E-05**	**14.75**	-6.02	**20.77**	1.48
VM-MG CCI P1	41.09	13.94	34.63	14.81	42.35	9.11	0.5503	-1.26	-7.72	6.46	0.27
VM-MG CCI P2	52.03	2.80	29.96	8.00	30.34	9.27	**9.74E-05**	**21.69**	-0.38	**22.07**	1.42
Peak KFA (deg)	-102.32	1.55	-105.22	2.92	-111.72	3.47	**0.0001**	**9.40**	**6.50**	2.90	1.42
Peak KFM (Nm/kg)	0.88	0.06	1.12	0.15	1.30	0.08	**1.20E-05**	-0.42	-0.18	-0.24	1.64
Peak ADA (deg)	22.52	2.34	23.68	2.95	31.35	0.70	**8.00E-06**	**-8.83**	**-7.67**	-1.16	1.77
Peak ADM (Nm/kg)	-0.33	0.04	-0.19	0.10	-0.13	0.08	**0.002**	**-0.20**	-0.06	**-0.14**	1.08
Peak HFA (deg)	88.77	1.35	88.64	1.53	101.92	1.12	**1.89E-11**	**-13.15**	**-13.28**	0.13	4.64
Peak HFM (Nm/kg)	-1.21	0.06	-1.24	0.09	-0.86	0.12	**4.53E-06**	**-0.35**	**-0.38**	0.03	1.85

Figure 5.19 shows the medial and lateral KCF curves for all three conditions of the STS task, and statistically significant changes in peak KCF are shown.

(a) STS: Medial KCF.

(b) STS: Lateral KCF.

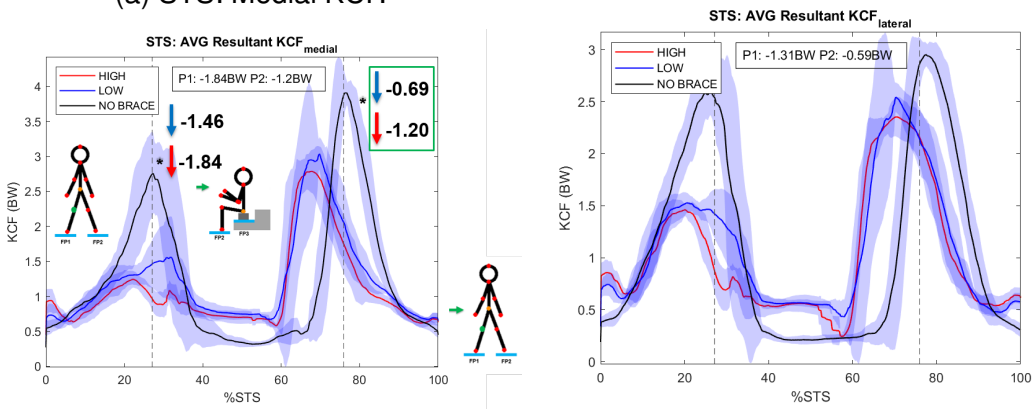

Figure 5.19: Medial and lateral KCF for STS. The dashed lines represent the transition points between standing up and sitting down.

The plots reveal two peak KCF locations, one at about 26 %, during sitting down eccentric contraction, and one at the beginning of the concentric contraction during the standing up motion. Both peaks exhibited statistically significant KCF reduction. Moreover, a statistically significant difference between levels of assistance was observed for the second peak medial KCF, with the low assistance level achieving a reduction of 0.69 BW, while the high assistance level achieved 1.20 BW. Likewise, the second lateral and second total peak KCF reduction magnitude were dependent on the assistance level.

The VL-BF CCI showed a reduction of 16.28 at the first peak for the high assistance condition (Fig. 5.20), which is in agreement with the observed KCF reductions. VL-LG CCI increased for both assistance levels during the second peak, however, no significant difference was found for VL-BF at this point. Similarly, VM-

MG showed an increased 21.69 in CCI for the second peak KCF, and VL-LG was higher by 14.75, however, no significant increase was observed in medial CCI for the first peak. Moreover, VM-ST CCI was reduced by 18.65 at the first peak for the low assistance condition.

(a) STS: VL-BF CCI.

(b) STS: VL-LG CCI.

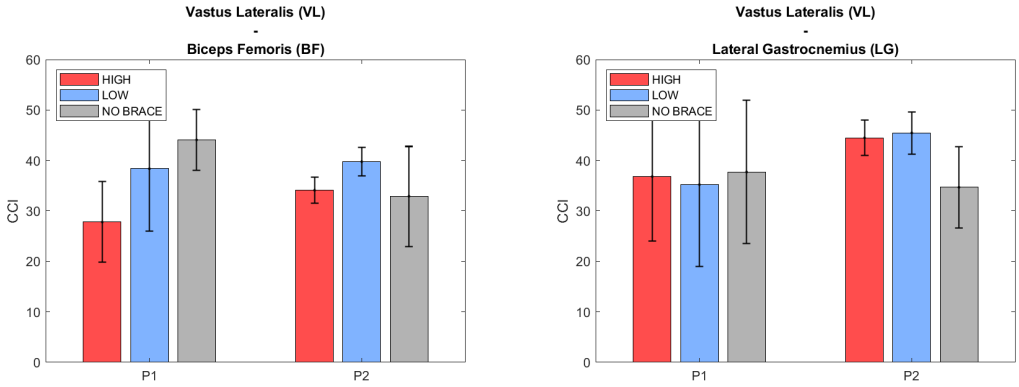

(c) STS: VM-ST CCI.

(d) STS: VM-MG CCI.

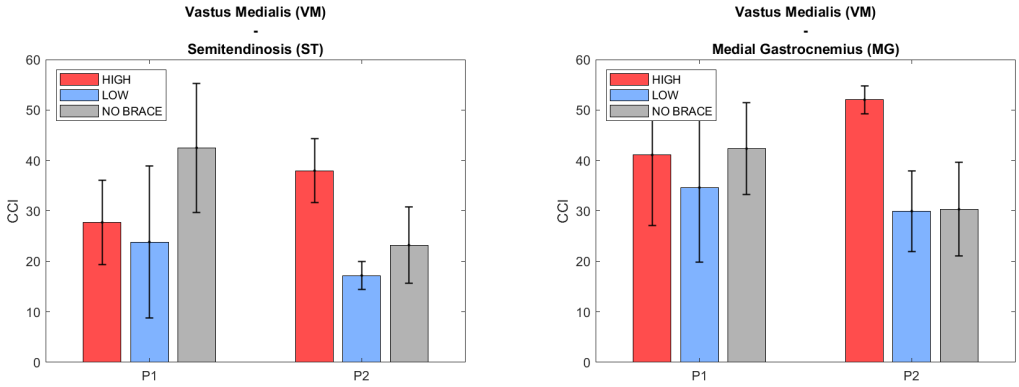

Figure 5.20: Co-Contraccion Index for STS task.

Peak KFA was reduced by $9.40°$ with the high assistance level. While a reduction of $6.50°$ was observed for the low assistance level, no statistically significant difference was observed between levels of assistance. Peak KFM was reduced by 0.42 Nm/kg and 0.18 Nm/kg for the high and low assistance levels respectively, and a statistically significant difference was found between these two effects.

The adjacent joints also experienced a reduced overall moment production, with the peak HFM reduced by 0.35 Nm/kg, and the ADM reduced by 0.2 Nm/kg during the high assistance trials. This rejects our hypothesis that the adjacent joints would increase torque production under knee assistance. This hypothesis was taken because a compensatory response at adjacent joints was expected based on the results found in Chapter 3.

(a) STS: KFA.

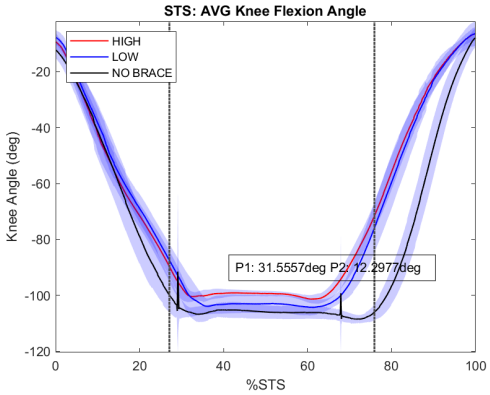

(b) STS: KFM.

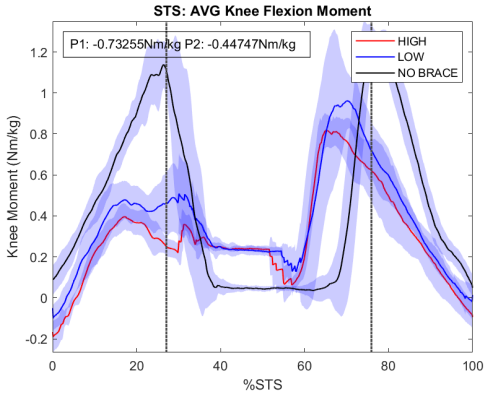

(c) STS: HFA.

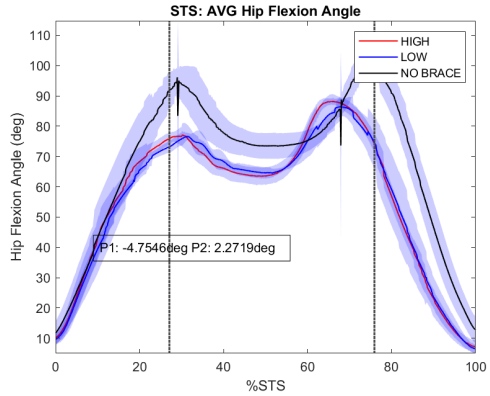

(d) STS: HFM.

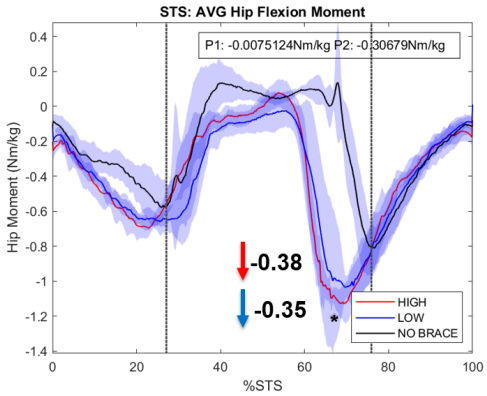

(e) STS: ADA.

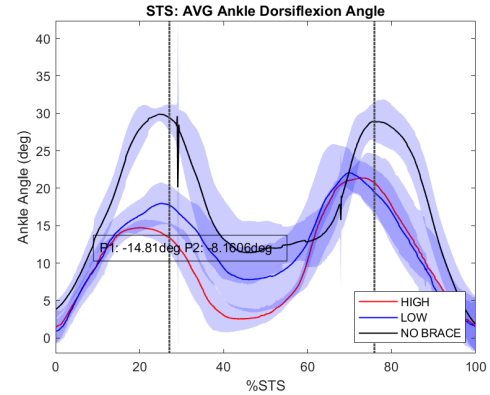

(f) STS: ADM.

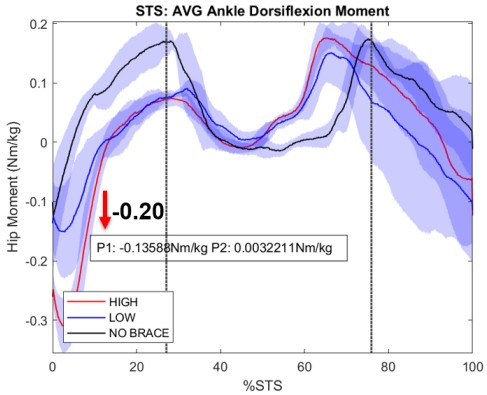

Figure 5.21: Knee, hip, and ankle kinematics and kinetics for STS. The dashed line represents the transition points between standing up and sitting down. KFA/KFM = Knee Flexion Angle/ Moment. HFA/HFM = Hip Flexion Angle/ Moment. ADA/ADM = Ankle Dorsiflexion Angle/ Moment.

Figure. 5.22 shows the muscle activity as predicted by OpenSim static opti-

mization simulations. While force production by VL and VM is reduced, increased activity is observed for MG, LG, and ST, which agrees with the increases observed in CCI.

(a) Biceps Femoris (b) Lateral Gastrocnemius (c) Medial Gastrocnemius

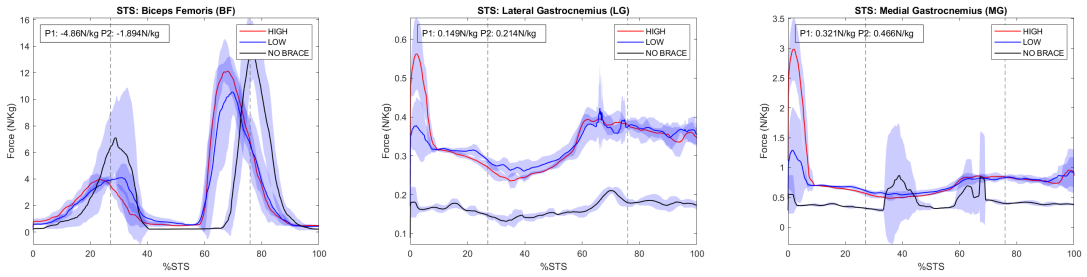

(d) Rectus Femoris (e) Semitendinosis (f) Soleus

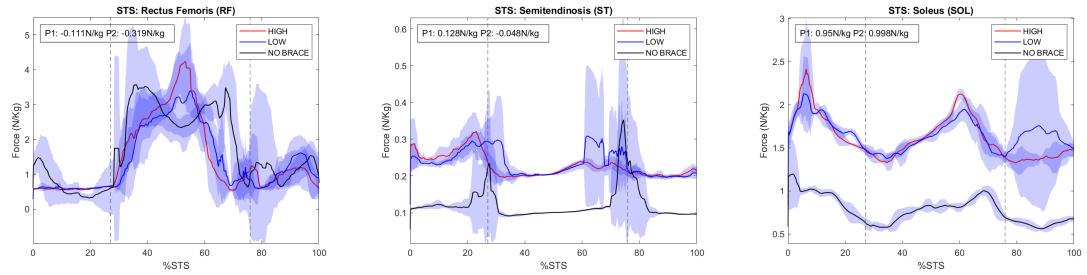

(g) Vastus Lateralis (h) Vastus Medialis

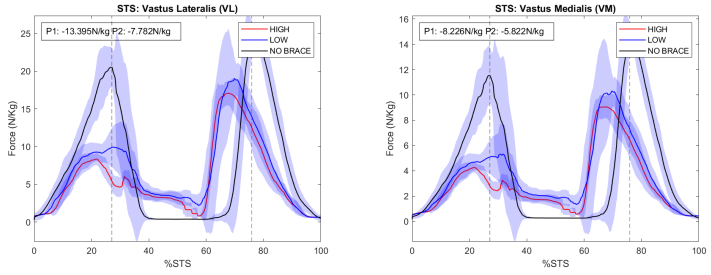

Figure 5.22: Static Optimization results for SA trials. Right leg muscle forces plots normalized to body weight in N/Kg.

The comparison between the measured external knee brace moment and the simulated approximation for the STS task are shown in Fig. 5.23. As we can observe, the assistive moment increases during eccentric contraction; this absorbed

elastic energy is stored, and later released during concentric contraction of the quadriceps.

(a) Measured KB-3.0 Moment. (b) Approximated KB-3.0 Moment.

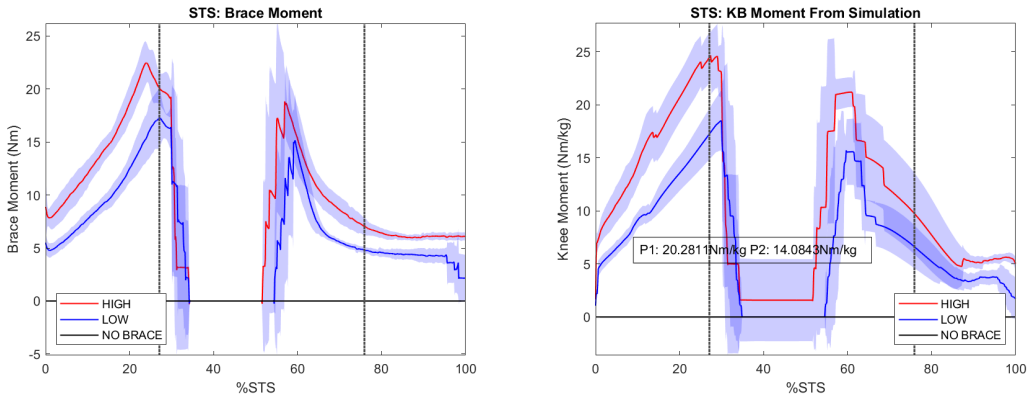

Figure 5.23: Comparison between the KB-3.0 measured external moment and the approximation curved used in the musculoskeletal simulation

5.3.4 Level Walking (W)

The result variables for each condition for the W task are summarized in Table. 5.9. Statistically significant results are highlighted.

Figure 5.24 shows the medial and lateral KCF curves for the two conditions tested for the W task, and statistically significant changes in peak KCF are shown. Two peaks were observed; the first peak occurs during early stance, and an increased medial and lateral KCF was observed as 0.87 BW and 0.21 BW respectively. The second peak occurs during late stance on the medial condyle, and a reduction of 0.64 BW was quantified. This reduction is in agreement with a statistically significant VM-MG CCI reduction of 25.74 (Fig. 5.25).

(a) W: Medial KCF. (b) W: Lateral KCF.

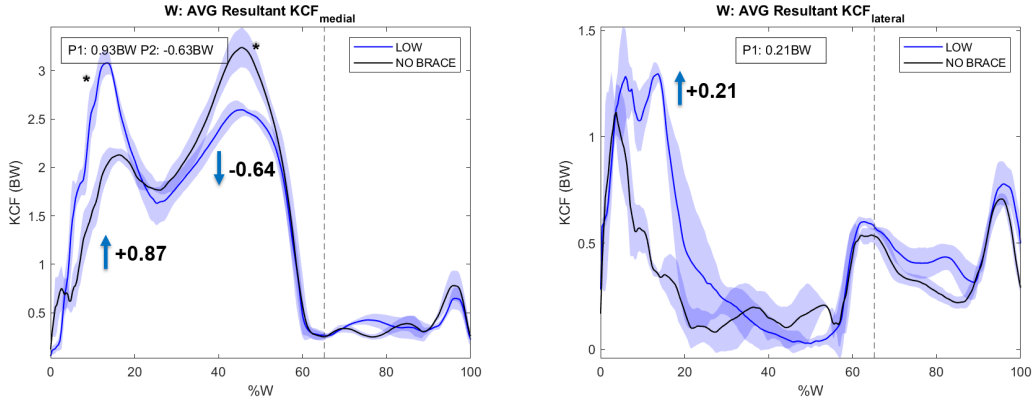

Figure 5.24: Medial and lateral KCF for STS. The dashed lines represent the transition points between standing up and sitting down.

(a) STS: VM-ST CCI. (b) STS: VM-MG CCI.

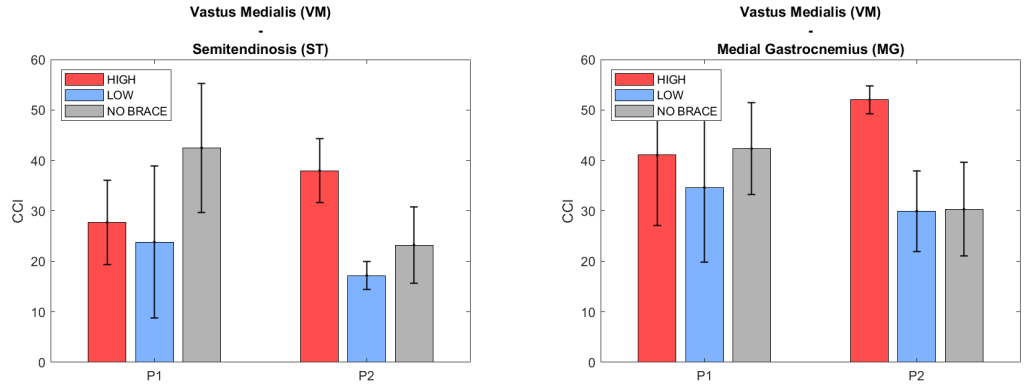

Figure 5.25: Co-Contraccion Index for STS task. Lateral CCI is not included due to technical issues with the VL EMG transducer

The increased peak KCF during early stance can be associated with a more flexed knee joint during this phase (Fig. 5.26). The hip joint was also more flexed $+2.75°$, suggesting a slightly crouched posture as compared to the no brace condition.

The external assistance caused an increased KFM at the first peak KCF, suggesting increased muscular activity, as opposed to what was hypothesized. This

Table 5.9: Resulting tibiofemoral contact forces, lower limb kinematics and kinetics for W task. P1 = Peak 1, P2 = Peak 2.

Assistance Level	**Low (L)**		**No Brace (N)**				
Prameter	**Mean**	**SD**	**Mean**	**SD**	**p-value**	**H-N**	**Cohen's d**
Medial KCF P1 (BW)	3.02	0.12	2.15	0.07	**1.09E-05**	0.87	8.86
Medial KCF P2 (BW)	2.61	0.09	3.25	0.21	**0.0013**	-0.64	3.96
Lateral KCF P1 (BW)	1.40	0.13	1.19	0.06	**0.0285**	0.21	2.07
Lateral KCF P2 (BW)	-	-	-	-	**-**	**-**	-
Total KCF P1 (BW)	4.38	0.12	2.53	0.13	**6.91E-07**	1.85	14.79
Total KCF P2 (BW)	2.63	0.16	3.23	0.27	**0.0077**	-0.60	2.70
VL-BF CCI P1	-	-	-	-	-	-	-
VL-BF CCI P2	-	-	-	-	-	-	-
VL-LG CCI P1	-	-	-	-	-	-	-
VL-LG CCI P2	-	-	-	-	**-**	**-**	-
VM-ST CCI P1	88.34	134.86	6.82	6.54	0.2727	81.52	0.85
VM-ST CCI P2	22.74	7.26	20.17	2.56	0.5305	2.57	0.47
VM-MG CCI P1	10.09	39.36	31.30	57.85	0.9875	-21.21	0.43
VM-MG CCI P2	4.30	5.28	30.04	3.19	**1.16E-04**	-25.74	5.90
Peak KFA (deg)	-59.40	15.16	-68.62	1.16	0.1818	9.22	0.86
Peak KFM (Nm/kg)	1.16	0.06	0.40	0.04	**4.83E-07**	0.76	14.90
Peak ADA (deg)	15.12	1.70	6.70	0.65	**9.05E-05**	8.42	6.54
Peak ADM (Nm/kg)	-1.43	0.05	-1.35	0.04	0.0557	-0.08	1.45
Peak HFA (deg)	28.35	0.69	25.60	0.56	**8.21E-04**	2.75	4.37
Peak HFM (Nm/kg)	-1.03	0.55	-1.16	0.12	0.0889	0.13	0.33

can be corroborated with Fig. 5.27, where VM and VL have an increased force production of 8.29 N/kg and 3.75 N/kg respectively.

Table 5.10: Muscle activity changes at peak KCF for the W trials.

Muscle	**P1 (↑)**	**P2 (↓)**	KCF Contributor?
BF	0	0	YES
LG	0	$\downarrow -0.92\ N/kg$	YES
MG	0	$\downarrow -4.57\ N/kg$	YES
RF	0	$\uparrow 0.87\ N/kg$	YES
ST	0	0	YES
SOL	$\uparrow 1.03\ N/kg$	$\uparrow 10.16\ N/kg$	NO
VL	$\uparrow 8.29\ N/kg$	0	YES
VM	$\uparrow 3.75\ N/kg$	0	YES

(a) W: KFA.

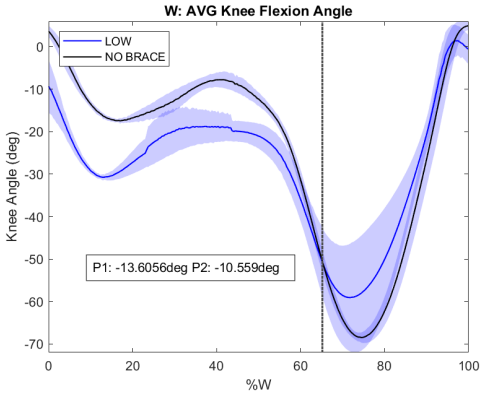

(b) W: KFM.

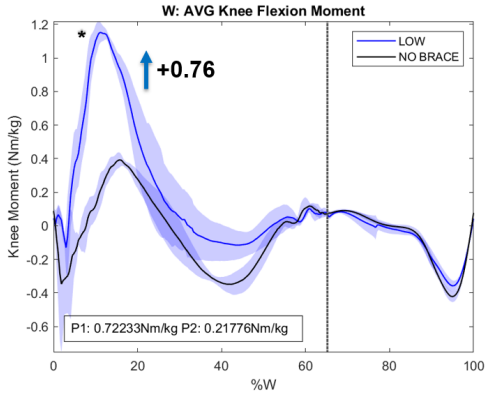

(c) W: HFA.

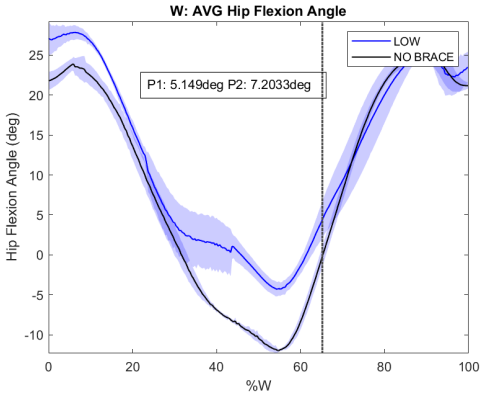

(d) W: HFM.

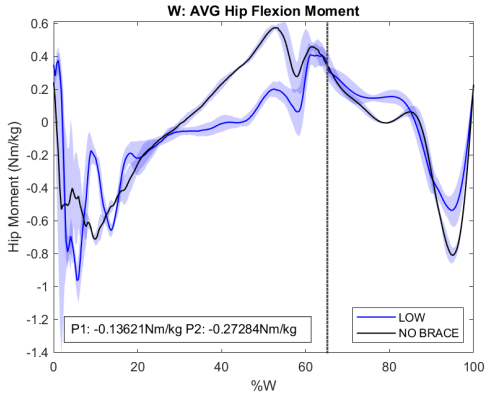

(e) W: ADA.

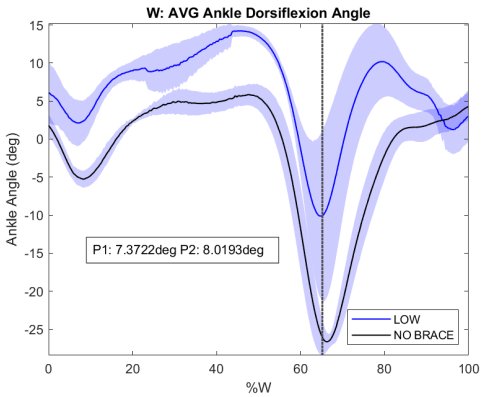

(f) W: ADM.

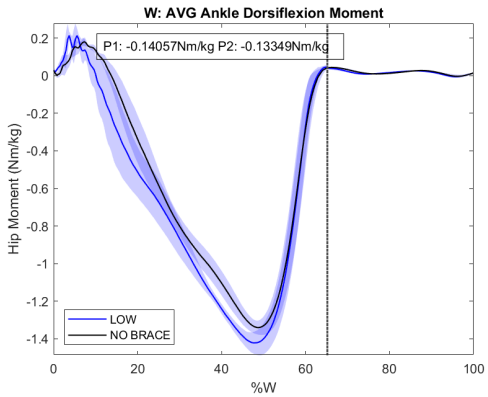

Figure 5.26: Knee, hip, and ankle kinematics and kinetics for W. The dashed line represent the transition points between stance phase and swing phase. KFA/KFM = Knee Flexionn Angle/ Moment. HFA/HFM = Hip Flexion Angle/ Moment. ADA/ADM = Ankle Dorsiflexion Angle/ Moment.

(a) Biceps Femoris (b) Lateral Gastrocnemius (c) Medial Gastrocnemius

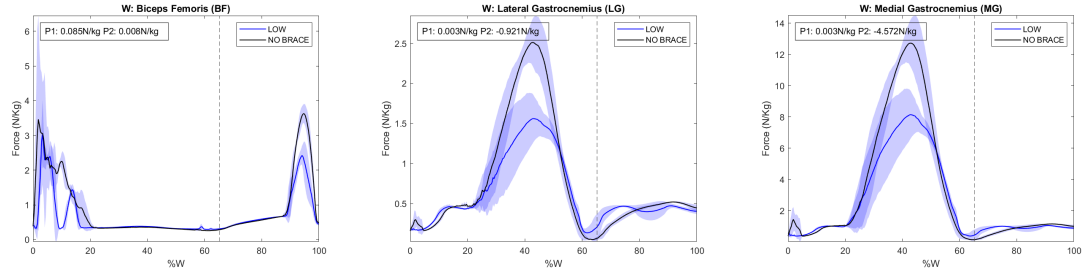

(d) Rectus Femoris (e) Semitendinosis (f) Soleus

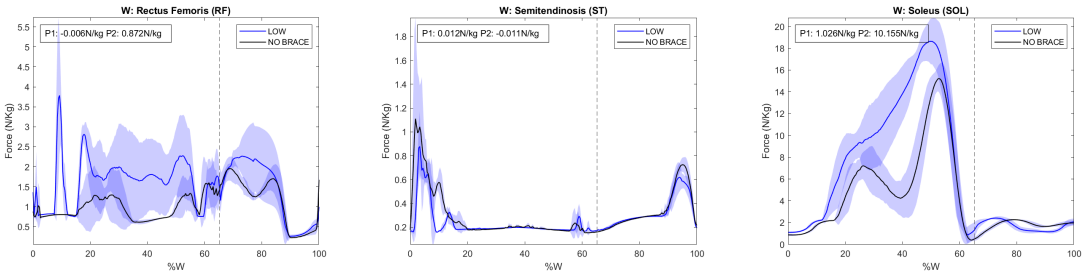

(g) Vastus Lateralis (h) Vastus Medialis

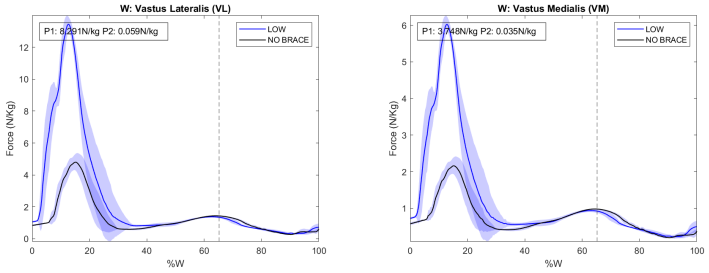

Figure 5.27: Static Optimization results for W trials. Right leg muscle forces plots normalized to body weight in N/Kg.

The comparison between the measured external knee brace moment and the simulated approximation for the W task is shown in Fig. 5.28. The knee brace starts with a preload to apply external moment during stance phase. This moment is disengaged during the swing phase.

(a) Measured KB-3.0 Moment.

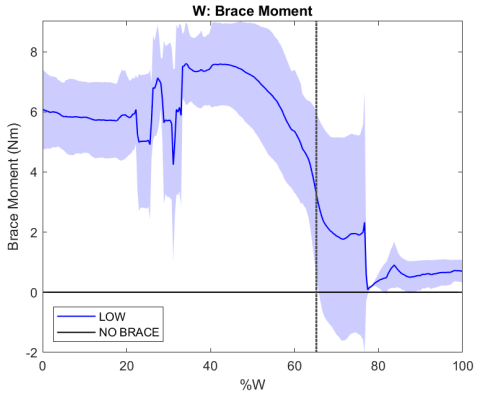

(b) Approximated KB-3.0 Moment.

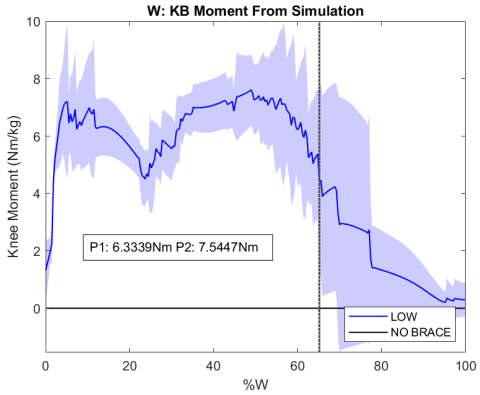

Figure 5.28: Comparison between the KB-3.0 measured external moment and the approximation curved used in the musculoskeletal simulation

5.4 Discussion

5.4.1 Stair Ascent

The KCF patterns estimated in our simulations are similar to those found in the literature. Fig. 5.29 shows a comparison between our total resultant KCF magnitude during SA and the pattern found by Costigan et al. (2002). While Costigan et al. (2002) analyzed the SA task including the swing phase and the stance phase until toe-off, we analyzed the stance phase until contralateral heel-strike, located at approximately 80 % in the plots by Costigan et al. (2002).

For this task, we hypothesized that the KCF would be reduced by a higher external knee brace assistive moment. While the second peak KCF showed a reduction of 0.84 BW for the medial KCF, there was a significant increase of 0.21 BW in the first peak medial KCF. Therefore we reject our hypothesis for the first peak

(a) SA: Total KCF.

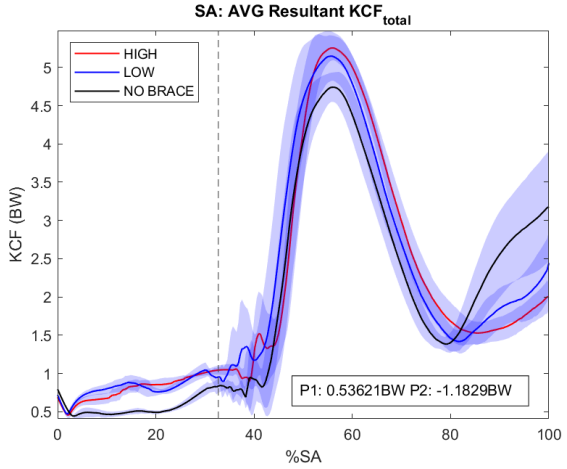

(b) SA: KCF from Costigan et al. (2002).

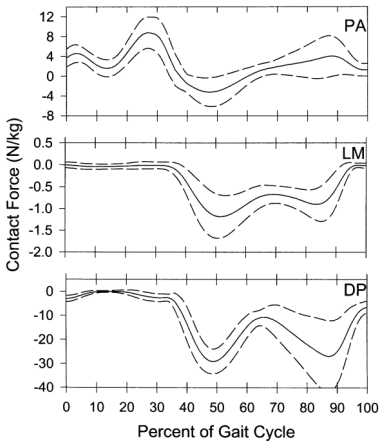

Figure 5.29: KCF comparison with the literature for the SA task. DP represents the distal-proximal KCF in Costigan et al. (2002), comparable to our total resultant KCF.

medial KCF.

The medial CCI was found to decrease by 25.40 for the high assistance condition during the first peak, and to increase by 13.71 during the second peak. Due to this inverse relationship as compared with medial KCF, the increased medial KCF magnitude can not be explained through CCI. Figure 5.30 shows the direct comparison between muscle activation as predicted by musculoskeletal simulation, and envelope EMG as obtained from measured data. We can clearly observe a discrepancy in VL, VM, RF, and SOL activation timings. This suggests that the effects of the knee brace assistance might be better explained through CCI values for the SA task. While a reduced medial CCI was determined, as hypothesized, no significant difference was detected between levels of assistance.

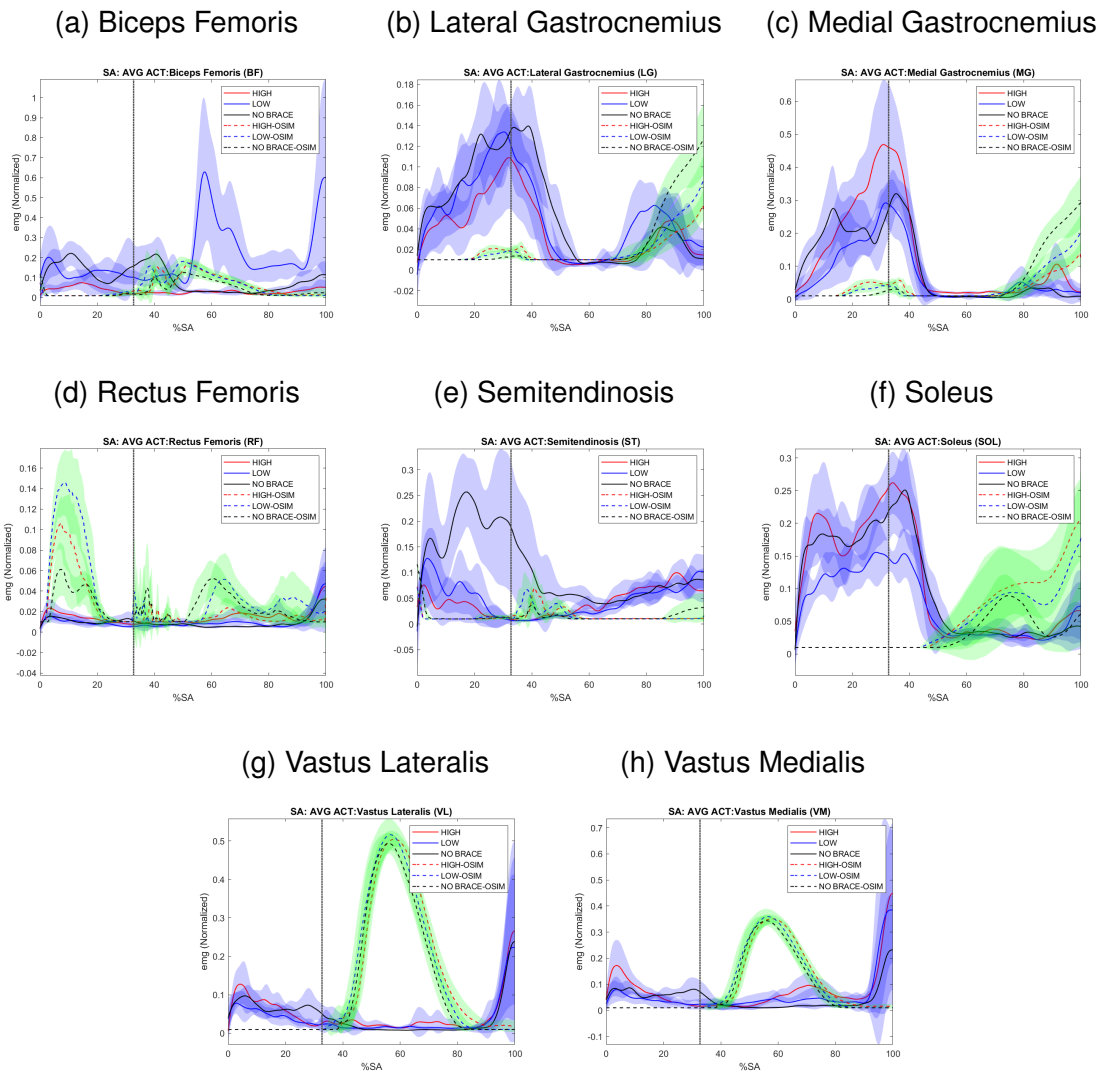

Figure 5.30: Normalized EMG envelope and predicted OpenSim muscle activation SA.

The hip extension moment was increased as a result of the external knee brace assistance. This confirms our hypothesis that this adjacent joint would be more loaded when knee assistance was provided. The knee brace timing, however, was not optimal, and this might have contributed to increased BF and ST activity, and higher hip extension moment during the step-up phase. Figure 5.31 shows the stored force magnitude on the knee brace, as compared with KCF and KFA. We

can observe that the energy release is triggered at the maximum KFA of $-70°$, while the peak KCF occurred between $-50°$ and $-55°$. The energy storage and release behavior is observed, nonetheless, as the stored force is held constant until the release point.

(a) High Assistance. (b) Low Assistance.

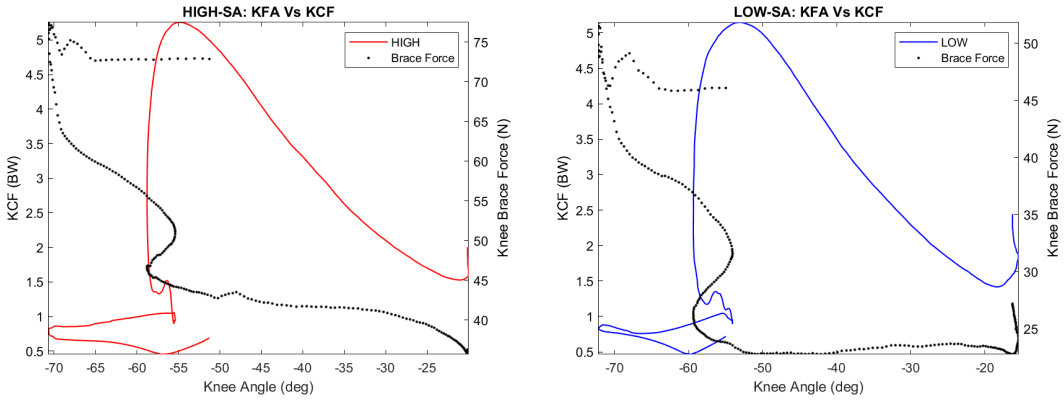

Figure 5.31: Stored force magnitude on the knee brace compared with KCF and KFA for SA trials.

SA: Subject Personal Assessment

The subject reported perceiving the device's assistance upon engagement. However, the engagement timing felt to happen before the maximum perceived force was exerted by the quads. This is in agreement with the timing discrepancy reported between the knee brace engagement and the peak KCF.

5.4.2 Stair Descent

Konrath et al. (2019) explored the KCF pattern during stair descent; Fig. 5.32 shows the comparison with our estimated KCF pattern. Our pattern includes the

late stance and the full swing phase, resembling the last 50 % of the plot by Konrath et al. (2019) plus the swing phase after toe-off.

(a) SD: Total KCF.

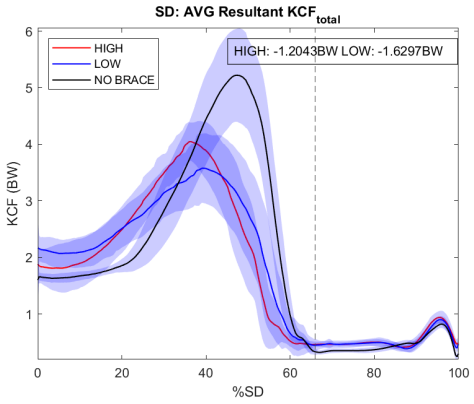

(b) SD: KCF from Konrath et al. (2019).

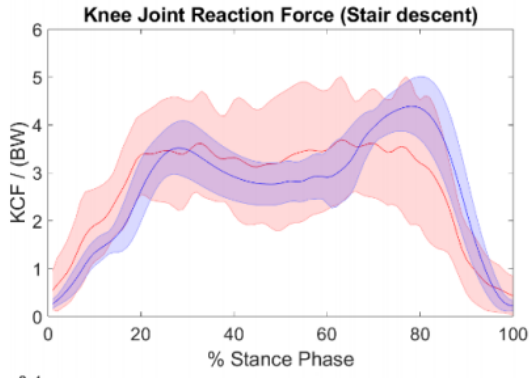

Figure 5.32: KCF comparison with the literature for the SD task.

For this task, we also hypothesized that the KCF would be reduced by a higher external knee brace assistive moment. The low-level assistance achieved a 0.41 BW reduction in peak KCF, the high assistance, however, did not achieve any statistically significant KCF reduction. This might suggest that an optimal tuning point exists for the magnitude of the external assistance to be provided in order to achieve a significant peak KCF reduction.

While the CCI did not show any statistically significant changes, Fig. 5.34 shows that the activation timings from the static optimization simulations were in agreement, up to some degree, with the analyzed envelope EMG signals. This suggests that the muscle force reductions shown in Fig. 5.17 could be used to explain the reduced peak KCF magnitude, however, a more robust and statistically powerful experiment would be needed.

The accurate timing for KB 3.0 energy release is also in agreement with the

reduction in medial pea KCF. As observed in Fig. 5.33, the disengagement point occurs shortly after the peak KCF at around 50° of knee flexion, helping absorb the eccentric loads at the knee joint during the peak KCF.

(a) High Assistance. (b) Low Assistance.

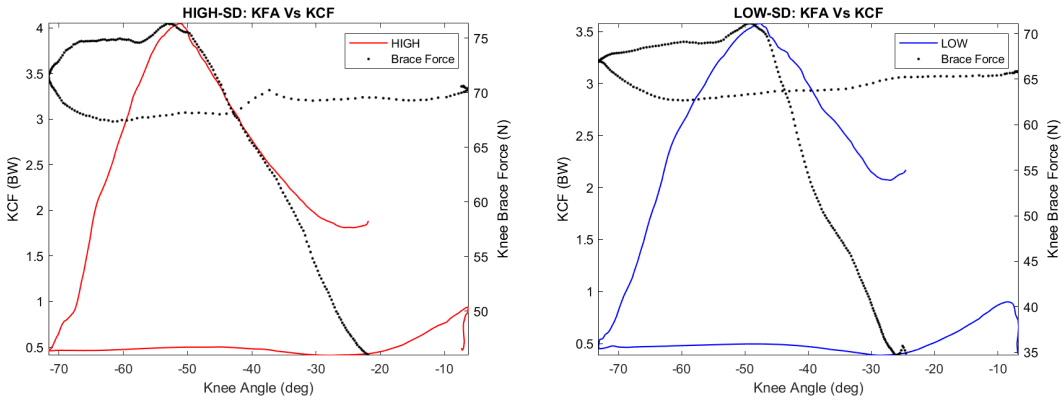

Figure 5.33: Stored force magnitude on the knee brace compared with KCF and KFA for SD trials.

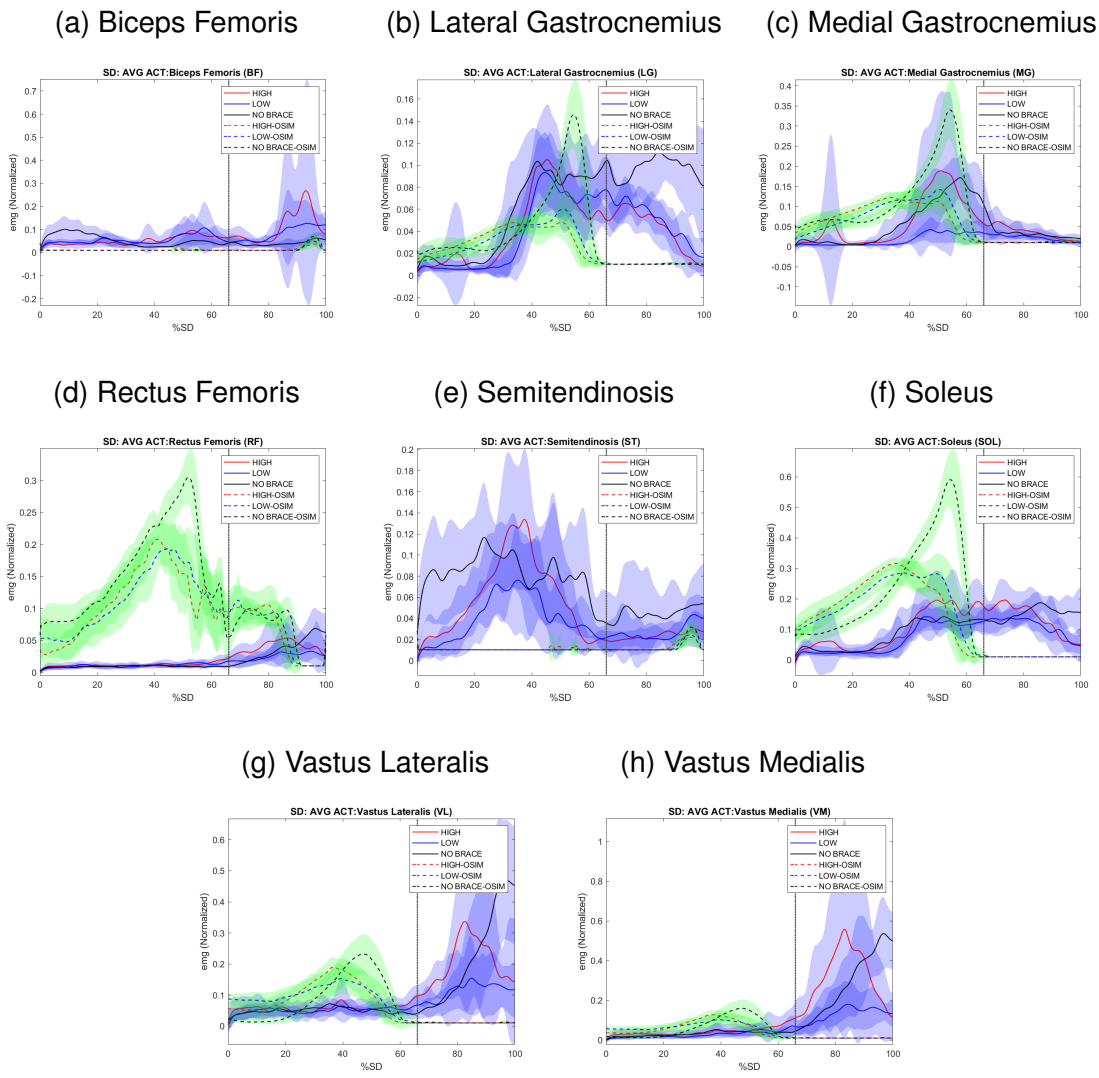

Figure 5.34: Normalized EMG envelope and predicted OpenSim muscle activation for SD trials.

SD: Subject Personal Assessment

The subject reported perceiving the knee brace assistance during eccentric contraction. In some trials, however, the unassisted leg was perceived to have a higher impact force at ground contact, which may imply bigger peak KCF at the unassisted knee. Lastly, the subject felt a tendency to internally rotate the hip during leg swing

after the eccentric contraction.

5.4.3 Stand-to-Sit-to-Stand

This is the first time to our knowledge that KCF is investigated for a full STS cycle task. The work by Bobbert et al. (2016), however, serves as a comparison in Fig. 5.35 for the Sit-to-Stand portion of our STS task (i.e. approximately the last 50 %).

(a) STS: Total KCF.

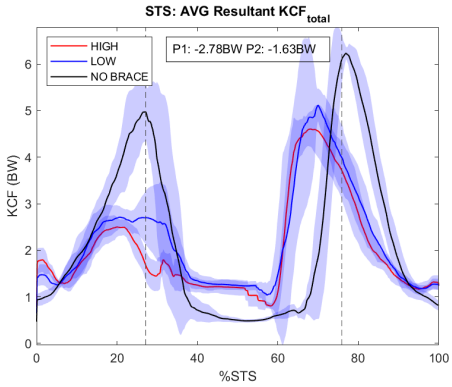

(b) STS: KCF from Bobbert et al. (2016).

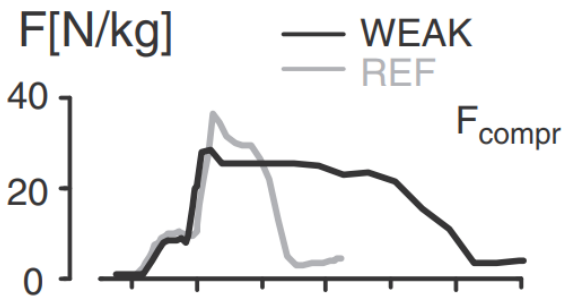

Figure 5.35: KCF comparison with the literature for the STS task. When normalized to body weight using $g = 9.8\ m/s^2$ the second peak is similar to what is found in the literature.

As hypothesized, peak KCF was reduced during both peaks detected. The medial KCF reduction achieved for the second peak with high assistance was 1.8 times larger than the reduction obtained with the low assistance, this is similar to the stiffness relationship between the respective elastic bands used, as the band for the high assistance condition was 1.7 times stiffer than the one used for the low assistance condition.

The KCF reduction effect magnitude during the first peak of the STS task was

not statistically dependent on the level of assistance used, the overall KCF reduction, however, was greater for the first peak as compared to the second peak. This greater reduction can be, in part, explained by a load shift from the assisted leg to the unassisted leg during the eccentric portion of the task. Figure 5.36 shows the vertical ground reaction forces (GRF) for the assisted (RIGHT) and unassisted (LEFT) legs during the STS task. For both high and low assistance conditions, the left vertical GRF was greater than the right vertical GRF during the first peak KCF. The reduction effect achieved at the second peak KCF can not be explained by redistribution in GRF, as the GRF distribution seems to be unaltered at the second peak KCF, during concentric contraction.

(a) No Brace (b) HIGH (c) LOW

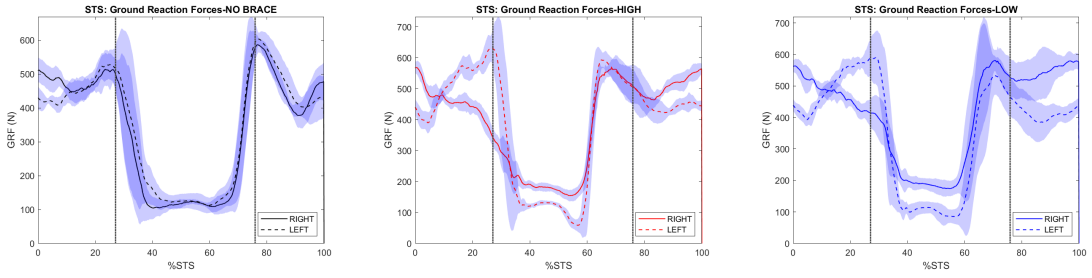

Figure 5.36: Ground Reaction Forces (GRF) for the assisted (RIGHT) and unassisted (LEFT) legs during STS task.

The KCF redistribution can also help explain the smaller KFM at the first peak KCF, during eccentric contraction (Fig. 5.21). The second peak KFM reduction, however, is better explained through kinematic changes and kinetic adaptations. The knee is less flexed during the assisted STS trials (Fig. 5.21), this causes a compensatory response at the hip joint, increasing hip extension moment and re-

ducing hip flexion angle while reducing knee extension moment.

The changes observed in CCI seem to be directly related to the musculoskeletal simulation results, moreover, the predicted muscle activation timings are in good agreement with the measured EMG envelope signals (Fig. 5.38). This indicates that the 13.39 N/kg and 8.23 N/kg reductions in VM and VL force production (Table 5.11) may indeed help explain the observed reduction in KCF despite the increases in VM-ST and VM-MG CCI.

Table 5.11: Muscle activity changes at peak KCF for the high assistance condition during STS trials.

Muscle	**P1 (↓)**	**P2 (↓)**	KCF Contributor?
BF	$\downarrow -4.86\ N/kg$	$\downarrow -1.89\ N/kg$	YES
LG	$\uparrow 0.15\ N/kg$	$\uparrow 0.21\ N/kg$	YES
MG	$\uparrow 0.32\ N/kg$	$\uparrow 0.47\ N/kg$	YES
RF	0	0	YES
ST	$\uparrow 0.13\ N/kg$	0	YES
SOL	$\uparrow 0.95\ N/kg$	$\uparrow 1.00\ N/kg$	NO
VL	$\downarrow -13.40\ N/kg$	$\downarrow -7.78\ N/kg$	YES
VM	$\downarrow -8.23\ N/kg$	$\downarrow -5.82\ N/kg$	YES

The timing for KB 3.0 energy release is shown in Fig. 5.37. During the energy absorption portion, the maximum force does not match the maximum KCF location. However, during the concentric contraction, the assistance is well synchronized with the peak KCF. This helps understand why the KCF reduction effect was more evident in the second KCF peak.

(a) High Assistance.

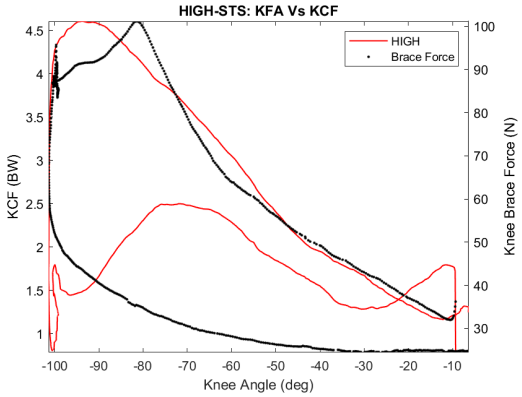

(b) Low Assistance.

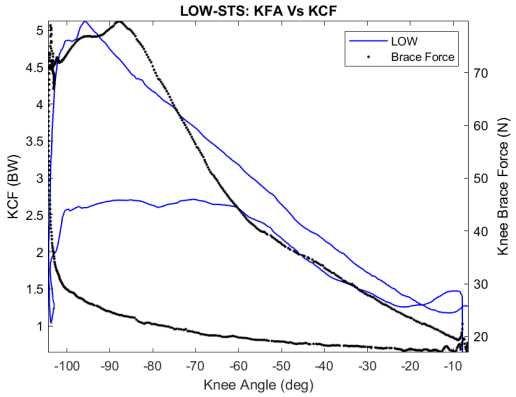

Figure 5.37: Stored force magnitude on the knee brace compared with KCF and KFA for STS trials.

STS: Subject Personal Assessment

The subject perceived the assistance at both levels, however, the subject reported a tendency to rely more on the calves for stability during eccentric contraction as the level of assistance increased. Moreover, the subject felt a tendency to be more gentle on the assisted leg while bearing more load on the unassisted leg during the high assistance condition. In general, the strapping method was found to be uncomfortable and painful after a long period of use, leaving marks on the skin once removed.

5.4.4 Level Walking

Tibiofemoral contact forces during level walking have been widely studied in the literature. The work by Hall et al. (2019), as well as the work by Lenton et al. (2018), can serve as a comparison reference. Fig. 5.39 shows the similarity between our KCF pattern, estimated for the W task, and the KCF pattern determined by Hall et

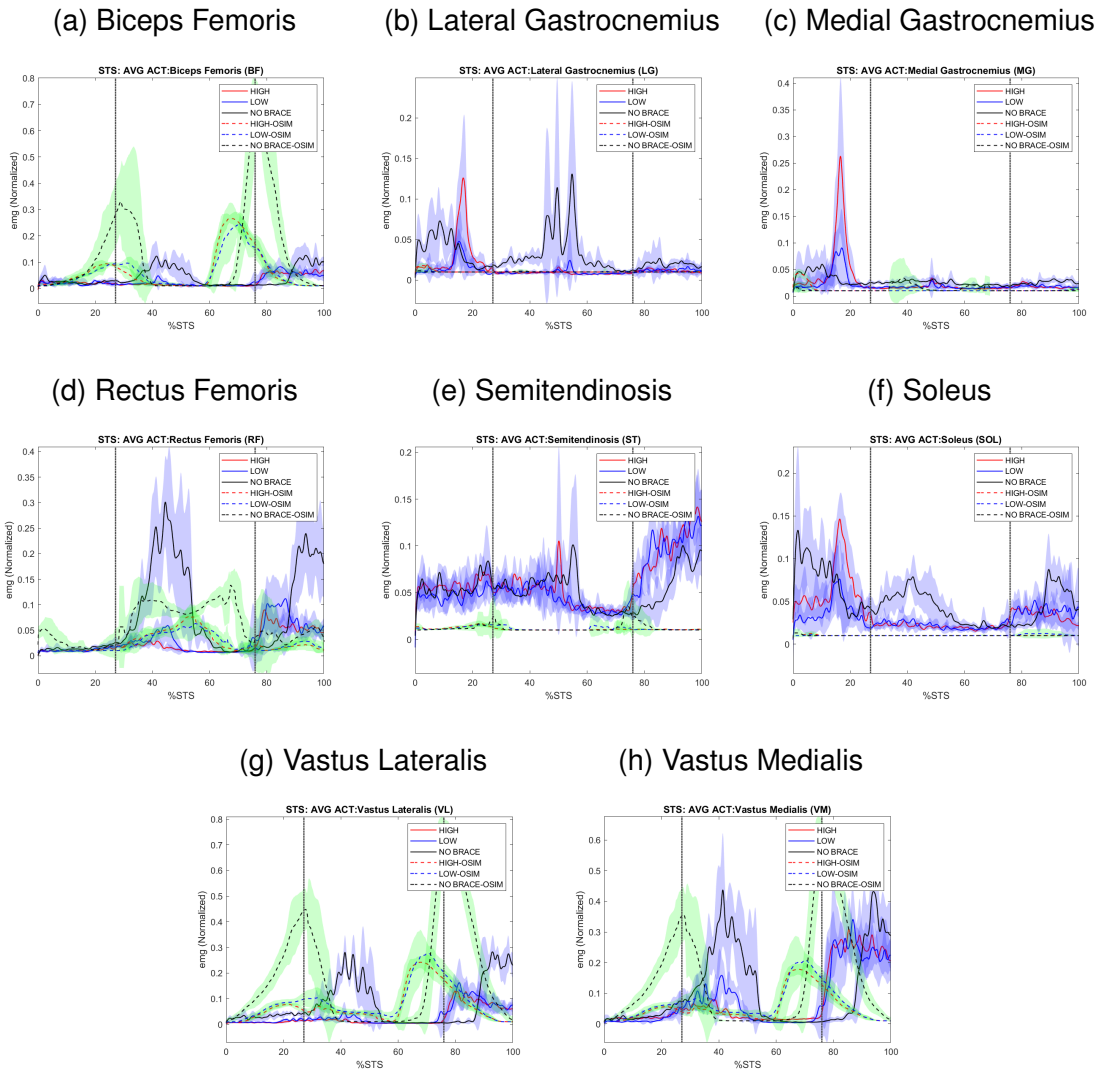

Figure 5.38: Normalized EMG envelope and predicted OpenSim muscle activation for STS trials.

al. (2019).

The external assistance caused an increased KCF peak at the beginning of the stance phase and a reduced KCF peak during late stance. The changes in CCI and muscle force estimation are in accordance with these results. When comparing predicted muscle activations with EMG, however, EMG envelopes show an increased activation for VM and RF during the second peak KCF.

(a) W: Total KCF.

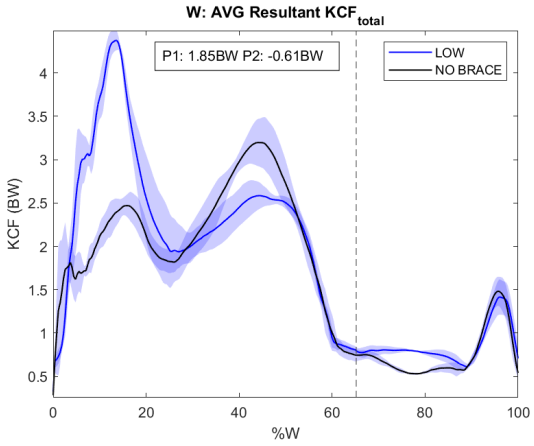

(b) W: KCF from Hall et al. (2019).

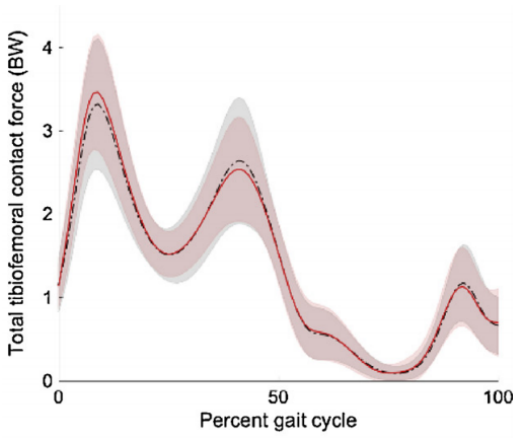

Figure 5.39: KCF comparison with the literature for the W task.

The increased VM and VL force production, as well as the increased first peak KCF during the W trials, in not necessarily explained through a weakness in the knee brace actuation principle. Instead, we can explain it by observing at the ground reaction forces in Fig. 5.40, realizing that there was a 265 N increase in peak GRF after heel strike. This higher heel strike impact is a direct result of wearing the brace regardless of the application of external assistance and, perhaps, a result of the conscious knowledge of the control variables that defined the behavior of the W finite state machine controller (i.e. accelerometer).

The timing for KB 3.0 energy release is shown in Fig. 5.41. The knee brace holds the preload until the knee flexion angle starts changing drastically (i.e. starting swing phase).

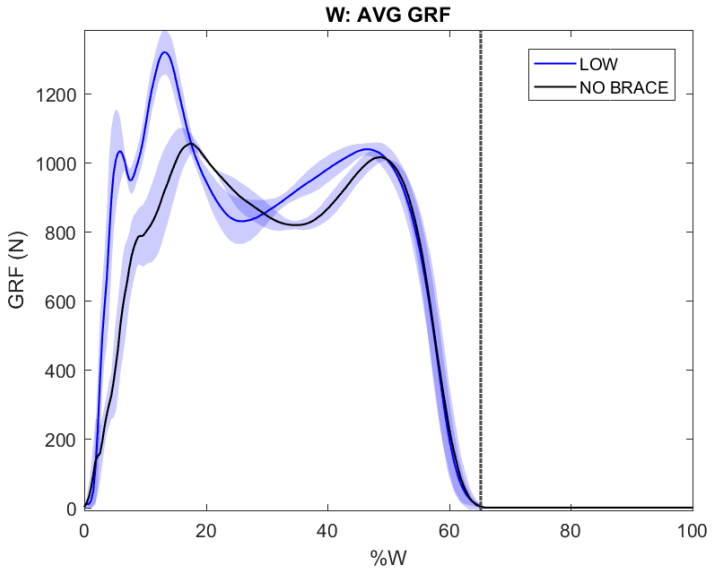

Figure 5.40: Ground reaction forces (GRF) for W trials.

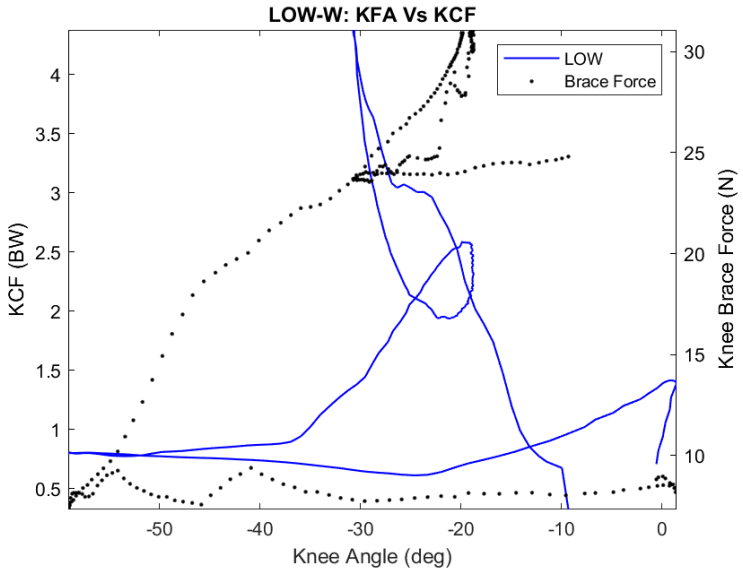

Figure 5.41: Stored force magnitude on the knee brace compared with KCF and KFA for W trials.

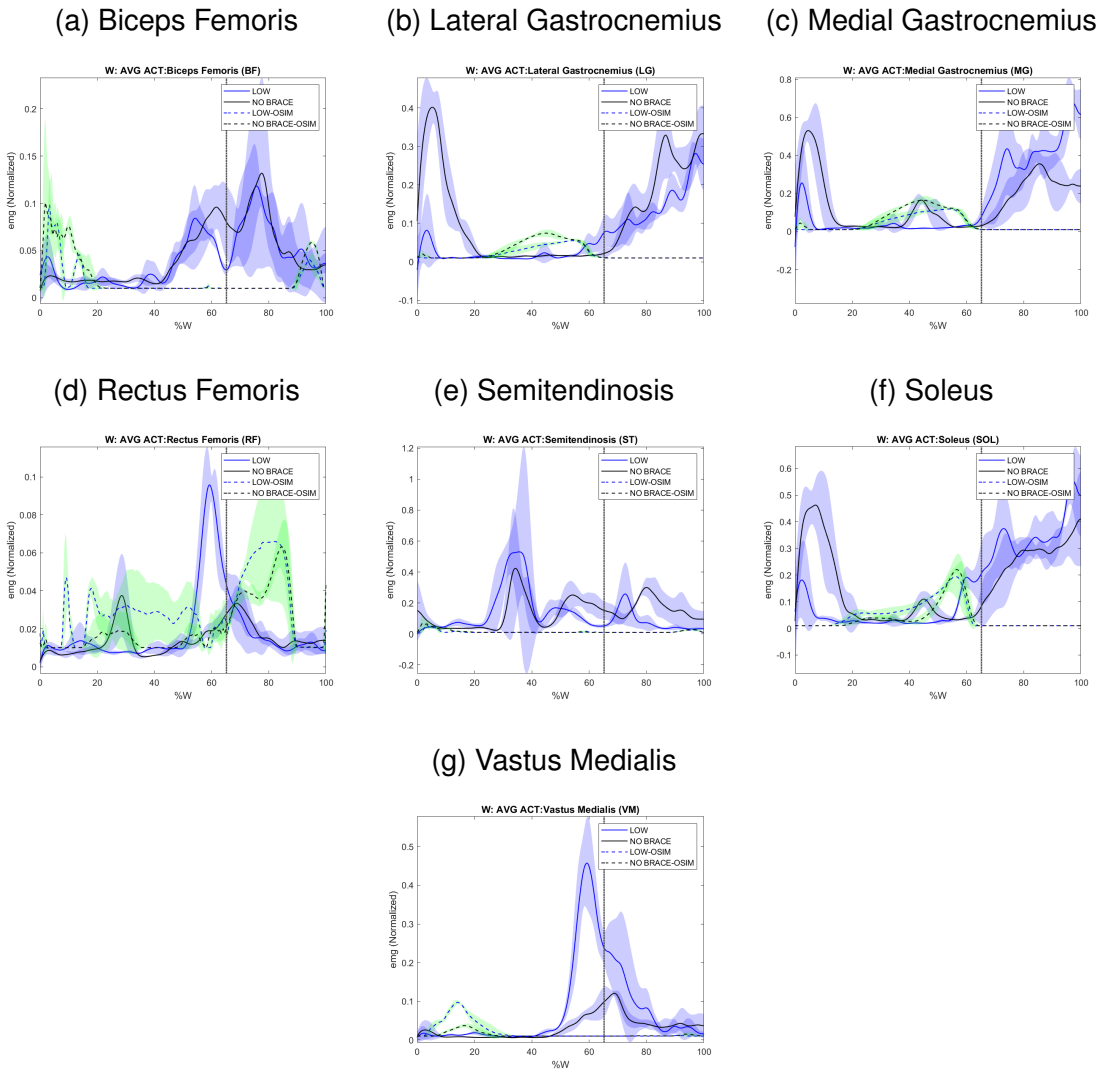

Figure 5.42: Normalized EMG envelope and predicted OpenSim muscle activation for W trials.

W: Subject Personal Assessment

During the W trials, the subject reported the need to step "harder" with the assisted leg in order for the device to properly identify the heel strike. The knee brace was uncomfortable to wear, and the pressure created by the straps on the skin created

a tendency on the subject to internally rotate the right hip during leg swing. The subject was not able to immediately perceive the device's assistance.

5.5 Conclusions

The hypotheses tested in this study had different outcomes according to the task under test. For SA, the device had an effect at the end of the SA cycle and was unable to reduce the highest peak KCF. It is possible that the poor timing with respect to the peak KCF hindered the potential benefits of external assistance. The device, however, caused reductions in medial CCI of up to 25.40 during the first peak. Modeling limitations can also introduce errors in the estimation of tibiofemoral contact forces, therefore, the reduction in CCI should be taken into account despite the increased peak KCF.

The SD trials had a better knee assistance timing with respect to peak KCF, and a -0.41 BW reduction in peak medial KCF was achieved with the low assistance level. Since the high assistance level did not achieve any significant KCF reduction, it seems that for SD exists a tuning point for assistance magnitude, beyond which the benefits of the external moment are hindered.

The STS trials exhibited an overall reduction in medial, lateral, and total KCF, and both peak KCF showed a statistically significant reduction. Based on our post-hoc analysis, it seems that the amount of medial KCF reduction during eccentric contraction is directly proportional to the stiffness of the elastic element used. As it was found, a 1.7 times increase in elastic band stiffness caused a 1.8 times

increase in second peak medial KCF reduction.

The walking trials had limited statistical power, due to the small number of trials analyzed, however, a reduction of 0.64 BW in medial KCF was observed for the second peak. Since the W trials yielded muscle activation patterns that notably differed from the measured and analyzed envelope EMG, implementing other optimization approaches would help compare and get a more conclusive result for this activity. In general, the effect sizes were found to be large in the best of cases; a new experiment design based on our results could be done in order to achieve smaller effect sizes and better statistical power.

The device achieved the highest KCF reductions under the tasks that involved the greatest amount of eccentric contraction. This is not surprising, since the design principle for KB-3.0 is based on energy storage from external moment. This means that KB-3.0 was configured to absorb the negative work normally done at the knee joint during eccentric contraction and store that energy to be delivered at the peak KCF.

In general, the device was painful to wear after long periods (over 1 h), a review and redesign of the limb-brace interface should be done in order to minimize the discomfort that could turn into undesired mechanical adaptations.

Chapter 6

Summary and Future Work

The aim of this dissertation was to develop a clutch-based energy storage and release knee bracing approach and quantify its effect in knee muscles co-contraction index (CCI), knee joint internal contact forces (KCF), and lower limb kinematics during four daily life activities; walking, sit and stand, stair ascent, and stair descent.

The device was designed to achieve high torque capabilities while being lightweight and having low power requirements. As compared with the literature, at 23 Nm, our device had torque capabilities comparable to powered exoskeletons such as Horst (2009). While at 2.58 kg of total weight, our design is overdimensioned can be optimized to reduce total weight. Moreover, in a practical setting, components used for experimental purposes such as the load cell are no longer needed, further reducing the total weight.

We designed and executed a testing protocol with one subject, with the purpose of evaluating the biomechanical effects of our assistive knee brace under four tasks: Stair Ascent (SA), Stair Descent (SD), Stand-to-Sit-to-Stand (STS),

and Level Walking(W). While not able to reduce the total KCF in all cases, significant reductions in medial KCF were observed on all tasks up to some degree. The knee brace was most effective under the STS task, presumably due to the amount of eccentric contraction involved, which implies high potential for energy absorption and storage as elastic potential energy by the knee brace. Our post-hoc analysis revealed a possible direct relationship between the stiffness of the elastic element used to store energy and the magnitude of medial KCF reduction. However, it is necessary to investigate this effect on a wider range of assistance values, since for SD the possible existence of an assistance threshold was identified, beyond which the benefits of external assistance are lost.

This dissertation identified the benefits of clutched external assistance to alleviate knee joint loading. We pointed out the kinematic, and muscular activity changes that can occur as an adaptation to the external assistance. This design approach has the potential to serve as the basis for the development of novel hybrid exoskeletons, orthoses, and assistive devices. The reduction of muscular force production observed for the STS task, in particular, can be further explored to find new applications to this assistive device design approach.

6.0.1 Improvements to KB-3.0 and suggestions for KB-4.0

Control System

Regarding improvements to our current design, KB-3.0, the control methodology should be refined to account for the knee flexion angle in real-time as well as the

energy stored in the system. This was not achieved in our KB-3.0 version due to a damaged component in our circuitry. Real-time spatial orientation could be included in the control system input variables. This can be achieved through IMU fusion; however, the computational power as well as the base sample frequency of the IMU implemented did not allow for this process to be responsive enough to be implemented in our current version.

Two novel control approaches that could be implemented in future versions of our device are the following:

- Real-time KCF estimation in order to identify optimal engagement timings. Pizzolato et al. (2017) used a similar approach for gait training; however, this would only be feasible in experimental settings, due to the need for motion capture and EMG data collection in order to execute real-time musculoskeletal simulations.

- Machine learning approach using multiple musculoskeletal simulation trials as training input. Yang & Peng (2020) implemented a Gaussian Process method as the mathematical foundation of the learning process, using EMG as the input variable for control. Although extensive experimental data would be initially required to train the system and achieve effective engagement timings, this approach has the potential to be implemented outside of experimental environments.

Mechanical Design

The mechanical design of KB-3.0 interfered with the Tibialis Anterior muscle. This is a muscle of interest if an EMG-driven musculoskeletal modeling approach is to be implemented.

The elastic band was coiled around the shaft as the only support, this caused the elastic band to come completely uncoiled after several contractions due to energy loss. Improving the attachment technique in order to allow for continuous use without constant adjustment would be necessary to allow for practical implementations of this device.

The electromagnetic brakes used needed a continuous electric current in order to keep the shaft fixed. At all times, at least one of the brakes is engaged, this indicates that replacing the brakes by normally engaged electromagnetic clutches would reduce the average and maximum power consumption of the device, allowing for longer battery life, and further improving our 20 W power consumption.

The frame used was based on a stock valgization knee brace that was not designed for the application of external assistance in the sagittal plane. While support straps and plastic surfaces were added to reduce discomfort, wearing the device was painful after long periods of use. A new ergonomic-oriented approach should be used to redesign the frame and strapping system to allow for long-periods practical implementations of future versions of our device.

Musculoskeletal Modeling

The modeling approach implemented in our study did not allow for a good correlation between EMG signals and Opensim predicted activations. While an EMG-driven simulation approach would allow for this correlation to improve, further indirect validation should be done in order to estimate the level of accuracy of the simulation.

References

Ackerman, I. N., Bucknill, A., Page, R. S., Broughton, N. S., Roberts, C., Cavka, B., ... Brand, C. A. (2015). The substantial personal burden experienced by younger people with hip or knee osteoarthritis. *Osteoarthritis and cartilage*, *23*(8), 1276–1284.

Ackerman, I. N., Kemp, J. L., Crossley, K. M., Culvenor, A. G., & Hinman, R. S. (2017). Hip and knee osteoarthritis affects younger people, too. *journal of orthopaedic & sports physical therapy*, *47*(2), 67–79.

Al Amer, H. S., Sabbahi, M. A., Alrowayeh, H. N., Bryan, W. J., & Olson, S. L. (2018). Electromyographic activity of quadriceps muscle during sit-to-stand in patients with unilateral knee osteoarthritis. *BMC research notes*, *11*(1), 356.

Anderson, F. C., & Pandy, M. G. (2001). Dynamic optimization of human walking. *Journal of biomechanical engineering*, *123*(5), 381–390.

Andriacchi, T. P., Mündermann, A., Smith, R. L., Alexander, E. J., Dyrby, C. O., & Koo, S. (2004). A framework for the in vivo pathomechanics of osteoarthritis at the knee. *Annals of biomedical engineering*, *32*(3), 447–457.

Asay, J. L., Mündermann, A., & Andriacchi, T. P. (2009). Adaptive patterns of movement during stair climbing in patients with knee osteoarthritis. *Journal of Orthopaedic Research*, *27*(3), 325–329.

Benoit, D., Lamontagne, M., Cerulli, G., & Liti, A. (2003). The clinical significance of electromyography normalisation techniques in subjects with anterior cruciate ligament injury during treadmill walking. *Gait & posture*, *18*(2), 56–63.

Bhala, N., Emberson, J., Merhi, A., Abramson, S., Arber, N., Baron, J., ... others (2013). *Vascular and upper gastrointestinal effects of non-steroidal anti-inflammatory drugs: meta-analyses of individual participant data from randomised trials.* Elsevier.

Bihlet, A. R., Byrjalsen, I., Bay-Jensen, A.-C., Andersen, J. R., Christiansen, C., Riis, B. J., & Karsdal, M. A. (2019). Associations between biomarkers of bone and cartilage turnover, gender, pain categories and radiographic severity in knee osteoarthritis. *Arthritis research & therapy*, *21*(1), 203.

Blazek, K., Favre, J., Asay, J., Erhart-Hledik, J., & Andriacchi, T. (2014). Age and obesity alter the relationship between femoral articular cartilage thickness and ambulatory loads in individuals without osteoarthritis. *Journal of Orthopaedic Research*, *32*(3), 394–402.

Bobbert, M. F., Kistemaker, D. A., Vaz, M. A., & Ackermann, M. (2016). Searching for strategies to reduce the mechanical demands of the sit-to-stand task with a muscle-actuated optimal control model. *Clinical Biomechanics*, *37*, 83–90.

Bouchouras, G., Patsika, G., Hatzitaki, V., & Kellis, E. (2015). Kinematics and knee muscle activation during sit-to-stand movement in women with knee osteoarthritis. *Clinical biomechanics*, *30*(6), 599–607.

Bourne, R. B., Chesworth, B. M., Davis, A. M., Mahomed, N. N., & Charron, K. D. (2010). Patient satisfaction after total knee arthroplasty: who is satisfied and who is not? *Clinical Orthopaedics and Related Research®*, *468*(1), 57–63.

Boyer, K. A. (2018). Biomechanical response to osteoarthritis pain treatment may impair long-term efficacy. *Exercise and sport sciences reviews*, *46*(2), 121–128.

Brandon, S. C., Miller, R. H., Thelen, D. G., & Deluzio, K. J. (2014). Selective lateral muscle activation in moderate medial knee osteoarthritis subjects does not unload medial knee condyle. *Journal of biomechanics*, *47*(6), 1409–1415.

Burden, A. (2009). How should we normalize electromyograms obtained from healthy participants. *What we*, *605*.

Burden, A., Trew, M., & Baltzopoulos, V. (2003). Normalisation of gait emgs: a re-examination. *Journal of Electromyography and Kinesiology*, *13*(6), 519–532.

Chaichaowarat, R., Kinugawa, J., & Kosuge, K. (2018). Cycling-enhanced knee exoskeleton using planar spiral spring. In *2018 40th annual international conference of the ieee engineering in medicine and biology society (embc)* (pp. 1–6).

Chawla, H., Nwachukwu, B., Van der List, J., Eggman, A., Pearle, A., & Ghomrawi, H. (2017). Cost effectiveness of patellofemoral versus total knee arthroplasty in younger patients. *Bone Joint J*, *99*(8), 1028–1036.

Chehab, E. F., Favre, J., Erhart-Hledik, J. C., & Andriacchi, T. P. (2014). Baseline knee adduction and flexion moments during walking are both associated with 5 year cartilage changes in patients with medial knee osteoarthritis. *Osteoarthritis and cartilage*, *22*(11), 1833–1839.

Chen, S., Sun, Y., Ma, G., Yin, X., & Liang, L. (2019). The wedge insole for the treatment of knee osteoarthritis: A systematic review protocol. *Medicine*, *98*(37).

Claes, S., Hermie, L., Verdonk, R., Bellemans, J., & Verdonk, P. (2013). Is osteoarthritis an inevitable consequence of anterior cruciate ligament reconstruction? a meta-analysis. *Knee Surgery, Sports Traumatology, Arthroscopy*, *21*(9), 1967–1976.

Costigan, P. A., Deluzio, K. J., & Wyss, U. P. (2002). Knee and hip kinetics during normal stair climbing. *Gait & posture*, *16*(1), 31–37.

Delp, S. L., Anderson, F. C., Arnold, A. S., Loan, P., Habib, A., John, C. T., ... Thelen, D. G. (2007). Opensim: open-source software to create and analyze dynamic simulations of movement. *IEEE transactions on biomedical engineering*, *54*(11), 1940–1950.

De Luca, C. J. (1979). Physiology and mathematics of myoelectric signals. *IEEE Transactions on Biomedical Engineering*(6), 313–325.

Deluzio, K., & Astephen, J. (2007). Biomechanical features of gait waveform data associated with knee osteoarthritis: an application of principal component analysis. *Gait & posture*, *25*(1), 86–93.

DeMers, M. S., Pal, S., & Delp, S. L. (2014). Changes in tibiofemoral forces due to variations in muscle activity during walking. *Journal of Orthopaedic Research*, *32*(6), 769–776.

Dieppe, P. A., & Lohmander, L. S. (2005). Pathogenesis and management of pain in osteoarthritis. *The Lancet*, *365*(9463), 965–973.

Dixon, P. C., Gomes, S., Preuss, R. A., & Robbins, S. M. (2018). Muscular cocontraction is related to varus thrust in patients with knee osteoarthritis. *Clinical Biomechanics*, *60*, 164–169.

Dollar, A. M., & Herr, H. (2008a). Design of a quasi-passive knee exoskeleton to assist running. In *Intelligent robots and systems, 2008. iros 2008. ieee/rsj international conference on* (pp. 747–754).

Dollar, A. M., & Herr, H. (2008b). Lower extremity exoskeletons and active orthoses: challenges and state-of-the-art. *IEEE Transactions on robotics*, *24*(1), 144–158.

Dorn, T. W., Wang, J. M., Hicks, J. L., & Delp, S. L. (2015). Predictive simulation generates human adaptations during loaded and inclined walking. *PloS one*, *10*(4), e0121407.

Erdemir, A., McLean, S., Herzog, W., & van den Bogert, A. J. (2007). Model-based estimation of muscle forces exerted during movements. *Clinical biomechanics*, *22*(2), 131–154.

Falconer, K., & Winter, D. (1985). Quantitative assessment of co-contraction at the ankle joint in walking. *Electromyography and clinical neurophysiology*, *25*(2-3), 135–149.

Felson, D. T., Goggins, J., Niu, J., Zhang, Y., & Hunter, D. J. (2004). The effect of body weight on progression of knee osteoarthritis is dependent on alignment. *Arthritis & Rheumatology*, *50*(12), 3904–3909.

Fitzgerald, G. K., Piva, S. R., & Irrgang, J. J. (2004). Reports of joint instability in knee osteoarthritis: its prevalence and relationship to physical function. *Arthritis Care & Research*, *51*(6), 941–946.

Fregly, B. J., Besier, T. F., Lloyd, D. G., Delp, S. L., Banks, S. A., Pandy, M. G., & D'lima, D. D. (2012). Grand challenge competition to predict in vivo knee loads. *Journal of Orthopaedic Research*, *30*(4), 503–513.

Gohal, C., Shanmugaraj, A., Tate, P., Horner, N. S., Bedi, A., Adili, A., & Khan, M. (2018). Effectiveness of valgus offloading knee braces in the treatment of medial compartment knee osteoarthritis: a systematic review. *Sports health*, *10*(6), 500–514.

Gupta, S., Hawker, G., Laporte, A., Croxford, R., & Coyte, P. (2005). The economic burden of disabling hip and knee osteoarthritis (oa) from the perspective of individuals living with this condition. *Rheumatology*, *44*(12), 1531–1537.

Hall, M., Diamond, L. E., Lenton, G. K., Pizzolato, C., & Saxby, D. J. (2019). Immediate effects of valgus knee bracing on tibiofemoral contact forces and knee muscle forces. *Gait & posture*, *68*, 55–62.

Handford, M. L., & Srinivasan, M. (2016). Robotic lower limb prosthesis design through simultaneous computer optimizations of human and prosthesis costs. *Scientific reports*, *6*, 19983.

Hang, J. R., Stanford, T. E., Graves, S. E., Davidson, D. C., de Steiger, R. N., & Miller, L. N. (2010). Outcome of revision of unicompartmental knee replacement: 1,948 cases from the australian orthopaedic association national joint replacement registry, 1999–2008. *Acta orthopaedica*, *81*(1), 95–98.

Hast, M. W., & Piazza, S. J. (2013). Dual-joint modeling for estimation of total knee replacement contact forces during locomotion. *Journal of biomechanical engineering*, *135*(2), 021013.

Hatfield, G. L., Hubley-Kozey, C. L., Wilson, J. L. A., & Dunbar, M. J. (2011). The effect of total knee arthroplasty on knee joint kinematics and kinetics during gait. *The Journal of arthroplasty*, *26*(2), 309–318.

Hatfield, G. L., Stanish, W. D., & Hubley-Kozey, C. L. (2015). Three-dimensional biomechanical gait characteristics at baseline are associated with progression to total knee arthroplasty. *Arthritis care & research*, *67*(7), 1004–1014.

Hawker, G., Stewart, L., French, M., Cibere, J., Jordan, J., March, L., ... Gooberman-Hill, R. (2008). Understanding the pain experience in hip and knee osteoarthritis–an oarsi/omeract initiative. *Osteoarthritis and cartilage*, *16*(4), 415–422.

Hawker, G. A., French, M. R., Waugh, E. J., Gignac, M. A., Cheung, C., & Murray, B. J. (2010). The multidimensionality of sleep quality and its relationship to fatigue in older adults with painful osteoarthritis. *Osteoarthritis and Cartilage*, *18*(11), 1365–1371.

Henriksen, M., Aaboe, J., & Bliddal, H. (2012). The relationship between pain and dynamic knee joint loading in knee osteoarthritis varies with radiographic disease severity. a cross sectional study. *The knee*, *19*(4), 392–398.

Herr, H. (2009). Exoskeletons and orthoses: classification, design challenges and future directions. *Journal of neuroengineering and rehabilitation*, *6*(1), 21.

Herzog, W., Longino, D., & Clark, A. (2003). The role of muscles in joint adaptation and degeneration. *Langenbeck's Archives of Surgery*, *388*(5), 305–315.

Hicks-Little, C. A., Peindl, R. D., Hubbard, T. J., Scannell, B. P., Springer, B. D., Odum, S. M., ... Cordova, M. L. (2011). Lower extremity joint kinematics during stair climbing in knee osteoarthritis. *Medicine & Science in Sports & Exercise*, *43*(3), 516–524.

Hodges, P. W., van den Hoorn, W., Wrigley, T. V., Hinman, R. S., Bowles, K.-A., Cicuttini, F., ... Bennell, K. (2016). Increased duration of co-contraction of medial knee muscles is associated with greater progression of knee osteoarthritis. *Manual therapy*, *21*, 151–158.

Horst, R. W. (2009). A bio-robotic leg orthosis for rehabilitation and mobility enhancement. In *2009 annual international conference of the ieee engineering in medicine and biology society* (pp. 5030–5033).

Horst, R. W., & Marcus, R. R. (2006). Flexcva: A continuously variable actuator for active orthotics. In *2006 international conference of the ieee engineering in medicine and biology society* (pp. 2425–2428).

Hortobágyi, T., Garry, J., Holbert, D., & Devita, P. (2004). Aberrations in the control of quadriceps muscle force in patients with knee osteoarthritis. *Arthritis Care & Research*, *51*(4), 562–569.

Hsu, R., Himeno, S., Coventry, M. B., & Chao, E. (1990). Normal axial alignment of the lower extremity and load-bearing distribution at the knee. *Clinical orthopaedics and related research*(255), 215–227.

Huang, S.-C., Wei, I.-P., Chien, H.-L., Wang, T.-M., Liu, Y.-H., Chen, H.-L., ... Lin, J.-G. (2008). Effects of severity of degeneration on gait patterns in patients with medial knee osteoarthritis. *Medical engineering & physics*, *30*(8), 997–1003.

Huetink, K., Van Der Voort, P., Bloem, J. L., Nelissen, R. G., & Meulenbelt, I. (2016). Genetic contribution to the development of radiographic knee osteoarthritis in a population presenting with nonacute knee symptoms a decade earlier. *Clinical Medicine Insights: Arthritis and Musculoskeletal Disorders*, *9*, CMAMD–S30657.

Hunter, D. J., Schofield, D., & Callander, E. (2014). The individual and socioeconomic impact of osteoarthritis. *Nature Reviews Rheumatology*, *10*(7), 437–441.

Johnson, F., Leitl, S., & Waugh, W. (1980). The distribution of load across the knee. a comparison of static and dynamic measurements. *Bone & Joint Journal*, *62*(3), 346–349.

Julin, J., Jämsen, E., Puolakka, T., Konttinen, Y. T., & Moilanen, T. (2010). Younger age increases the risk of early prosthesis failure following primary total knee replacement for osteoarthritis: a follow-up study of 32,019 total knee replacements in the finnish arthroplasty register. *Acta orthopaedica*, *81*(4), 413–419.

Jun, S., Zhou, X., Ramsey, D. K., & Krovi, V. N. (2015). Smart knee brace design with parallel coupled compliant plate mechanism and pennate elastic band spring. *Journal of Mechanisms and Robotics*, *7*(4), 041024.

Kaufman, K. R., Hughes, C., Morrey, B. F., Morrey, M., & An, K.-N. (2001). Gait characteristics of patients with knee osteoarthritis. *Journal of biomechanics*, *34*(7), 907–915.

Kim, D., & Hwang, J.-M. (2018). The center of pressure and ankle muscle cocontraction in response to anterior-posterior perturbations. *PloS one*, *13*(11), e0207667.

Kim, H. J., Fernandez, J. W., Akbarshahi, M., Walter, J. P., Fregly, B. J., & Pandy, M. G. (2009). Evaluation of predicted knee-joint muscle forces during gait using an instrumented knee implant. *Journal of Orthopaedic Research*, *27*(10), 1326–1331.

Kim, Y.-H., Park, W.-M., & Phuong, B. T. T. (2010). Effect of joint center location on in-vivo joint contact forces during walking. In *Asme 2010 summer bioengineering conference* (pp. 267–268).

Kinney, A. L., Besier, T. F., D'Lima, D. D., & Fregly, B. J. (2013). Update on grand challenge competition to predict in vivo knee loads. *Journal of biomechanical engineering*, *135*(2), 021012.

Kinney, A. L., Besier, T. F., Silder, A., Delp, S. L., D'Lima, D. D., & Fregly, B. J. (2013). Changes in in vivo knee contact forces through gait modification. *Journal of Orthopaedic Research*, *31*(3), 434–440.

Knarr, B. A., Zeni Jr, J. A., & Higginson, J. S. (2012). Comparison of electromyography and joint moment as indicators of co-contraction. *Journal of Electromyography and Kinesiology*, *22*(4), 607–611.

Knowlton, C. B., Wimmer, M. A., & Lundberg, H. J. (2012). Grand challenge competition: A parametric numerical model to predict in vivo medial and lateral knee forces in walking gaits. In *Asme 2012 summer bioengineering conference* (pp. 199–200).

Koh, I. J., Cho, W.-S., Choi, N. Y., Kim, T. K., Group, K. K. R., et al. (2014). Causes, risk factors, and trends in failures after tka in korea over the past 5 years: a multicenter study. *Clinical Orthopaedics and Related Research®*, *472*(1), 316–326.

Konrath, J. M., Karatsidis, A., Schepers, H. M., Bellusci, G., de Zee, M., & Andersen, M. S. (2019). Estimation of the knee adduction moment and joint contact force during daily living activities using inertial motion capture. *Sensors*, *19*(7), 1681.

Koo, S., & Andriacchi, T. P. (2007). A comparison of the influence of global functional loads vs. local contact anatomy on articular cartilage thickness at the knee. *Journal of biomechanics*, *40*(13), 2961–2966.

Koo, S., Rylander, J. H., & Andriacchi, T. P. (2011). Knee joint kinematics during walking influences the spatial cartilage thickness distribution in the knee. *Journal of biomechanics*, *44*(7), 1405–1409.

Kotlarz, H., Gunnarsson, C. L., Fang, H., & Rizzo, J. A. (2009). Insurer and out-of-pocket costs of osteoarthritis in the us: Evidence from national survey data. *Arthritis & Rheumatism: Official Journal of the American College of Rheumatology*, *60*(12), 3546–3553.

Kutzner, I., Küther, S., Heinlein, B., Dymke, J., Bender, A., Halder, A. M., & Bergmann, G. (2011). The effect of valgus braces on medial compartment load of the knee joint–in vivo load measurements in three subjects. *Journal of biomechanics*, *44*(7), 1354–1360.

Kutzner, I., Trepczynski, A., Heller, M. O., & Bergmann, G. (2013). Knee adduction moment and medial contact force–facts about their correlation during gait. *PloS one*, *8*(12), e81036.

Landry, S. C., McKean, K. A., Hubley-Kozey, C. L., Stanish, W. D., & Deluzio, K. J. (2007). Knee biomechanics of moderate oa patients measured during gait at a self-selected and fast walking speed. *Journal of biomechanics*, *40*(8), 1754–1761.

Lehman, G. J., & McGill, S. M. (1999). The importance of normalization in the interpretation of surface electromyography: a proof of principle. *Journal of manipulative and physiological therapeutics*, *22*(7), 444–446.

Leigh, J. P., Seavey, W., & Leistikow, B. (2001). Estimating the costs of job related arthritis. *The Journal of rheumatology*, *28*(7), 1647–1654.

Lenton, G. K., Bishop, P. J., Saxby, D. J., Doyle, T. L., Pizzolato, C., Billing, D., & Lloyd, D. G. (2018). Tibiofemoral joint contact forces increase with load magnitude and walking speed but remain almost unchanged with different types of carried load. *PloS one*, *13*(11), e0206859.

Lerner, Z. F., DeMers, M. S., Delp, S. L., & Browning, R. C. (2015). How tibiofemoral alignment and contact locations affect predictions of medial and lateral tibiofemoral contact forces. *Journal of biomechanics*, *48*(4), 644–650.

Liao, Y., Zhou, Z., & Wang, Q. (2015). Biokex: A bionic knee exoskeleton with proxy-based sliding mode control. In *Industrial technology (icit), 2015 ieee international conference on* (pp. 125–130).

Liikavainio, T., Bragge, T., Hakkarainen, M., Karjalainen, P. A., & Arokoski, J. P. (2010). Gait and muscle activation changes in men with knee osteoarthritis. *The Knee*, *17*(1), 69–76.

Lin, Y.-C., Walter, J. P., Banks, S. A., Pandy, M. G., & Fregly, B. J. (2010). Simultaneous prediction of muscle and contact forces in the knee during gait. *Journal of biomechanics*, *43*(5), 945–952.

Lin, Y.-C., Walter, J. P., & Pandy, M. G. (2018). Predictive simulations of neuromuscular coordination and joint-contact loading in human gait. *Annals of biomedical engineering*, *46*(8), 1216–1227.

Lindström, L. (1973). *On the frequency spectrum of emg signals*. Department of Clinical Neurophysiology, Sahlgren Hospital.

Liu, H.-x., Shang, P., Ying, X.-Z., & Zhang, Y. (2016). Shorter survival rate in varus-aligned knees after total knee arthroplasty. *Knee Surgery, Sports Traumatology, Arthroscopy*, *24*(8), 2663–2671.

Losina, E., Paltiel, A. D., Weinstein, A. M., Yelin, E., Hunter, D. J., Chen, S. P., ... others (2015). Lifetime medical costs of knee osteoarthritis management in the united states: impact of extending indications for total knee arthroplasty. *Arthritis care & research*, *67*(2), 203–215.

Manal, K., & Buchanan, T. S. (2012). Predictions of condylar contact during normal and medial thrust gait. In *Asme 2012 summer bioengineering conference* (pp. 197–198).

Meireles, S., De Groote, F., Verschueren, S., Maganaris, C., & Jonkers, I. (2014). Subjects with severe knee osteoarthritis reduce medio-lateral forces during gait at the expense of compressive knee contact forces. *Osteoarthritis and Cartilage*, *22*, S99–S100.

Meireles, S., Reeves, N. D., Jones, R. K., Smith, C. R., Thelen, D. G., & Jonkers, I. (2019). Patients with medial knee osteoarthritis reduce medial knee contact forces by altering trunk kinematics, progression speed, and stepping strategy during stair ascent and descent: a pilot study. *Journal of applied biomechanics*, *35*(4), 280–289.

Meireles, S., Wesseling, M., Smith, C. R., Thelen, D. G., Verschueren, S., & Jonkers, I. (2017). Medial knee loading is altered in subjects with early osteoarthritis during gait but not during step-up-and-over task. *PloS one*, *12*(11), e0187583.

Merletti, R., & Di Torino, P. (1999). Standards for reporting emg data. *J Electromyogr Kinesiol*, *9*(1), 3–4.

Metcalfe, A., Stewart, C., Postans, N., Dodds, A., Holt, C. A., & Roberts, A. (2013). The effect of osteoarthritis of the knee on the biomechanics of other joints in the lower limbs. *The bone & joint journal*, *95*(3), 348–353.

Mills, K., Hunt, M. A., Leigh, R., & Ferber, R. (2013). A systematic review and meta-analysis of lower limb neuromuscular alterations associated with knee osteoarthritis during level walking. *Clinical Biomechanics*, *28*(7), 713–724.

Miyazaki, T., Wada, M., Kawahara, H., Sato, M., Baba, H., & Shimada, S. (2002). Dynamic load at baseline can predict radiographic disease progression in medial compartment knee osteoarthritis. *Annals of the rheumatic diseases*, *61*(7), 617–622.

Morrison, J. (1970). The mechanics of the knee joint in relation to normal walking. *Journal of biomechanics*, *3*(1), 51–61.

Moyer, R. F., Birmingham, T. B., Chesworth, B. M., Kean, C., & Giffin, J. R. (2010). Alignment, body mass and their interaction on dynamic knee joint load in patients with knee osteoarthritis. *Osteoarthritis and cartilage*, *18*(7), 888–893.

Mündermann, A., Dyrby, C. O., & Andriacchi, T. P. (2005). Secondary gait changes in patients with medial compartment knee osteoarthritis: increased load at the ankle, knee, and hip during walking. *Arthritis & Rheumatism*, *52*(9), 2835–2844.

Mündermann, A., Dyrby, C. O., D'Lima, D. D., Colwell, C. W., & Andriacchi, T. P. (2008). In vivo knee loading characteristics during activities of daily living as measured by an instrumented total knee replacement. *Journal of Orthopaedic Research*, *26*(9), 1167–1172.

Murphy, L., & Helmick, C. G. (2012). The impact of osteoarthritis in the united states: a population-health perspective. *AJN The American Journal of Nursing*, *112*(3), S13–S19.

Murphy, L., Schwartz, T. A., Helmick, C. G., Renner, J. B., Tudor, G., Koch, G., ... Jordan, J. M. (2008). Lifetime risk of symptomatic knee osteoarthritis. *Arthritis Care & Research: Official Journal of the American College of Rheumatology*, *59*(9), 1207–1213.

Muthuri, S., McWilliams, D., Doherty, M., & Zhang, W. (2011). History of knee injuries and knee osteoarthritis: a meta-analysis of observational studies. *Osteoarthritis and Cartilage*, *19*(11), 1286–1293.

Nguyen, V. Q., Umberger, B. R., & Sup, F. C. (2019). Predictive simulation of human walking augmented by a powered ankle exoskeleton. In *2019 ieee 16th international conference on rehabilitation robotics (icorr)* (pp. 53–58).

Ong, K. L., Runa, M., Lau, E., & Altman, R. D. (2019). Cost-of-illness of knee osteoarthritis: potential cost savings by not undergoing arthroplasty within the first 2 years. *ClinicoEconomics and outcomes research: CEOR*, *11*, 245.

Patsika, G., Kellis, E., & Amiridis, I. G. (2011). Neuromuscular efficiency during sit to stand movement in women with knee osteoarthritis. *Journal of Electromyography and Kinesiology*, *21*(5), 689–694.

Peterson, D. S., & Martin, P. E. (2010). Effects of age and walking speed on coactivation and cost of walking in healthy adults. *Gait & posture*, *31*(3), 355–359.

Pizzolato, C., Reggiani, M., Saxby, D. J., Ceseracciu, E., Modenese, L., & Lloyd, D. G. (2017). Biofeedback for gait retraining based on real-time estimation of tibiofemoral joint contact forces. *IEEE Transactions on Neural Systems and Rehabilitation Engineering*, *25*(9), 1612–1621.

Pollo, F. E., Otis, J. C., Backus, S. I., Warren, R. F., & Wickiewicz, T. L. (2002). Reduction of medial compartment loads with valgus bracing of the osteoarthritic knee. *The American Journal of Sports Medicine*, *30*(3), 414–421.

Poulsen, E., Goncalves, G. H., Bricca, A., Roos, E. M., Thorlund, J. B., & Juhl, C. B. (2019). Knee osteoarthritis risk is increased 4-6 fold after knee injury–a systematic review and meta-analysis. *Br J Sports Med*, bjsports–2018.

Purevsuren, T., Dorj, A., Kim, K., & Kim, Y. H. (2016). Prediction of medial and lateral contact force of the knee joint during normal and turning gait after total knee replacement. *Proceedings of the Institution of Mechanical Engineers, Part H: Journal of Engineering in Medicine*, *230*(4), 288–297.

Ramanujam, A., Cirnigliaro, C. M., Garbarini, E., Asselin, P., Pilkar, R., & Forrest, G. F. (2018). Neuromechanical adaptations during a robotic powered exoskeleton assisted walking session. *The journal of spinal cord medicine*, *41*(5), 518–528.

Ravi, B., Croxford, R., Reichmann, W. M., Losina, E., Katz, J. N., & Hawker, G. A. (2012). The changing demographics of total joint arthroplasty recipients in the united states and ontario from 2001 to 2007. *Best practice & research Clinical rheumatology*, *26*(5), 637–647.

Roche, M., Law, T. Y., Kurowicki, J., Rosas, S., & Rush III, A. J. (2018). Effect of obesity on total knee arthroplasty costs and revision rate. *The journal of knee surgery*, *31*(01), 038–042.

Roebroeck, M., Doorenbosch, C., Harlaar, J., Jacobs, R., & Lankhorst, G. (1994). Biomechanics and muscular activity during sit-to-stand transfer. *Clinical Biomechanics*, *9*(4), 235–244.

Rosenfalck, P. (1969). Intra-and extracellular potential fields of active nerve and muscle fibres. *Acta Phisiologica Scandinavica*, *321*.

Rudolph, K., Axe, M., & Snyder-Mackler, L. (2000). Dynamic stability after acl injury: who can hop? *Knee Surgery, Sports Traumatology, Arthroscopy*, *8*(5), 262–269.

Salam, A., Awan, M. W., Mahmood, T., Rukh, M. S., & Seffat, N. (2019). Application of lateral wedge in knee osteoarthritis for improving pain and quality of life. *Journal of Liaquat University of Medical & Health Sciences*, *18*(02), 146–151.

Schween, R., Gehring, D., & Gollhofer, A. (2015). Immediate effects of an elastic knee sleeve on frontal plane gait biomechanics in knee osteoarthritis. *PloS one*, *10*(1), e0115782.

Seireg, A., & Arvikar, R. (1973). A mathematical model for evaluation of forces in lower extremeties of the musculo-skeletal system. *Journal of biomechanics*, *6*(3), 313–326.

Seth, A., Sherman, M., Reinbolt, J. A., & Delp, S. L. (2011). Opensim: a musculoskeletal modeling and simulation framework for in silico investigations and exchange. *Procedia Iutam*, *2*, 212–232.

Shakoor, N., Agrawal, A., & Block, J. A. (2008). Reduced lower extremity vibratory perception in osteoarthritis of the knee. *Arthritis Care & Research: Official Journal of the American College of Rheumatology*, *59*(1), 117–121.

Shannak, O., Palan, J., & Esler, C. (2017). A regional registry study of 216 patients investigating if patient satisfaction after total knee arthroplasty changes over a time period of five to 20 years. *The Knee*, *24*(4), 824–828.

Sharma, L., & Pai, Y.-C. (1997). Impaired proprioception and osteoarthritis. *Current Opinion in Rheumatology*, *9*(3), 253–258.

Shepherd, M. K., & Rouse, E. J. (2017). Design and validation of a torque-controllable knee exoskeleton for sit-to-stand assistance. *IEEE/ASME Transactions on Mechatronics*, *22*(4), 1695–1704.

Shimura, Y., Kurosawa, H., Ishijima, M., Liu, L., Kaneko, H., Futami, I., ... others (2013). The sources of pain in knee osteoarthritis are changing dependent upon the progression of the disease. *Osteoarthritis and Cartilage*, *21*, S262.

Shimura, Y., Kurosawa, H., Sugawara, Y., Tsuchiya, M., Sawa, M., Kaneko, H., ... others (2013). The factors associated with pain severity in patients with knee osteoarthritis vary according to the radiographic disease severity: a cross-sectional study. *Osteoarthritis and Cartilage*, *21*(9), 1179–1184.

Silverwood, V., Blagojevic-Bucknall, M., Jinks, C., Jordan, J., Protheroe, J., & Jordan, K. (2015). Current evidence on risk factors for knee osteoarthritis in older adults: a systematic review and meta-analysis. *Osteoarthritis and cartilage*, *23*(4), 507–515.

Sinclair, J., Brooks, D., Edmundson, C., & Hobbs, S. (2012). The efficacy of emg mvc normalization techniques for running analyses. *Journal of Biomechanics*(45), S623.

Sloan, M., Premkumar, A., & Sheth, N. P. (2018). Projected volume of primary total joint arthroplasty in the us, 2014 to 2030. *JBJS*, *100*(17), 1455–1460.

Souissi, H., Zory, R., Bredin, J., & Gerus, P. (2017). Comparison of methodologies to assess muscle co-contraction during gait. *Journal of biomechanics*, *57*, 141–145.

Spyropoulos, G., Tsatalas, T., Tsaopoulos, D. E., Sideris, V., & Giakas, G. (2013). Biomechanics of sit-to-stand transition after muscle damage. *Gait & posture*, *38*(1), 62–67.

Srivastava, R., Sanghi, D., Singh, A., Avasthi, S., Agarwal, S., & Natu, S. (2011). 297 is radiology a determinant of pain, stiffness and functional disability in knee osteoarthritis? *Osteoarthritis and Cartilage*, *19*, S139.

Steadman, J. R., Briggs, K. K., Pomeroy, S. M., & Wijdicks, C. A. (2016). Current state of unloading braces for knee osteoarthritis. *Knee Surgery, Sports Traumatology, Arthroscopy*, *24*(1), 42–50.

Steele, K. M., Jackson, R. W., Shuman, B. R., & Collins, S. H. (2017). Muscle recruitment and coordination with an ankle exoskeleton. *Journal of biomechanics*, *59*, 50–58.

Sutton, P. M., & Holloway, E. S. (2013). The young osteoarthritic knee: dilemmas in management. *BMC medicine*, *11*(1), 14.

Taylor, W. R., Heller, M. O., Bergmann, G., & Duda, G. N. (2004). Tibio-femoral loading during human gait and stair climbing. *Journal of Orthopaedic Research*, *22*(3), 625–632.

Thorp, L. E., Sumner, D. R., Block, J. A., Moisio, K. C., Shott, S., & Wimmer, M. A. (2006). Knee joint loading differs in individuals with mild compared with moderate medial knee osteoarthritis. *Arthritis & Rheumatology*, *54*(12), 3842–3849.

Trelle, S., Reichenbach, S., Wandel, S., Hildebrand, P., Tschannen, B., Villiger, P. M., ... Jüni, P. (2011). Cardiovascular safety of non-steroidal anti-inflammatory drugs: network meta-analysis. *Bmj*, *342*, c7086.

Trepczynski, A., Kutzner, I., Schwachmeyer, V., Heller, M. O., Pfitzner, T., & Duda, G. N. (2018). Impact of antagonistic muscle co-contraction on in vivo knee contact forces. *Journal of neuroengineering and rehabilitation*, *15*(1), 101.

Turcot, K., Armand, S., Fritschy, D., Hoffmeyer, P., & Suvà, D. (2012). Sit-to-stand alterations in advanced knee osteoarthritis. *Gait & posture*, *36*(1), 68–72.

van Ingen Schenau, G., Boots, P., De Groot, G., Snackers, R., & Van Woensel, W. (1992). The constrained control of force and position in multi-joint movements. *Neuroscience*, *46*(1), 197–207.

Van Rossom, S., Smith, C. R., Thelen, D. G., Vanwanseele, B., Van Assche, D., & Jonkers, I. (2018). Knee joint loading in healthy adults during functional exercises: implications for rehabilitation guidelines. *journal of orthopaedic & sports physical therapy*, *48*(3), 162–173.

Varadarajan, K. M., Moynihan, A. L., D'Lima, D., Colwell, C. W., & Li, G. (2008). In vivo contact kinematics and contact forces of the knee after total knee arthroplasty during dynamic weight-bearing activities. *Journal of biomechanics*, *41*(10), 2159–2168.

Vos, T., Barber, R. M., Bell, B., Bertozzi-Villa, A., Biryukov, S., Bolliger, I., ... others (2015). Global, regional, and national incidence, prevalence, and years lived with disability for 301 acute and chronic diseases and injuries in 188 countries, 1990–2013: a systematic analysis for the global burden of disease study 2013. *The Lancet*, *386*(9995), 743–800.

Wang, X., Guo, S., Qu, B., Song, M., & Qu, H. (2020). Design of a passive gait-based ankle-foot exoskeleton with self-adaptive capability. *Chinese Journal of Mechanical Engineering*, *33*(1), 1–11.

Wang, X., Guo, S., Qu, H., & Song, M. (2019). Design of a purely mechanical sensor-controller integrated system for walking assistance on an ankle-foot exoskeleton. *Sensors*, *19*(14), 3196.

Winby, C. R., Lloyd, D. G., Besier, T. F., & Kirk, T. B. (2009). Muscle and external load contribution to knee joint contact loads during normal gait. *Journal of biomechanics*, *42*(14), 2294–2300.

Witte, K. A., Fatschel, A. M., & Collins, S. H. (2017). Design of a lightweight, tethered, torque-controlled knee exoskeleton. In *Rehabilitation robotics (icorr), 2017 international conference on* (pp. 1646–1653).

Wretenberg, P., & Arborelius, U. P. (1994). Power and work produced in different leg muscle groups when rising from a chair. *European journal of applied physiology and occupational physiology*, *68*(5), 413–417.

Yandell, M. B., Tacca, J. R., & Zelik, K. E. (2019). Design of a low profile, unpowered ankle exoskeleton that fits under clothes: overcoming practical barriers to widespread societal adoption. *IEEE Transactions on Neural Systems and Rehabilitation Engineering*, *27*(4), 712–723.

Yang, J., & Peng, C. (2020). Evolving control of human-exoskeleton system using gaussian process with local model. *Biomedical Signal Processing and Control*, *58*, 101844.

Yusuf, E., Bijsterbosch, J., Slagboom, P. E., Rosendaal, F. R., Huizinga, T. W., & Kloppenburg, M. (2011). Body mass index and alignment and their interaction as risk factors for progression of knees with radiographic signs of osteoarthritis. *Osteoarthritis and cartilage*, *19*(9), 1117–1122.

Zeni Jr, J. A., & Higginson, J. S. (2009). Dynamic knee joint stiffness in subjects with a progressive increase in severity of knee osteoarthritis. *Clinical biomechanics*, *24*(4), 366–371.

Zhao, D., Banks, S. A., D'Lima, D. D., Colwell, C. W., & Fregly, B. J. (2007). In vivo medial and lateral tibial loads during dynamic and high flexion activities. *Journal of Orthopaedic Research*, *25*(5), 593–602.

Zhao, D., Banks, S. A., Mitchell, K. H., D'Lima, D. D., Colwell, C. W., & Fregly, B. J. (2007). Correlation between the knee adduction torque and medial contact force for a variety of gait patterns. *Journal of orthopaedic research*, *25*(6), 789–797.

Appendices

Appendix A

Load Cells: Technical Information

In Tables A.1 and A.2, F_{Calib} represents the tension load value at which the load cell was statically held during data collection at the corresponding nominal force value. $\overline{R}_A$ represents the mean value of the samples read during the static calibration period for each nominal force value. σ_{R_A} represents the standard deviation corresponding to $\overline{R}_A$. F_A represents the force value obtained from the Arduino readings after adjusting with the model determined from the calibration. e is the reading error ($F_A - \overline{R}_A$). $\%e$ is the percentage error (e/F_{Calib}).

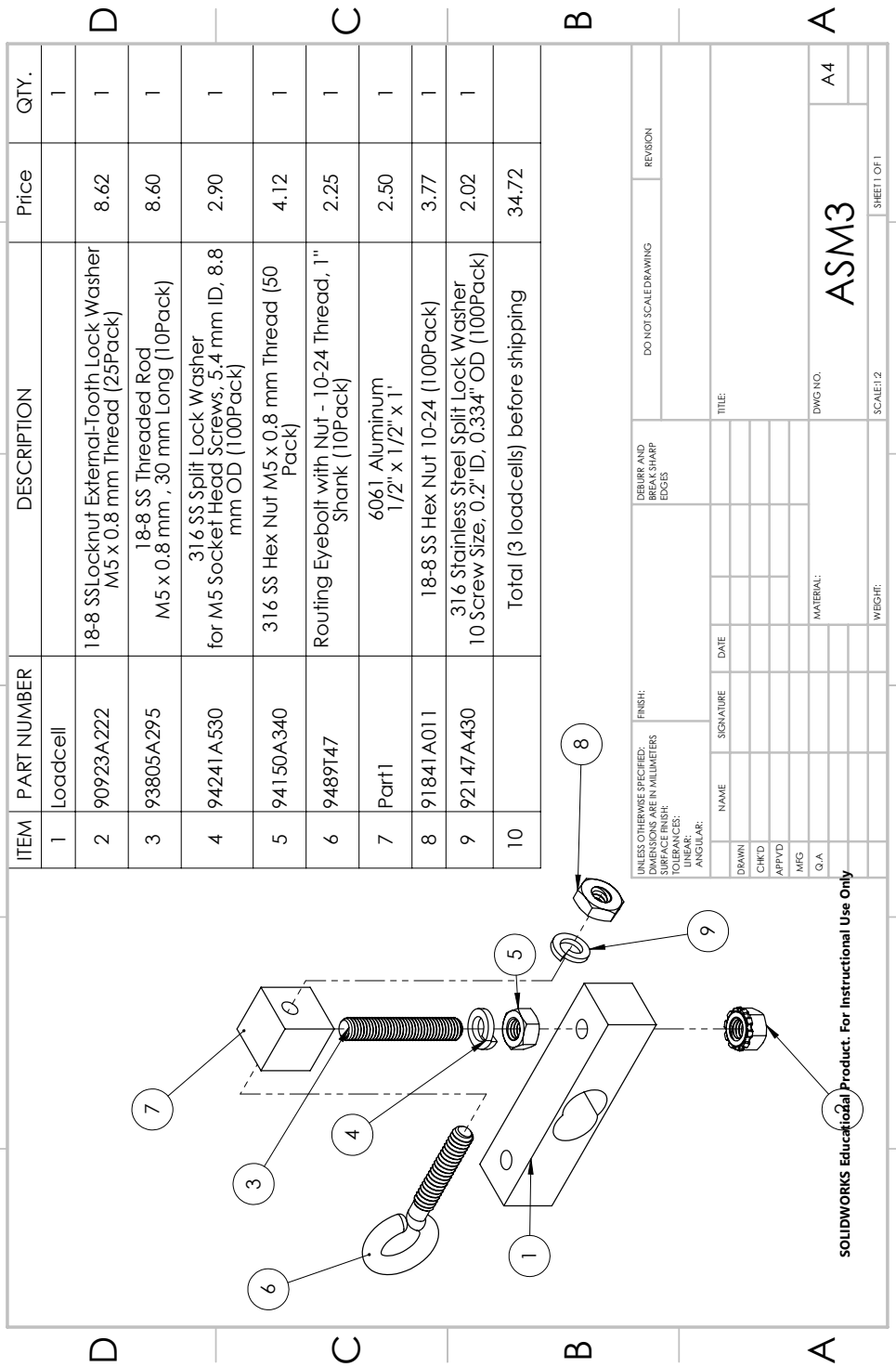

Figure A.1: Load cell assembly with BOM. Two symmetrical assembly sets are required for each load cell.

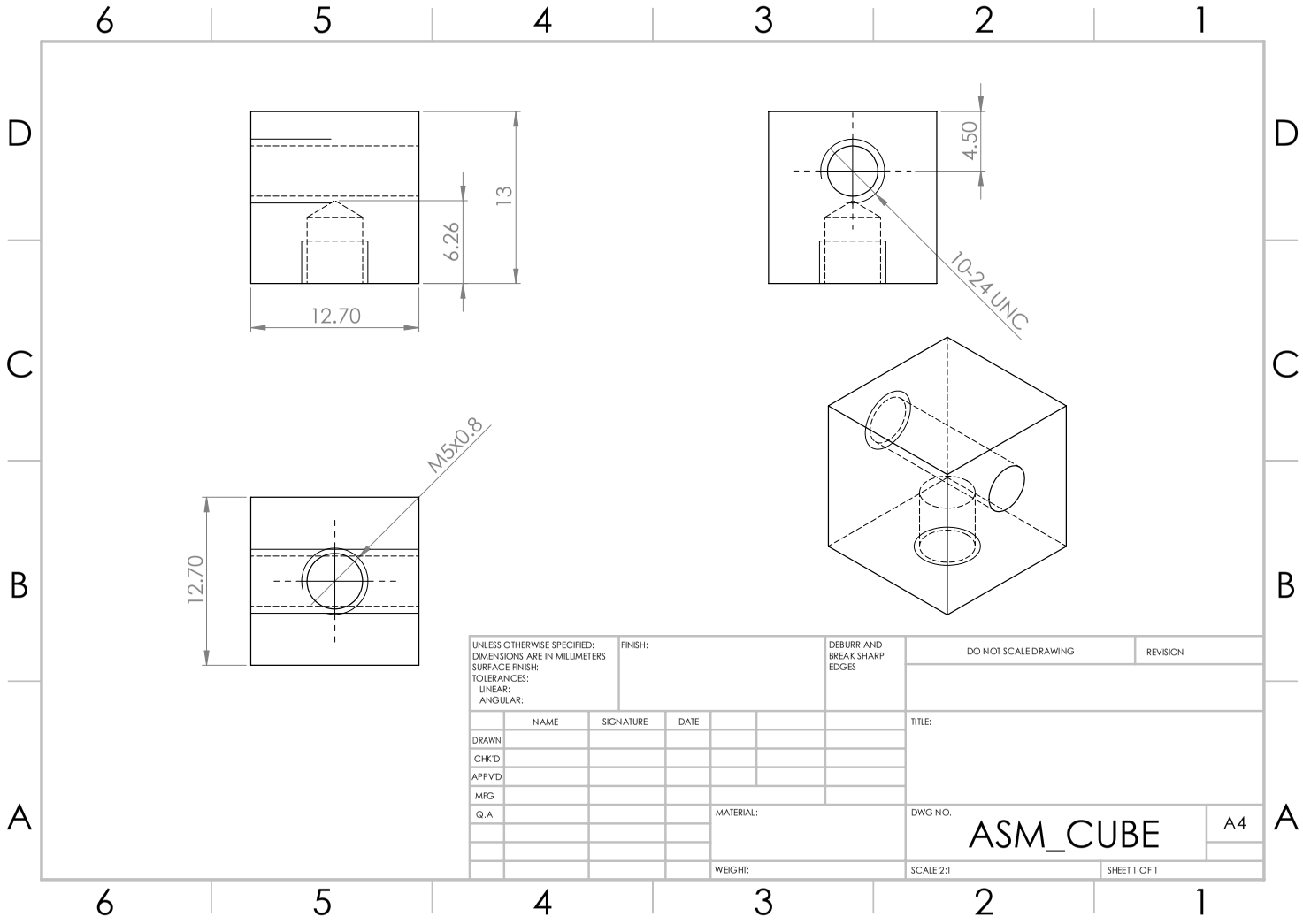

Figure A.2: Part1 drawing. This part is located as ITEM 7 in the BOM showed in Fig. A.1.

Table A.1: Calibration data for Lower Medial load cell (LM).

$F_{Calib}(N)$	$\overline{R}_A$	σ_{R_A}	F_A	e	$\%e$
10.10	96.81	4.62	10.16	0.06	0.61%
20.10	151.64	5.36	20.03	-0.07	-0.37%
30.00	206.36	5.94	29.87	-0.13	-0.43%
40.10	263.33	7.63	40.12	0.02	0.05%
50.00	318.34	7.77	50.02	0.02	0.03%
60.00	373.30	8.52	59.90	-0.10	-0.16%
70.50	431.84	9.63	70.43	-0.07	-0.09%
80.10	486.42	10.33	80.25	0.15	0.19%
90.40	543.73	11.19	90.56	0.16	0.18%
100.20	597.39	12.18	100.22	0.02	0.02%
110.10	654.01	13.54	110.40	0.30	0.27%
120.40	708.24	14.14	120.16	-0.24	-0.20%
130.10	763.49	14.75	130.10	0.00	0.00%

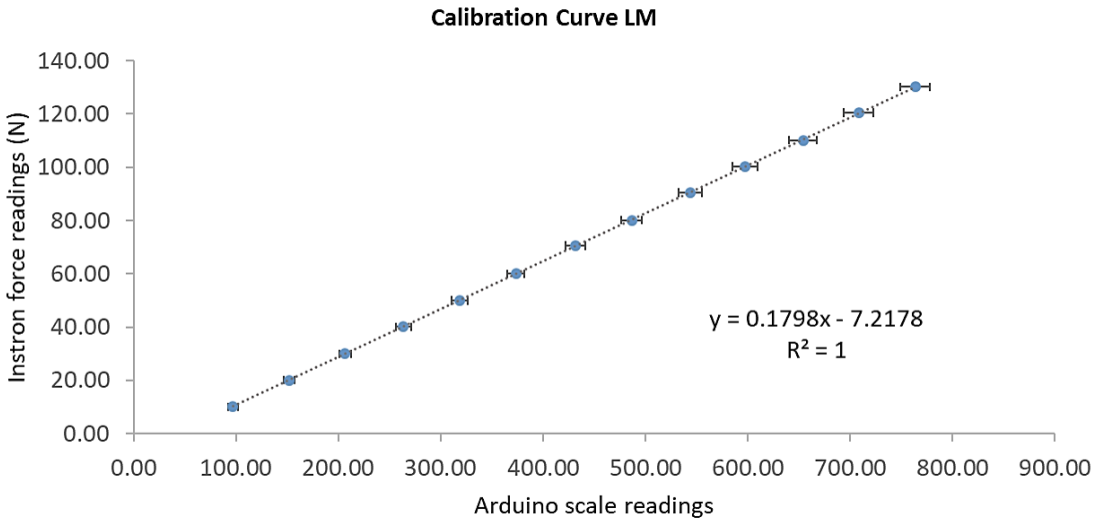

Figure A.3: Calibration curve for LM load cell.

Table A.2: Calibration data for Lower Lateral load cell (LL).

$F_{Calib}(N)$	$\overline{R}_A$	σ_{R_A}	F_A	e	$\%e$
10.10	83.19	4.44	10.05	-0.05	-0.51%
20.10	141.08	4.96	20.24	0.14	0.71%
30.20	196.77	5.80	30.05	-0.15	-0.50%
40.30	254.38	6.66	40.20	-0.10	-0.26%
50.40	310.27	7.61	50.04	-0.36	-0.72%
60.20	367.79	8.46	60.17	-0.03	-0.05%
70.10	425.93	9.28	70.40	0.30	0.43%
80.30	483.37	10.54	80.52	0.22	0.27%
90.00	538.80	11.48	90.28	0.28	0.31%
100.40	594.78	12.19	100.14	-0.26	-0.26%
110.20	652.29	12.74	110.27	0.07	0.06%
120.20	709.94	14.32	120.42	0.22	0.18%
130.40	765.26	15.19	130.16	-0.24	-0.18%

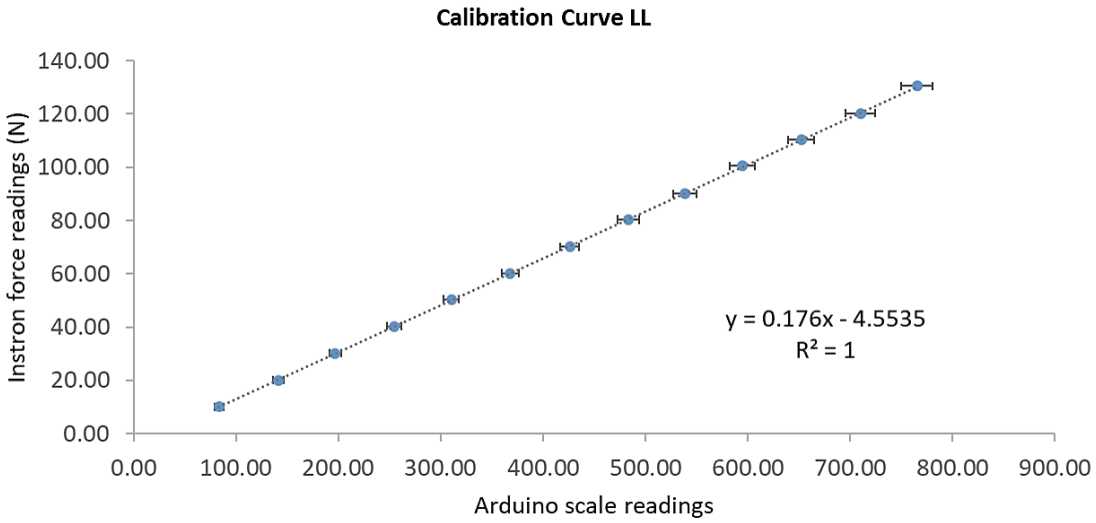

Figure A.4: Calibration curve for LL load cell.